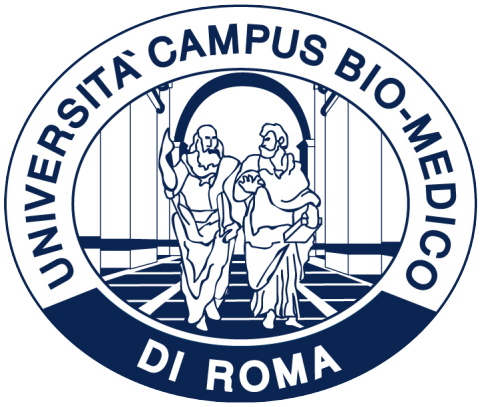

Università Campus Bio-Medico di Roma

Corso di dottorato di ricerca in Bioingegneria e Bioscienze
XXXIV ciclo a.a. 2018-2019

Towards a novel platform to study embodiment

François Le Jeune

Supervisor
Prof. Giovanni Di Pino
Co-Supervisor
Prof. Domenico Formica

September 2022

Abstract

Body representation defines the general representation of our body in our brain. It is composed of a complex sub-division of representations [1] that can be regrouped into two main concepts: the body image and the body schema. Whereas the body image is a conscious aggregation of our feelings and emotions towards our body, the body schema is an implicit model of the metric properties of our body integrating limb dimensions and position in space. A pathological body schema resulting from an amputation can provoke phantom limb pain from the missing limb. A solution to restore a healthy body representation in amputees could be to equip them with prostheses that could replicate the sensations of their former limb. An obstacle to this solution is the abandonment rate of prostheses from their users, who mainly report the lack of feedback from the device. Those inputs direct towards the necessity to promote the embodiment of the prostheses. Embodiment is a complex phenomenon that takes place when we perceive that we own a body part and that we are responsible for its action, senses respectively referred as ownership and agency. However, little is known on the brain process of embodiment so far. Therefore there is a need to cast light on its grey areas to be able to understand the necessary characteristics that a prosthesis must have to be fully embodied and thus integrated into the user's body schema. The present work presents the development and validation of components of a platform aimed at the comprehensive study of the brain processes underlying embodiment. A first component of the platform was developed integrating motion capture and virtual reality into a virtual environment to study the embodiment and its effect on the body schema. The platform was validated and the study showed through the assessment of tactile distance perception that experiencing an elongated arm in immersive virtual reality effectively modifies the body schema. It was additionally found that in this study the body schema alteration was mainly due to the sense of vision whereas the role of the visuo-tactile congruent feedback - typically eliciting ownership - appeared irrelevant. The second component of the platform

consisting in an robot-aided transcranial magnetic stimulation system was developed and validated through the test of control approaches for subjects' movement tracking and compensation. A hybrid force-position control and a selective impedance control were found to be the best choices for our future applications. Finally, the author obtained theoretical and practical hands-on knowledge on the use of electroencephalography to monitor the brain activity through a study of a preferred hand posture in the body schema. Results did not provide any evidence of such a hypothesis from an electrophysiological point of view.

Contents

List of Publications

[1] François Le Jeune, Marco D'Alonzo, et al. "A Novel Platform to Assess the Effects of the Rubber Hand Illusion on the Tactile Reference Frame". In: *2019 Summer School on Neurorehabilitation (SSNR2019)*. 2019, pp. 12–13.

[2] François Le Jeune, Marco D'Alonzo, et al. "Manipulating The Body Representation: Assessment Of A Novel Platform". In: *2020 42nd Annual International Conference of the IEEE Engineering in Medicine & Biology Society (EMBC)*. IEEE. 2020, pp. 3248–3251.

[3] François Le Jeune, Marco D'Alonzo, et al. "Experiencing an elongated forearm in virtual reality increases the tactile distance perception on the corresponding real limb". 2023, In preparation.

[4] Alessia Noccaro, François Le Jeune, et al. "Evaluation of control approaches for TMS robot-aided platform during head motion". 2023, In preparation.

List of Figures

List of Tables

Chapter 1

Introduction

The general knowledge of our body and its implementation in our brain is called the *body representation*. Several currents of thoughts still diverge today in defining the concepts underlying the body representation and their boundaries [1, 2], but a so-far accepted consensus is that body representation is governed by two main concepts: the *body image* and the *body schema* (also respectively referred as somatorepresentation and somatoperception [3]). The body image is generally defined as a person's conscious perception of their body and the resulting thoughts and feelings towards it. It plays an important role in the way we conceive ourselves and influences our psychology and behavior, in such a way that a pathological body image can for instance lead to dramatic eating disorders [4]. On the other hand, the body schema is defined as an implicit model of the metric properties of our body including information about our limbs position and dimensions [2]. It acts as reference frame for perception of the environment through our body (somatosensation) [5–8] and is involved in the process of movement planning for action. The multi-modal sensory inputs we receive from our interaction with the environment continuously update the body schema which in turn ensures an accurate perception and realisation of the planned actions. However, the body schema can also be pathological, and one of the main causes is the amputation of a limb. An amputation is a sudden and traumatic modification of the body schema which very often results in a famous and widely studied pathology known as the phantom limb (PL) [9] in which patients report still feeling their missing limb while visually perceiving its absence, and sometimes coupled with pain arising from the missing limb i.e phantom limb pain (PLP) [10–15]. Furthermore, amputation is also likely to impact patients' feelings towards their body, but so-far

little attention has been paid to the alteration of the body image caused by the amputation [16, 17]. Some temporary treatments of PLP have been previously proposed, such as the famous "mirror-box illusion" which reduced PLP in upper-limb amputated patients after observing the reflection of their healthy hand moving where their amputated contralateral hand should be [18, 19]. Nevertheless, a new - and likely more permanent - promising way of treating the altered body representation of amputees could be to replace their lost limb with a prosthesis which would feel natural enough to make them feel like its part of their own body. This would be possible through efferent control over the prosthesis, but above all through afferent multisensory feedback from the prosthesis. The latter is the goal of the RESHAPE ERC research project (REstoring the Self with embodiable HAnd ProsthesEs) lead by Prof. Giovanni Di Pino since 2016, focused on trans-radial upper limb amputation resulting in the loss of the hand [20].

The loss of a limb is a rare but traumatic event that, in 2017, concerned 57.7 millions of people worldwide, Western Europe being the third world region (after East and South Asia) with the highest number of prevalent traumatic amputation [21]. Post-operation, amputees might chose to use a prosthesis to substitute their lost limb. As modern as upper limb prostheses sound, the first appearance of a functional hand prosthesis in history actually dates back to the Second Punic War (218-201 B.C) when a Roman general named Marcus Sergius wore an iron hand to support his shield after loosing his hand in battle [22]. Jumping forward in time, the first mechanically actuated hand prosthesis was designed by Ambroise Paré, a French military surgeon, in 1564 [23] and the first powered prosthesis was a pneumatic hand designed in 1915 in Germany [24]. A new control solution for upper limb prostheses emerged more recently: the myoelectric control. Developed in the 60s, myoelectric prostheses are externally powered (embedded batteries) devices actuated by electric motors and controlled by the contraction of the user's residual limb's muscles [25, 26]. Myoelectric control on prostheses is still widely used today, and has brought about an interesting variety of solutions for upper limbs prostheses, from the classic myoelectric prosthesis controlled by (co)contraction of the remaining muscles of the stump, to most recent and promising technique of osseointegration of the prosthesis into the user's body, sometimes combined with targeted muscle reinnervation (see Fig. 1.1).

In spite of the recent technical improvements, the question of prostheses abandonment, especially from upper limb amputees, is still much discussed. The situation is even more critical as the technological improvements in the control of the devices do not seem to tackle the problem. Quite on the

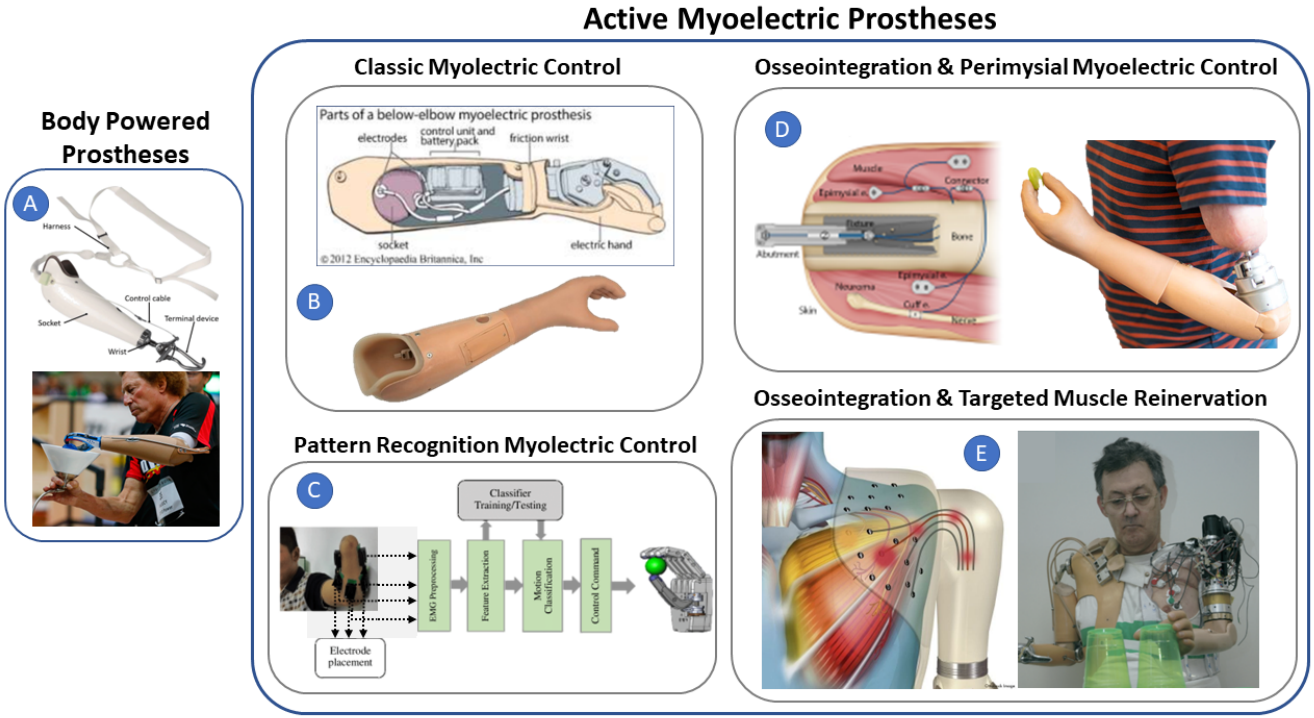

Figure 1.1: Examples of modern solutions for upper limb amputation. **Panel A**: Body powered "hook-like" upper limb prosthesis [27] **Panel B**: Inside view of a classic myoelectric prosthesis components and a commercialized example (Otto Bock HealthCare GmbH). **Panel C**: Pattern recognition myoelectric control [28]. **Panel D**: Osseointegration technique with stump-implanted myoelectrodes [29]. **Panel E**: Targeted Muscle Reinervation technique for shoulder disarticulation prosthesis [30]

contrary, they seem to enhance it: indeed, despite being more technologically advanced than their mechanical counterpart, myoelectric prostheses suffer from a greater abandonment rate [31]. Regarding the functionality of prostheses, users principally accuse the lack of sensory feedback such as force and tactile feedback, especially impacting their grasping function [32, 33]. These findings are the first clues towards the development of prostheses fully acceptable by their users and to consequently restore the healthiness of the representation they have of their body through the integration of the prosthesis into their body schema [34, 35]. Interestingly, these first clues i.e the sensory feedback from a object external to our body, are actually part of a more general concept: the *embodiment*.

The embodiment is a complex phenomenon still vastly investigated today that arises when we perceive that a body part -but not only- is our own, part of our body. It is composed of several sub-concepts, being mainly the *ownership* and the *agency*. Ownership describes the feeling that a body part belongs to us, whereas agency is defined by the feeling of being responsible for an action performed by a body parts [36, 37]. The embodiment phenomenon takes place through congruent integration of motor planning and matching multisensory feedback perceived through somotosensation [38–40] and results in the creation of our body representation [41]. Probably the most interesting aspect of the embodiment process is the fact that it can be related not only to our body parts, but also towards objects initially *external* to our body [42–47]. This groundbreaking aspect of the embodiment was brought to light by Botvinick and Cohen in 1998 with the now famous Rubber Hand Illusion (RHI) paradigm. They demonstrated that the sense of ownership over a rubber hand could be elicited by congruently brush-stroking the visible rubber hand and the hidden real hand of participants, or in other words, by giving participants coherent visuo-tactile feedback from the fake hand [48]. RHI paradigm applications to hand prostheses for amputees have quickly been successfully tested, for example with sensory targeted reinnervation patients who perceived a vivid embodiment illusion towards the prosthesis when it was visually stimulated synchronously with the tactile stimulation on the reinnervation site [49]. Prosthesis integration into the body schema has even been pushed forward by closing the loop between myoelectric efferent control over the prosthesis and almost-natural sensory feedback through implanted electrodes on the ulnar and median nerve fascicles [50]. Further investigations have also speculated that an effective embodiment over a limb or a tool would positively impact the ability of the user to proficiently control it [51, 52]. We thus are getting closer to the objective: successfully restoring the natural feeling of a healthy limb through a prosthesis that

would promote its embodiment, which would in turn restore the healthiness the body representation of amputees (perception of integrity), altered by the amputation [45, 53, 54]. Thus, embodiment appears as the binder between an artificial limb and the body representation, but for now it is likely that we only unveiled the first layers of the brain mechanisms behind the embodiment. Questions still remain, hence the necessity to go further in depth in the investigation of the underlying aspects of the embodiment and the different possibilities to promote and enhance it.

What aspects of a fake limb would promote embodiment? Whereas modifying different aspects of a real prosthesis (aesthetics, noise, weight, dimensions, etc.) to understand their influence on embodiment would be complex and costly, virtual reality (VR) offers the convenience of being highly malleable in terms of visual and audio feedback. Besides, it becomes also possible to act on the proprioceptive and tactile feedback that users perceive from their virtual body and environment when VR is coupled with motion tracking and haptic technologies [53], developing the senses ownership and agency on top of the sense of self-location given by the first-person perspective over their virtual avatar [55]. A platform integrating such technologies would enable the fine tuning of afferent sensorimotor parameters coming from a virtual limb or prosthesis in order to determine the ones necessary to achieve an optimal embodiment [56]. Additionally, VR has proven to present alleviating properties on the PLP through a vast number of studies [57–66] and to be be an promising tool for neurorehabilitation in general [67, 68], giving a further therapeutic purpose to such a platform.

How to measure embodiment? Embodiment is generally measured through explicit and subjective measurements such as an embodiment questionnaires [48] and through physiological measurements such as skin conductance response (SCR) [41] or as recently highlighted, blood flow to the investigated limb [69]. Furthermore, brain areas related to ownership are believed to be the ventral premotor cortices, intraparietal cortices, and the cerebellum. Indeed, rated ownership illusion strength has been correlated with the degree of premotor and cerebellar activity [70, 71]. Besides, the frontal cortex where motor plans for voluntary action are processed, and its connectivity to the parietal areas that monitor outcomes of these actions are known to play an important role on the sense of agency [72]. Hence, monitoring the brain activity related to these areas appears as an interesting method to investigate the levels of embodiment, and electroencephalography (EEG) has indeed recently began to be used for this purpose [73–75]. EEG has the additional benefits of being portable and compatible with movement, unlike magnetoencephalography (MEG) or functional magnetic resonance imaging

(fMRI). Furthermore, the EEG cap can even be worn together with a virtual reality headset.
Now, can we externally stimulate embodiment, not by sensorimotor stimulation but by directly stimulating the related brain areas? Transcranial magnetic stimulation (TMS) is a non-invasive and painless technique used to stimulate areas of the cerebral cortex by polarising neurons through an electromagnetic field generated by a coil placed on the scalp. Since it was first described by Barker in 1985 [76], TMS have seen its use increase especially over the last decades as a clinical therapeutic application for neurological or mental health disorders [77] as well as in the research field to investigate and modulate human brain functions [78]. Interestingly, TMS has already been used to modulate the RHI [79], and has recently been successfully used to promote agency [80] and ownership with VR feedback [81]. Using TMS during embodiment tasks thus could enable to define in further details the brain areas to be targeted and the optimal neuromodulation paradigm to enhance a prosthesis embodiment. However, classic TMS constrains the subject movements during stimulation, which would strongly limit the experimental protocols. Therefore, the development of a robot-aided TMS system, tracking and compensating for the subjects movements would open up the way to a wide range of dynamical experimental protocols. Finally, the inter-compatibility of VR, motion tracking, haptic stimulation, EEG and robot-aided TMS enables the integration of these technologies into a comprehensive platform that would act as a test bench for a broad range of studies aimed at expanding knowledge on embodiment.

The present doctoral thesis presents the development and validation through different experimental studies of components of such a platform integrating VR, motion capture, robot-aided TMS and EEG, aimed at performing comprehensive experimental studies on embodiment both with healthy and amputated participants.
In the second chapter, we introduce the first component of the platform composed of the integration of several motion capture devices and a VR system into a custom virtual environment designed to study embodiment over virtual limbs. We successively present the feasibility of such a study with the developed component.
The third chapter presents an application of the platform introduced in chapter 2 to the study of the body schema manipulation through embodiment of an elongated virtual arm and its effect on the tactile distance perception.
The forth chapter is dedicated to the development of the second component of the platform, namely the robot-aided transcranial magnetic stimulation

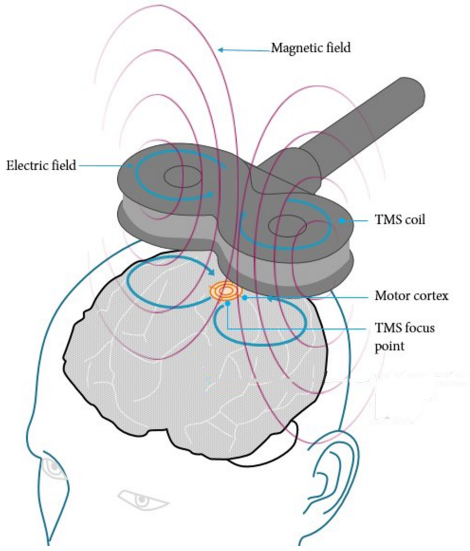

Figure 1.2: Schema of transcranial magnetic stimulation functioning. Adapted from [82]

platform, and to its validation through the comparison of three different robot control approaches.
To conclude the study and validation of the technologies involved in the future platform, we present in chapter five an EEG study aimed at providing evidence from an electrophysiological point of view of a preferred hand posture in the body schema. This study simultaneously enabled the author to obtain hands-on knowledge on how to process and analyse human electroencephalographic data.
Finally, chapter six summarizes the findings and the relevance of the present work, and proposes a plan for the future steps towards the completion of the embodiment platform.

Figure 1.3: Objective of the final platform. In this hypothetical scene, an amputated patient is participating to an embodiment study. They are immersed in a virtual environment where they experience the feeling of owning a prosthesis with changeable features. Their movement is tracked and replicated in the virtual environment through motion capture. The robot-aided TMS platform stimulates the brain areas responsible for the embodiment, and the patient's brain activity is recorded through the electroencephalography cap.

Chapter 2

Embodiment of virtual limbs through virtual reality and motion capture: platform development and feasibility study

2.1 Background

As introduced in chapter 1 the sense of embodiment refers to the particular perceptual status when part of one's own body is identified as self. By integrating an external and new object into the body schema, the RHI alters the body representation. Besides, it has been reported that the RHI also induces in participants a shift of the perceived location of their real hand towards the fake hand, a phenomenon known as the proprioceptive drift (PD) [48, 83–88]. The RHI has been replicated in a virtual environment i.e the virtual hand illusion (VHI) for the first time in 2008 by Mel Slater and colleagues using stereo glasses to view a three-dimensional (3D) virtual image of a virtual arm in the place of the real one and by tapping and stroking the hand of the participant congruently with the visual stroking of the virtual hand [89]. At that time, authors already viewed the embodiment of a virtual body as "an invaluable tool for the understanding of the brain mechanisms underlying body ownership" and that a virtual body owned by participants would have a significant application in the research on limb prostheses. In

the following years, the VHI and VR in general have indeed proven powerful tools to induce embodiment over a virtual limb or a complete virtual body through visuo-tactile integration [90, 91], visuo-motor integration [92, 93] and visuo-motor-tactile integration [94, 95]. Furthermore, with the objective of studying the embodiment of *external* objects, we chose VR over video or augmented reality (AR) imaging because the latter visual feedback methods show participants an image based on their real hand, inducing a strong top-down influence on the ownership rating [96]. Hence, for the reasons specific to our main axis of research presented in chapter 1 and supported by the vast literature on the topic, we developed a platform consisting in a highly immersive VR application integrating optical motion capture devices. In a feasibility study, we then investigated the possibility of eliciting the embodiment of a virtual forearm of different lengths with the developed platform through two experimental protocols : the first one is inspired from an study performed by Kilteni and colleagues in 2012 in which they used a similar platform integrating motion capture into a VR environment to study the extent to which virtual body parts with unnatural dimensions could be integrated into the body schema through embodiment based on synchronous visuo-motor-tactile feedback (VMT-VHI) [97]. They found that ownership scores were high both for incongruent and congruent stimulations and without significant difference between each other, but that the illusion strength decreased with limb elongation. We replicated their protocol to verify that we could achieve similar results with our platform. The second protocol is a classical VHI paradigm employed to understand if embodiment could also be achieved through our platform with only visuo-tactile synchronous stimulation (VT-VHI). The aim of the feasibility study was not to compare the protocols, but to investigate if they could individually elicit embodiment over virtual limbs of different lengths.

2.2 Platform development

2.2.1 Hardware apparatus

Virtual Reality System

As virtual reality system, we used a first generation HTC Vive VR kit (HTC Corporation) composed of a VR headset (Head Mounted Device - HMD), one controller, and two infrared cameras (base stations) that track the motion of the HMD and of the controller. We chose this system for its "plug and play" convenience, low price (799$ in 2016), and easy integration into Unity

(virtual environment engine) through the SteamVR Unity Plugin (Valve Corporation) already available. The headset technical specifications offer a high (1080 x 1200) pixels-per-eye resolution (2160x1200 total), a 90Hz frame rate and a 110° horizontal field of view (human horizontal field of view being of 114° [98]), as well as a room-scale tracking system [99]. We however decided not to exploit the motion tracking features provided by the HTC Vive, except for head motion because of its lack of accuracy and precision for scientific research [100, 101].

Motion Tracking Systems

To track the arm and forearm movement of participants, we used four Optitrack 13W infrared cameras (NatualPoint Inc.) together with passive optical markers and Optitrack's software Motive (Version 2.1.1 Final). We chose this solution for its low cost, its sufficiently precise and accurate motion tracking of the upper body [102], and its easy integration into Unity through the available Optitrack Unity plugin. The cameras benefit from a 0.30mm accuracy, a sampling frequency of 240 FPS, and can track optical markers up to a 9m range [103] which is largely sufficient for our maximum tracking distance of 3.40m. To track the hand and fingers movement of participants, we used a Leap Motion device (Ultraleap, Inc.). This device was also chosen for its low cost, plug and play convenience and for the availability of a plugin for easy integration into Unity. The Leap Motion reconstructs in real-time a 3D model of the hand including bones and joints from the hand image captured by its two embedded infrared cameras. It operates at a sampling frequency of 120Hz and its tracking works best within a 0.60m range [104]. Finally, head motion tracking, performed by the HTC Vive cameras (base stations) together with the inertial measurement units (IMUs) embedded in the headset itself, typically runs at sampling frequency of 90Hz. The platform workspace is a volume inside of a metallic structure of 2.40m x 2.00m x 1.80m for volume of 8.64m^2.

2.2.2 Software development

Virtual Environment

The virtual environment used for our experiments were developed with Unity (Version 2018.3.3f1), a game engine used to create games and other applications (Unity Software Inc.) using C# as primary scripting API. We chose it for its free access and its compatibility with the previously mentioned technologies. The virtual experimental room was created using Unity's user

interface: four white walls, a white ceiling and a floor. In the center of the virtual room, we placed a table and two chairs, one on both sides of the table. Using the open-source 3D computer graphics middleware MakeHuman, we created generic female and male avatars which we used as participants or experimenter avatar. We imported the avatars as assets in our Unity environment, and positioned the participant avatar seated on one of the chairs in a position we called "default" i.e with the right arm alongside the body and the left forearm on the table. When necessary, we positioned the experimenter avatar on the other chair, facing the participant avatar and holding a paintbrush in the right hand and over the participant avatar's left index finger.
All motion capture data were streamed in real-time to the Unity application. Optitrack motion tracking data were streamed through the Optitrack Unity Plugin (version 1.1.0) [105], Leap Motion hand tracking data through the Leap Motion's Core Assets for Unity (Version 4.3.4) [106], and information between the HTC Vive and Unity (motion tracking and visual feedback) were exchanged through the SteamVR Unity Plugin (version 1.2.2) [107]. See Fig. 2.1 for a complete overview of hardware and software integration into the Unity application.

Virtual Avatars Animation

The animations of the avatars were based on motion capture, meaning that movements of both avatars were coming from online or offline motion tracking data. More specifically, we used the tracked angular positions of the arm, forearm, hand and fingers. To animate the experimenter avatar during the VHI paradigm, we used an offline motion tracking recording of a real person performing the brush-stroking. We then imported the recorded angular trajectories of the person's arm, forearm and hand in Unity and programmed the avatar's arm, forearm and hand to follow the predefined trajectories when the virtual brush-stroking was activated. The animation of the participant's avatar was an online replication of the movements performed by the participant. The avatar's arm and forearm movements were replicated from the Optitrack motion tracking data, whereas the avatar's hand and fingers movements were replicated from the Leap Motion data. As previously specified, the sampling frequencies of the motion tracking systems are all equal or superior to the VR headset display frequency (90Hz) and thus the running frequency of the VR application we developed. This therefore enables a smooth real-time visual replication of the participant's movement on their avatar.

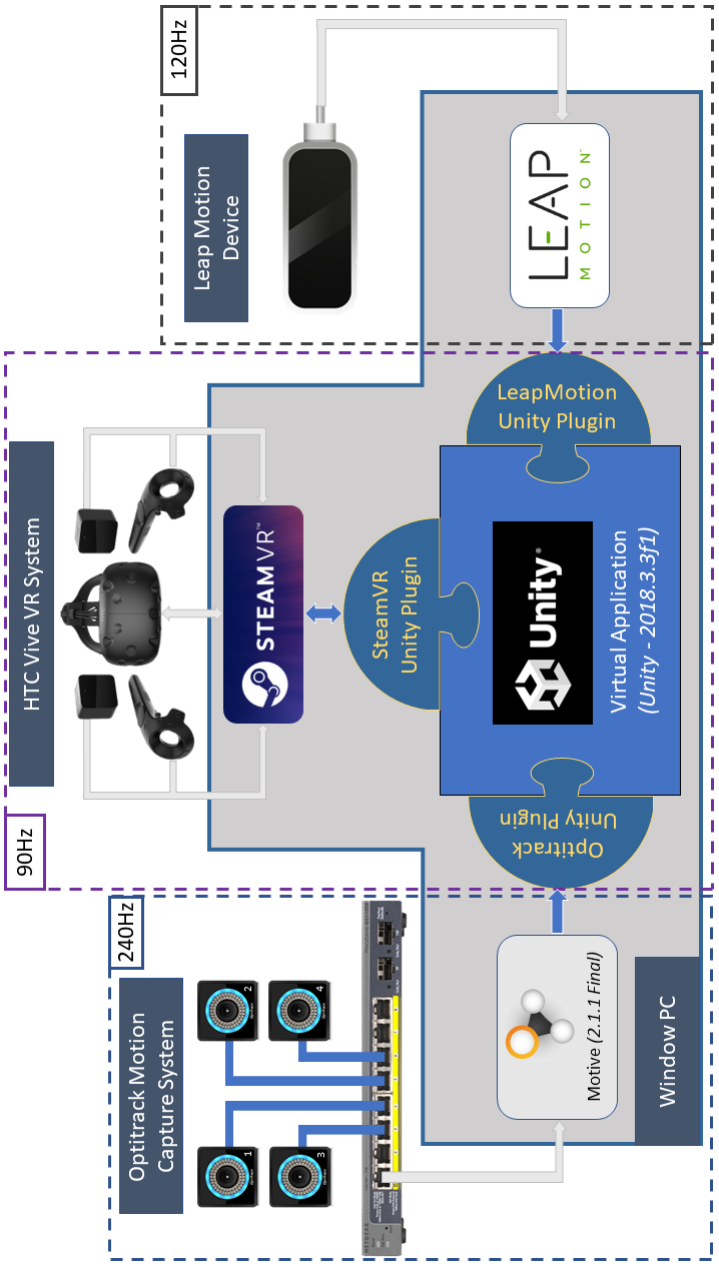

Figure 2.1: Integration of the motion capture and virtual reality systems into the Unity application.

2.3 Feasibility Study

2.3.1 Materials and Methods

Participants

Eight volunteers (3 females, age = 28.5± 1.69 [mean ± standard deviation]) naïve to the RHI or VHI paradigm, participated in the study (one for each condition). Seven were right handed. All participants were healthy and claimed to have normal hand sensation and normal or corrected to normal vision. Informed consent according to the Declaration of Helsinki (BMJ 1991; 302:1194) and to the Ethical Committee of the Campus Bio-Medico University, was obtained before conducting the experiments.

Real Environment

In the real environment, the participant is seated comfortably in a chair in front of a table and is equipped with the VR head mounted device (HMD) covering the eyes. They are positioned at the center of the motion capture workspace while VR infrared cameras are placed outside of the workspace, oriented towards the HMD. On the table is placed a large paper goniometer to perform the angle estimation used to evaluate the proprioceptive drift.

Virtual Environment

In the virtual environment, participants see their virtual body coincident with their real body in a first-person perspective. The physical appearance of the avatar can be switched between a male and female appearance, and the length of the left arm and left forearm can be modified to match the morphology of the subject. The participant's avatar is seated in front of a table. Two different virtual environments were developed to test the different experimental protocols. For the VT-VHI experiment, a virtual experimenter is seated in front of the subject on the other side of the table, in a room similar to the real one. The virtual experimenter is holding a virtual paint brush in the right hand to perform the stroking on the participant avatar's left index. When animated, the experimenter avatar performs the brush-stroking of the participant avatar's left hand index finger. The forearm of the subject's avatar can be elongated up to twice or three times the size of the participants real forearm. For the VMT-VHI, the subject is seated in the same position as previously mentioned, but without any virtual experimenter and a virtual piece of cardboard is present on the table. The possible elongations are the

same as in the VT-VHI experiment. For a detailed version of the experimental apparatus, see section 2.2.

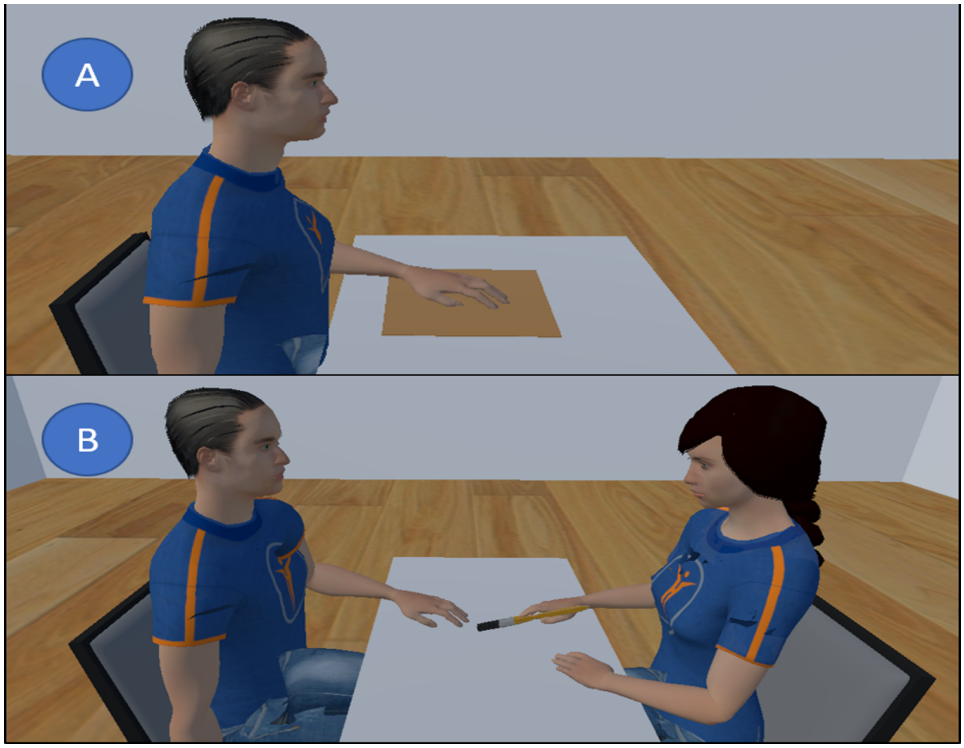

Figure 2.2: Visualization of the virtual environment without forearm elongation. **Panel A:** Environment of the VMT-VHI. **Panel B:** environment of the VT-VHI.

Haptic Stimulation

During the VT-VHI condition, the haptic stimulation was performed by an experimenter standing on the other side of the table and manually brush stroking the index finger of the subject congruently or incongruently with the visual feedback of the participant, depending on the condition. In the case of the VMT-VHI, a piece of cardboard was placed on the table, under the hand of the subject, and the haptic stimulation was performed through the tactile feedback felt by the participant when exploring the piece of cardboard with the left hand.

2.3.2 Experimental Procedure

Visuo-motor-tactile VHI

In order to reproduce the experiment performed in [97], we decided to test four different conditions: one incongruent condition with virtual forearm length equal to the real one (I), and three congruent conditions with virtual forearm lengths equal to (C1), twice (C2), or three times the real one (C3). In all conditions, the right arm of the subject was not tracked, and the subject was asked to keep it still alongside the body. It would remain in this position during the whole experiment, except for the angle estimation tasks. The right arm of the avatar was positioned accordingly. The left arm of the subject was initially placed as rest on the table, with the left hand placed on the piece of cardboard. In the familiarization phase, the participants were first asked to look around the room and especially at the virtual body. The virtual forearm was not yet elongated, and its length was equal to the real one in all conditions. Subjects were then asked to explore the material they felt under the left hand by touching it with the left hand. The movements performed by the subject were accordingly reproduced by the avatar. Subjects experiencing the congruent conditions were provided with visuo-motor and visuo-tactile correlation, as they saw the virtual hand touching the virtual piece of cardboard while feeling its texture. The subject experiencing the incongruent condition however, was only provided with visuo-motor correlation. The virtual piece of cardboard was placed out of reach, farther in front of the avatar's left hand, hence providing the subject with a visuo-tactile mismatch. In the experimental phase, the virtual left forearm of the avatar was then elongated accordingly to the condition (I and C1: no elongation, C2: twice the real length, C3: three times the real length). They were then asked to stroke again the surface they felt under their hand for ninety seconds. Finally, the subjects were told the experiment was over and showed the virtual forearm at the real length for a few seconds before removing the HMD and filling a questionnaire.

The visuo-tactile VHI

Four conditions similar to the one's of the VMT-VHI were tested. One congruent (C1) and one incongruent (I) brushing condition were tested for a virtual forearm length equal to the real one. Two other congruent brushing conditions were tested, one for a virtual arm length of twice the real one (C2) and one for a virtual arm length three times the real one (C3). The first part of the experimental protocol consists in a familiarization phase with the

virtual avatar to provide the participant with the sense of agency over the virtual avatar. In the virtual environment, the participant's avatar is seated on a chair in front of a table and the virtual experimenter is seated on the other side, arms crossed. The right arm of the subject is not tracked, and the subject is asked to keep it still and alongside the body. It would remain in this position during the whole experiment, except for the angle estimation tasks. The right arm of the avatar was positioned accordingly. The motion tracking of the left arm, hand and fingers was activated, and participants were asked to explore the surrounding area (without touching anything) by moving their chest, left arm, left hand and fingers while looking at the virtual body moving accordingly. In particular, participants were asked to pay close attention to the virtual left hand and fingers. Then, participants were asked to close their eyes and to put their arm and hand down on the table, and to remain still with the hand palm down, in a relaxed position. When this was done, the motion tracking was disabled. Participants were then asked to open their eyes and pay close attention to the left hand they were seeing, and the brushing session was started for ninety seconds. The virtual forearm was not yet elongated, and its length was equal to the real one. In all conditions, the visual brushing was performed by the virtual experimenter on the index finger of the virtual left hand, and the tactile brushing was performed by the experimenter on the index finger of the left hand of the subject. Subjects experiencing the congruent conditions were provided with visuo-tactile correlation, as they saw the virtual left hand index finger being brushed while feeling a brushing on their own left hand index finger. For the subject experiencing the incongruent condition however, a temporal delay of two seconds between the virtual and the real brushing was set, resulting in a visuo-tactile mismatch. In the experimental phase, the virtual left forearm of the avatar was then elongated accordingly to the condition (I and C1: no elongation, C2: twice the real length, C3: three times the real length). Participants were then asked again to remain still while looking at the left hand while brush-stroking took place for ninety seconds. Finally, the subjects were told the experiment was over and showed the virtual forearm at the real length for a few seconds before removing the HMD and filling a questionnaire.

Embodiment outcomes

In order to measure the strength of the illusion on different conditions, each participant filled-in a questionnaire at the end of the trial. The questionnaire included the six statements list designed in [97]. Three of the statements

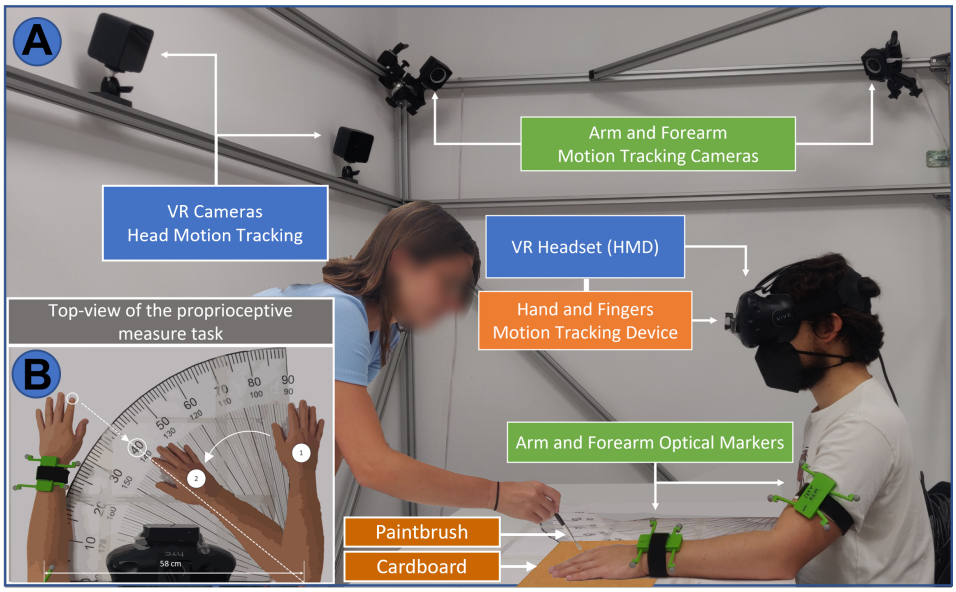

Figure 2.3: Real world experimental setup. **Panel A**: experimental setup with subject in default position. Blue squares: HTC Vive devices (Infrared cameras and HMD). Green squares: Optitrack related equipment (Infrared cameras and reflective optical markers). Orange square: Leap Motion device. Brown squares: tactile stimulation tools. **Panel B**: Proprioceptive drift measurement technique.

(i.e. illusion statements) referred to the extent of sensory transfer into the virtual hand and its self-attribution during the trial; whereas the other three statements (i.e. control statements) served as controls for compliance, suggestibility, and "placebo effect". Participants were asked to rate the extent to which these statements did or did not apply to their experience, by using a seven-point analogue scale. On this scale, -3 meant "absolutely certain that it did not apply," 0 meant "uncertain whether it applied or not," and +3 meant "absolutely certain that it applied". The RHI index, expressed as the difference between the mean score of the illusion statements and the mean score of the control statements [56], was calculated for each condition and employed as illusion outcome. In addition to the six statements, participants were asked to rate vividness and prevalence of self-attribution of the rubber hand [70, 108]. The vividness was defined as how life-like and realistic the illusion was when it was experienced; it was rated from 1 to 9. The prevalence rating (from 0% to 100%) reflected the percentage of

time that the illusion was experienced (equivalent to the continuance of the illusion).
To measure the PD, before and after the experimental phase participants were asked to close their eyes, and the display was turned black. They were helped placing their right arm on the table so that their elbow and forearm were placed on the correct position of the goniometer. They were then asked to point with their right hand's index towards the position where they felt their left hand's index, moving only the forearm and keeping the elbow at the same position (i.e. angle estimation task). After that, they were asked to put their right arm back to its position alongside the body. Post-experimental estimation minus pre-experimental estimation positive differences of the estimated position of the hand indicate a drift of the perceived location of the real hand toward the virtual hand.

2.3.3 Results and Discussion

The incongruent condition resulted in high embodiment scores (Fig. 2.4, first column). In the VMT-VHI experiment, such results could be explained by the remaining visuo-motor congruence of the arm movement, whereas in the VT-VHI experiment, the participant who underwent the incongruent condition mentioned that she did not perceived the stimulation as asynchronous but rather as synchronous with a slight mistake from the experimenter, and her strong PD could probably be considered as an outlier in a data distribution with a larger number of subjects. Nevertheless, Kilteni and colleagues similarly found high ownership scores for the incongruent condition, and no significant difference with the congruent condition [97], hinting towards a prevalence of visuo-motor congruency over the visuo-tactile synchronicity modality in the embodiment process. PD results (Fig. 2.4, bottom graph) for congruent conditions of the VMT-VHI experiement show a trend in line with [97], but not in the case of the VT-VHI. Considering all congruent conditions together, embodiment scores resulted as follows (across participants values, mean $\pm$ standard deviation): RHI Index 3.44 $\pm$ 1.77, Vividness 7.33 $\pm$ 0.81, Prevalence 70.0 $\pm$ 21.9%. Hence, despite the very limited number of participants tested in this study which does not enable to perform any statistical analysis, the results of the RHI index, the vividness score and the prevalence score of the congruent conditions of both experiments show embodiment results in line with previous studies [56, 97] for both experimental protocols, directing towards the possibility to evoke embodiment illusion of an elongated arm with the developed platform.

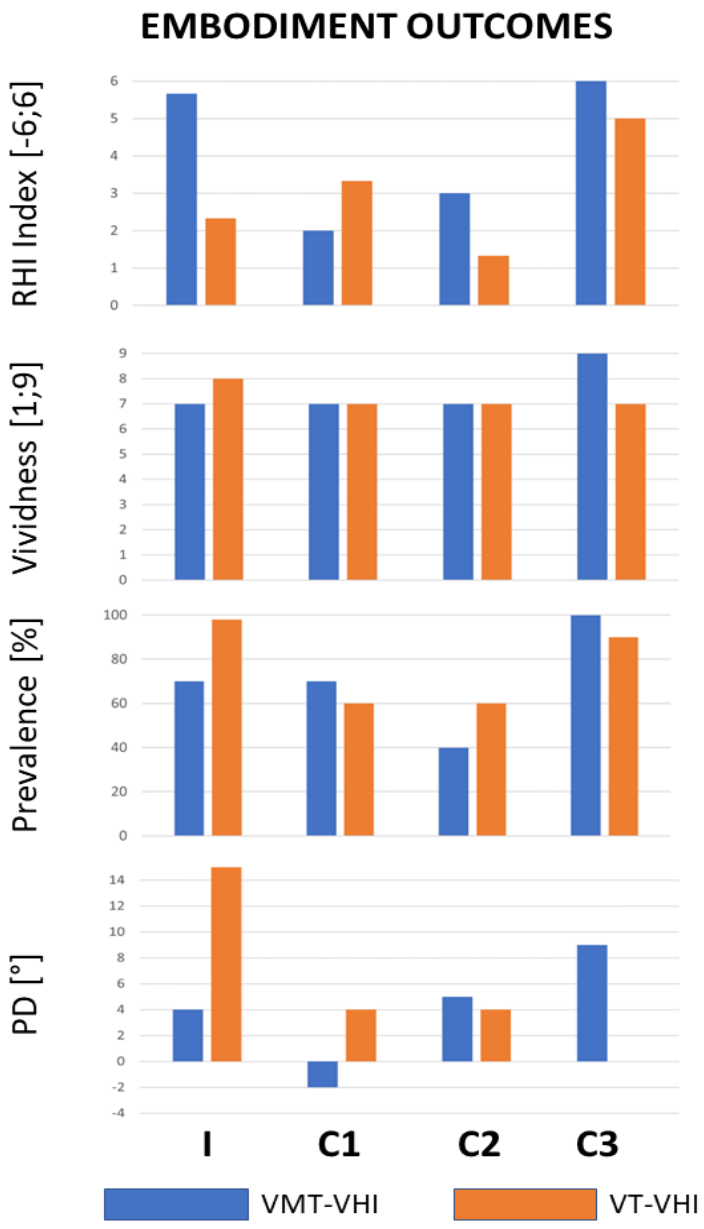

Figure 2.4: Embodiment outcomes of the feasibility study. From top to bottom: RHI Index, Vividness of the VHI, Prevalence of the VHI, and PD.

2.4 Conclusion

We developed a platform aimed at eliciting embodiment over a virtual limb. To investigate the feasibility of such manipulation, we tested two different experimental protocols to induce embodiment of a virtual arm of different lengths: a reproduction of the visuo-tactile-motor experiment performed in [97] and a VHI paradigm that reproduced the typical RHI where only congruent visuo-tactile stimulation was employed. Obtained results were in line with existing literature on the topic and it was thus decided to proceed with further studies with the developed platform.

Chapter 3

Experiencing an elongated forearm in virtual reality increases the tactile distance perception on the corresponding real limb

3.1 Background

Sensory feedback is mandatory to experience the environment and guide the physical interaction with its components. Sensing means measuring parameters and requires a unit of measure and a reference frame to which compare the measure. Especially when the environment is experienced through our body (i.e. in somatosensation), it has been suggested that we employ our body as a reference frame [7, 8] and its metric properties as unit of measure. This could be feasible because the brain creates an implicit model of the metric properties of our body [5, 6]: the body schema [2], and of the space where the interaction occurs. In touch, the perception of the distance between two stimulated points, i.e. tactile distance perception (TDP), depends on the part of the body which is stimulated. Such phenomenon, known as the Weber illusion [109], is certainly linked to the different tactile receptor density of different body parts, but there is more; a tactile resolution variation of 340% results in a variation of only 30% in TDP [110, 111]. Hence, besides receptor density which should account for coding the distance between the

two stimulated points in the primary somatosensory cortex, a subsequent neural process should be involved in the Weber illusion. This may likely be the creation of the body schema, which is a higher-order representation of the body, continuously updated by multimodal sensory input [2, 3, 112, 113]. In this case, a change of the body schema achieved through sensory modulation would have been reflected upon an alteration of the tactile perception of the distance. Indeed, by visually deforming the hand and forearm with magnifying and reducing lenses for about 1 hour the TDP relative to the participant's forearm would change with respect to the not altered control part [114]. In another experiment inspired by the Pinocchio illusion [115], inducing in participants the proprioceptive illusion of an elongation of the index finger achieved by stimulating the spindles of the right arm biceps with a vibrator placed on the tendon (known as tendon-vibration illusion) while participants held their left index finger with their right arm, significantly increased the TDP on said index finger [116]. Those studies confirmed that the perceived size of the body impacts on TDP, which is in line with the body schema acting as reference frame for touch. Interestingly, modifying the perception of the environment by changing the perceived dimensions of the body has also been proven possible by integrating a fake body part into the body schema through congruent visuo-tactile stimulation. After a synchronous Rubber Hand Illusion (RHI) paradigm [48] administrated with a larger fake hand, participants actively felt identical objects in both hands (one in each hand) and perceived the object held by the tested hand larger than the object held by the non-altered control contralateral hand [117]. Similarly, a change of the visually perceived sizes of objects was found when participants were under the illusion of owning (after congruent visuo-tactile stimulation) a giant or miniature body [118]. In the same way, inducing ownership (through a RHI paradigm) over a fake hand placed in a distal farther position than the real hand should induce the feeling of having a longer arm. This has been demonstrated both in real and in virtual environment [41, 88, 97]. However, to our knowledge, no previous study has investigated the possible change in passive tactile perception following a modification of the body schema induced by a RHI paradigm. Thus, we tested a large number of participants with a RHI paradigm in virtual reality, a Virtual Hand Illusion (VHI), to induce the feeling of having an elongated forearm and investigated the evolution of the TDP on the corresponding body part following different forearm length. We hypothesized that the synchronous brush-stroking of a hand at the end of an elongated forearm would have enhanced the TDP and that the amount of TDP changes would have positively correlated to the forearm elongation and the achieved level

of embodiment of the hand. The asynchronous stimulation in an elongated upper limb has been acquired as control condition.

3.2 Materials & Methods

3.2.1 Participants

Sixty-nine participants (33 females, 6 left-handed, aged 23.9±5.6) were enrolled in the experiment in order have twenty-three participants per group of condition (three conditions tested) in the between-subjects analysis on the first tested condition (see 2.4 for detailed explanation). This number of enrolled participants per group has been based on the TDP task (TDPT) data distribution from the study of Taylor-Clarke and colleagues (Taylor-Clarke et al. 2004) to show a 7% mean shift in TDP between pre and post VHI, achieving an effect size of 0.32, a power superior to 0.8 and considering an independent t-test. All participants reported to have normal tactile sensation of the hand, forearm, and forehead, and normal or corrected-to-normal vision. All participants provided written informed consent before the experiment in accordance with the Declaration of Helsinki and following amendments. The experiment was conducted after approval of the Ethics Committee of Università Campus Bio-Medico di Roma (EMBODY protocol).

3.2.2 Setup

The experimental setup consists in a table and a chair placed at the center of a 2.40m x 2.00m x 1.80m metallic structure. The participant sat comfortably on the chair inside the structure. A large paper goniometer (58cm radius) was displayed upon the table. Participants visualized the immersive virtual environment through a virtual reality (VR) system (HTC Vive, HTC Corporation). They wore a VR headset (head mounted device - HMD) and the HMD movement was tracked by two infrared cameras (base-stations). To enhance the immersion of participants inside the virtual environment and their sense of agency over the virtual upper limb, the movements of their real left arm, forearm, hand, and fingers were tracked by motion capture systems. Arm and forearm movements were tracked with four infra-red cameras (Optitrack 13W, Natural Point, Inc) and reflective optical markers worn by the participant. Finger movement was not tracked by the Optitrack cameras because of the small, fixed volume of cameras workspace it requires around the hand, which would have highly limited the arm movement. Thus, a fingers motion tracking device attached on the HMD was employed (Leap

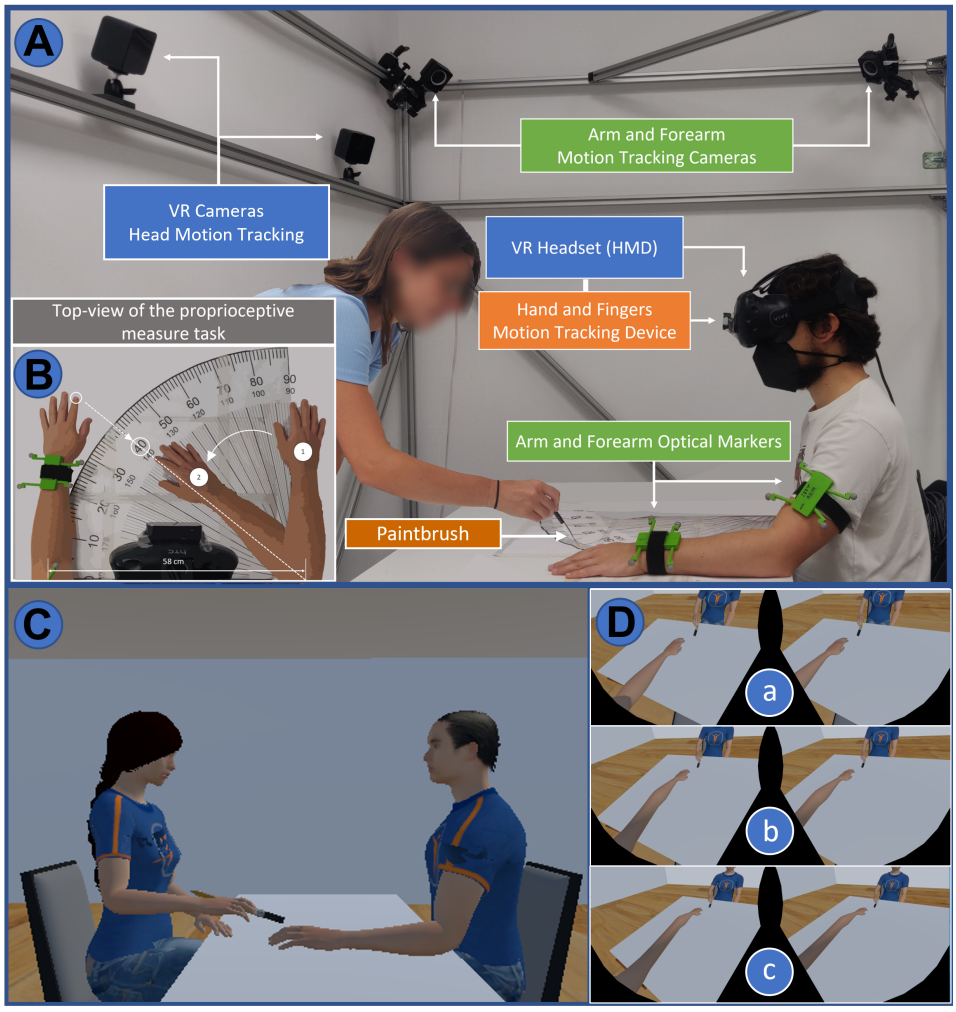

Figure 3.1: Real world and virtual experimental setup. **Panel A**: experimental setup with subject in default position. Blue squares: HTC Vive devices (Infrared cameras and HMD). Green squares: Optitrack related equipment (Infrared cameras and reflective optical markers). Orange square: Leap Motion device. Brown squares: tactile stimulation tools. **Panel B**: Proprioceptive drift measurement technique. **Panel C**: Sideview of the virtual environment. Virtual experimenter (left) holding the paintbrush and participant avatar (right) in initial position without forearm elongation. **Panel D**: Participant's 1PP of the virtual environment without forearm elongation **(a)**, with 20cm elongation **(b)**, with 40cm elongation **(c)**.

Motion, Ultraleap). The device embeds two infrared camera which enables finger tracking when the hand is in its field of view. We developed a VR environment using the game engine Unity (version 2018.3.0, Unity Technologies). The virtual environment replicates the lab room where the experiment was run, including table and chair. In the virtual environment, participants see in a first-person perspective (1PP) their avatar's body (male or female) sitting in front of the virtual table. In the default position, both the real participant and the participant's avatar have the left forearm (palm down) on the table and the right arm alongside the body. The left forearm of the participant avatar can be elongated by different lengths (20cm or 40cm). A virtual experimenter is seated on the other side of the table, in front of the participant avatar, holding a virtual paintbrush in the right hand to perform the stroking. When animated, the virtual experimenter performs the brushing on the participant avatar's left hand index finger. The brushing animation of the virtual experimenter was replicated from a previous motion capture recording of a real experimenter performing the brush stroking. The virtual avatars were created with the open-source software MakeHumanTM.

3.2.3 Experiment

General procedure

The experiment investigated the effects on TDP of the embodiment illusion over a virtual forearm elongated by 20cm (20S) and 40cm (40S) after a synchronous VHI, where an asynchronous VHI with a 20cm forearm elongation (20A) was used as control condition. Firstly, the virtual environment was turned pitch black, and participants underwent a preliminary TDPT (pre-TDPT) to measure their baseline TDP (see 2.3.2 for detailed information). Then, when VR was activated, participants were instructed to look at their surroundings (moving only their head) to familiarize themselves with the virtual environment. To give participants agency over the arm and hand of the avatar, favorizing their embodiment, participants were then asked in a first phase to raise and move their left arm for ninety seconds (without making any left fingers or wrist movement) while looking at the corresponding virtual arm which moved accordingly thanks to the motion tracking. In a second phase, they were instructed to place the palm of their left hand at a short distance in front of their face and to move their hand and fingers for ninety seconds while looking at their virtual counterparts which moved accordingly thanks to the fingers motion tracking device. Finally, participants were instructed to place back their left arm in the default position, and to keep

it still until further notice. The VR environment was turned pitch black. Participants then performed a proprioceptive measure (pre-PM), in which they had to indicate the felt position of the tip of their left index finger (see 2.3.2 for detailed information). The left virtual forearm was then elongated by 20cm or 40cm depending on the condition. The virtual environment was illuminated again, and the participants were asked to look and pay close attention to the (virtual) hand. To perform the VHI, the animation relative to the virtual brush stroking was then started and the experimenter started the tactile stimulation by brush stroking the real left index finger of the participant synchronously or asynchronously (depending on the condition) with respect to the visual virtual brush stroking performed by the virtual experimenter on the left index finger of the avatar of the participant. Brush stroking lasted ninety seconds. Following the VHI, a proprioceptive measure (post-PM) was immediately performed, followed by a post-TDPT. Participants then were asked to answer a questionnaire evaluating the strength of the embodiment illusion elicited by the VHI. The latest steps, starting from the proprioceptive measure prior to the VHI were repeated for every VHI condition, and conditions were tested in a pseudo-random order among participants. The whole procedure, including the preparation of the participant, lasted around one hour and half.

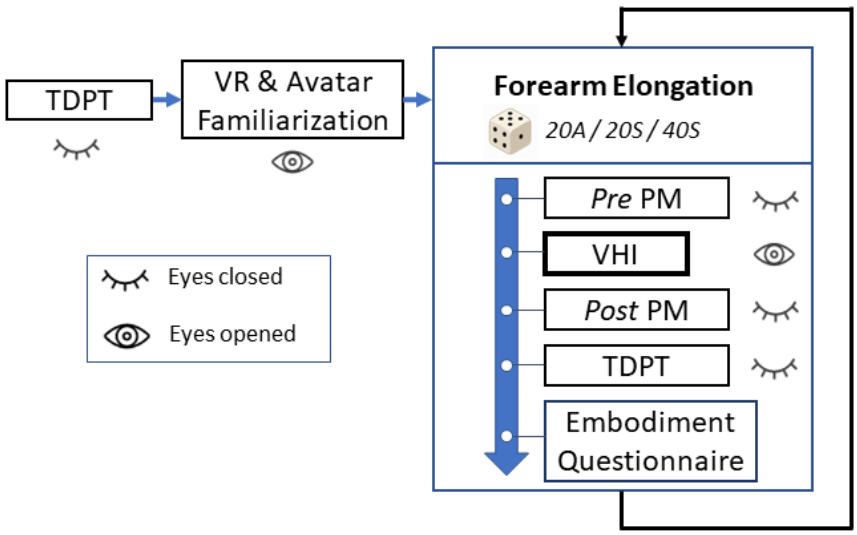

Figure 3.2: Experimental protocol of the experiment.

Measures

To measure the embodiment outcomes following the VHI, participants were asked to fill a self-evaluation questionnaire (adapted from [48, 56]) to evaluate the strength of the ownership illusion over the virtual hand. Three of the statements (Q1, Q2 and Q3) were ownership related and referred to the extent of sensory transfer into the virtual hand and its self-attribution during the VHI. The six other statements (Q4, Q5, Q6, Q7, Q8 and Q9) served as control items to assess compliance, suggestibility, and placebo effect (see 6 for the detailed questionnaire). For each statement, participants were asked to rate the extent to which these statements did or did not apply to their experience, by using a seven-point Likert scale. On this scale, -3 meant:" I am absolutely certain it did not apply", 0 meant:" uncertain whether it applied or not" and +3 meant:" I am absolutely certain it applied". The statements were presented to participants in a random order. The embodiment outcome of the VHI was taken from the questionnaire results and computed as the RHI Index. The RHI Index is defined as the difference between the mean score of the ownership statements and the mean score of the control statements [119]. To measure the proprioceptive drift (PD) of the felt position of their left hand caused by the VHI [48], participants were helped placing their right arm on the paper goniometer in the starting position (90°). To measure where they perceived the position of the tip of their index finger, they were instructed to point with their right index finger towards the felt position of the tip of their left index finger by rotating the right forearm while keeping it in a straight line with the hand and index finger and the elbow in position, like the hand of a clock. We registered the corresponding angle and helped participants placing their right arm back alongside their body. Angular values were converted to an elbow-index perceived distance expressed in millimeters: participants forearms were always positioned on the extremities of the goniometer so that their in-between distance would be of 580mm (see Fig. 3.1, **Panel B**) and a simple trigonometric formula was used to obtain the elbow-index distance corresponding to the given angular value (Θ). The proprioceptive measure (PM) was performed right before (pre) and after (post) every VHI and the resulting PD was calculated as the difference between the post-proprioceptive measure and the pre-proprioceptive measure.

$$\begin{aligned} PM &= 580 \times tan(\Theta) \\ PD &= PM_{POST} - PM_{PRE} \end{aligned} \tag{3.1}$$

To measure the TDP, participants underwent a TDP task (TDPT). During the TDPT, blindfolded participants received fifty-six couples of tactile stimu-

lation: one on the forearm (investigated TDP), and one on the forehead (used as reference TDP) in a random order. Tactile stimulations were performed using fork-like tools composed of two blunt tips with a specific distance between each other. After each couple of stimulation, participants were asked to report in which of the two stimulation the distance felt between the tips of the forks was higher: they were instructed to answer "one" if the first stimulation was felt larger, "two" it was the second. We recorded the body part on which the stimulation distance was felt bigger. Distances between the tips of the forks were chosen based on a previous study using a similar task [114]. In all couples of stimulations, we used a reference fork 45mm wide, and a fork with 30mm, 35mm, 40mm, 45mm, 50mm, 55mm or 60mm between-tips distance. The order, body part, and distance of the stimulations were randomized and balanced among the fifty-six couples of stimulations (twenty-eight unique couples of stimulations, each one performed twice). From the participants responses, we calculated the percentage of "forearm" answers (%FA) for each difference (ΔL) between the length of the forearm stimulation ($L_{forearm}$) and the length of the forehead stimulation ($L_{forehead}$).

$$\begin{aligned} &\Delta L = L_{forearm} - L_{forehead} \\ &\Delta L \in [-15, -10, -5, 0, 5, 10, 15] \end{aligned} \tag{3.2}$$

The TDP was measured by the point of subjective equality (PSE). In this study, the PSE is defined as the extra between-tips distance needed on the forearm stimulation compared to the forehead stimulation, so that both between-tips distances are felt as equal. Thus, an augmentation of the TDP on the forearm would result in reduction of the PSE. It is measured in millimeters. To calculate the PSE, we proceeded as follows: for every participant and every TDPT (Pre, 20A, 20S, 40S) we plotted the %FA (y-axis) in function of the ΔL (x-axis) as independent variable and fitted the data distribution with the following psychophysics sigmoid function (Fig. 3.4):

$$P(\Delta L, PSE, EA) = \frac{100}{1 + exp(-\frac{\Delta L - PSE}{0.5 \times EA})} \tag{3.3}$$

where P is the probability (expressed as a percentage) of feeling the larger stimulation of the forearm. EA is the esteem accuracy and represents the ΔL value of the point in which the line tangent to the curve at the point of coordinates (PSE, 50%) reaches the value P = 100%. It is the inverse of twice the slope of the curve at (PSE, 50%). Considering that we expected a change

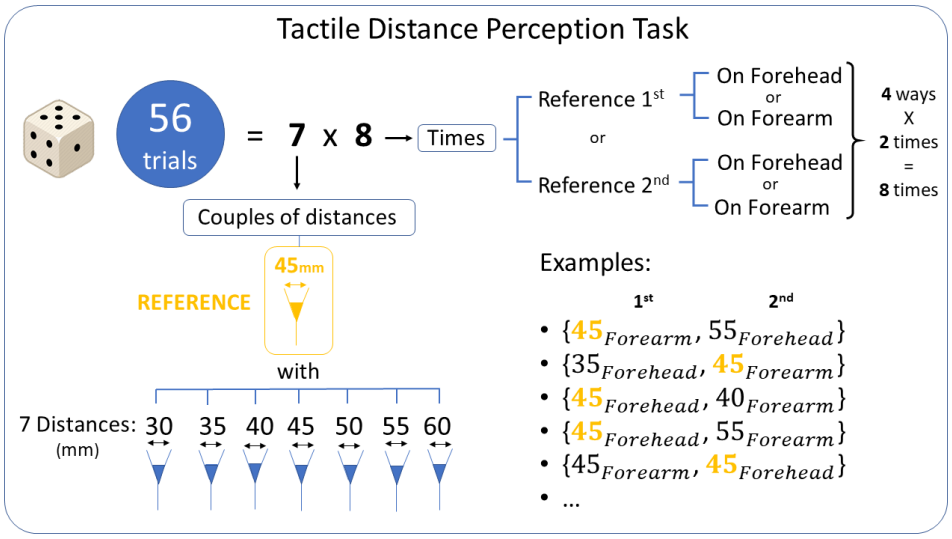

Figure 3.3: Tactile Distance Perception Task. 7 couples of distances tested in 4 different ways (28 different trials); each way repeated twice: 56 trials in total.

in TDP and not in tactile accuracy, the EA was not further considered in the study. From the fitted curve, the PSE can be defined as:

$$PSE = \Delta L | P_{50\%} \tag{3.4}$$

It represents the ΔL value of the point in which the curve corresponds to the P = 50% value, i.e the ΔL value for which the larger stimulation has the same probability to be felt on the forearm as on the forehead (perceived equality of distances). PSE values were obtained as a result of the fittings. The threshold of the fittings' goodness-of-fit was fixed at 0.6 and the data from participants who did not satisfy the threshold were discarded out of the analysis. Finally, we computed for each condition the variation of PSE i.e ΔPSE, as the difference between the post PSE (after the VHI) and the pre PSE (PSE after the previous condition, or baseline PSE for the first tested condition). Finally, for correlation purposes we calculated the relative forearm elongation (RFE) for each participant and each synchronous condition elongation (E, 20cm or 40cm) as the ratio between the length of the virtual elongated forearm and the length of their real forearm (D):

$$RFE_{condition} = \frac{D + E_{condition}}{D} \tag{3.5}$$

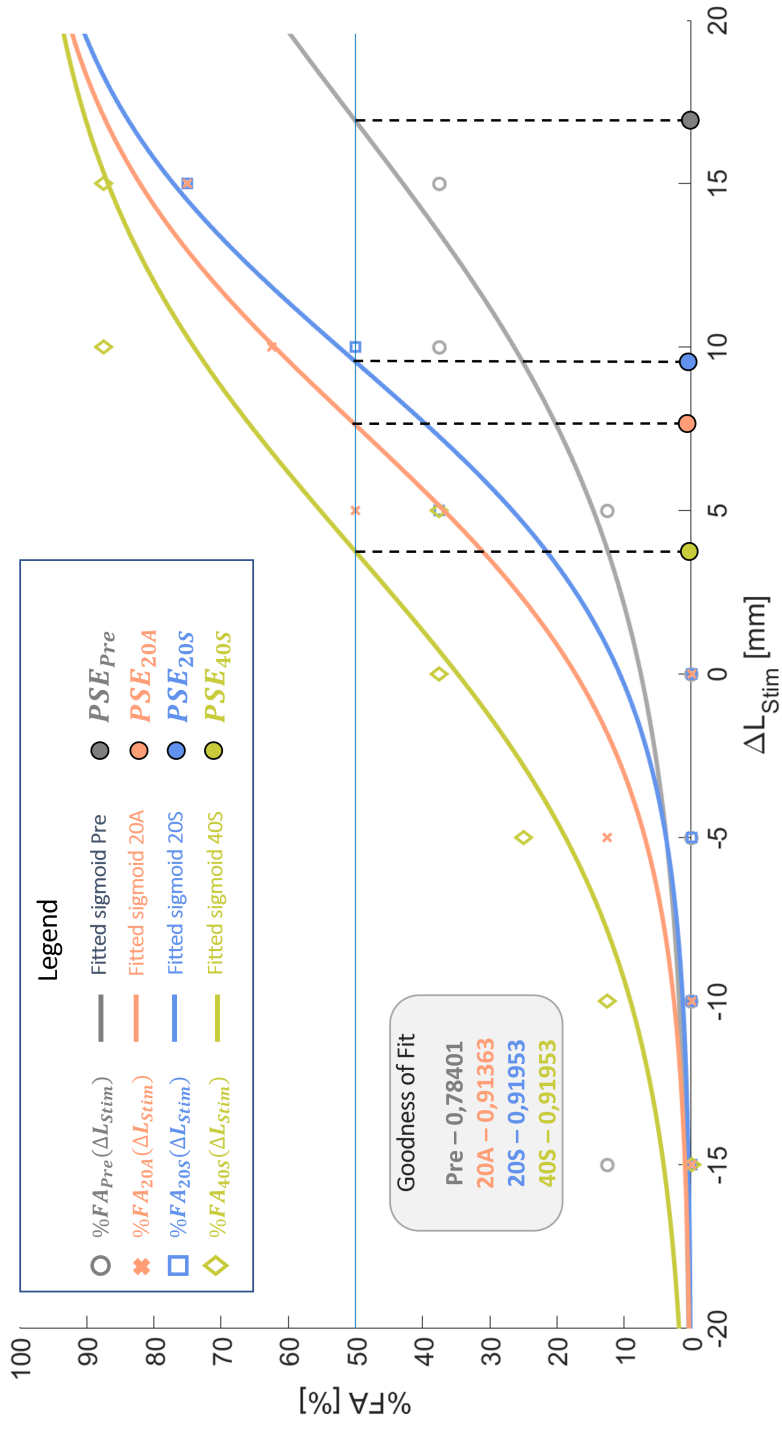

Figure 3.4: Example of a typical TDPT results plot from one participant. Raw results are the %FA in function of the ΔL. They are identified with grey empty circles (Pre), red crosses (20A), blue squares (20S), and green diamonds (40S). Continuous curves are their color-corresponding fitted sigmoid curves with their goodness-of-fit values specified in the bottom-left-hand corner. Colored circles indicate the graphical definition of the PSE.

3.2.4 Data analysis

Two separate analyses were performed. The general analysis was a within-subjects analysis (i.e., repeated measures). However, we considered the possibility that by undergoing different conditions successively without a pause between them one condition could have an influence on the successive one and that by repeating the VHI, its intensity might decrease. Therefore, to discard these possible effects from the analysis, a between-subject analysis was planned regarding only the data relative to the first condition presented to participants, thus three independent groups (of 23 subjects each) were formed depending on the first condition tested. In both analyses, the significance threshold was set to p-values lower than 0.05 for all statistical tests. Correlation analyses were performed between RHI Index and ΔPSE, between PD and ΔPSE, between RFE_{20S} and ΔPSE_{20S}, and between RFE_{40S} and ΔPSE_{40S}. For variation variables PD and ΔPSE we evaluated the significance of their difference from 0 for each condition using one-sample t-tests.

General analysis

Among all conditions, ΔPSE and PD data were distributed normally (Shapiro-Wilk test, p¿0.05) but not RHI Index data. We used pre-planned Wilcoxon's signed-rank t-tests to evaluate the effects of the VHI synchronicity (20A vs 20S) and forearm elongation (20S vs 40S) on RHI Index (Bonferroni corrected for two comparisons). We used pre-planned Student's paired t-tests to evaluate the effects of synchronicity (20A vs 20S) and elongation (20S vs 40S) on PD and ΔPSE (Bonferroni corrected for two comparisons). Difference from 0 of variation variables PD and ΔPSE were evaluated using one-sample Student t-tests. We used Student's t tests to investigate any difference of distribution in pre measures between conditions (20A vs 20S and 20S vs 40S) for the PD and ΔPSE (Bonferroni corrected for two comparisons). For correlation analysis, Spearman's ρ was calculated between RHI Index and ΔPSE, between RFE_{20S} and ΔPSE_{20S}, and between RFE_{40S} and ΔPSE_{40S} (RFE_{20S} and RFE_{40S} not normally distributed). Pearson's r was calculated between PD and ΔPSE.

First condition analysis

Among each group, all data (RHI Index, PD, ΔPSE) were normally distributed. We used pre-planned Student's unpaired t-tests to evaluate the effects of synchronicity (20A vs 20S) and elongation (20S vs 40S) on RHI

Index, PD and ΔPSE (Bonferroni corrected for two comparisons). Difference from 0 of variation variables PD and ΔPSE were evaluated using one-sample Student t-tests. We used Student's t-tests to investigate any distribution difference in pre measures between conditions for the PD and ΔPSE (Bonferroni corrected for two comparisons). For correlation analysis, Pearson's r was calculated between RHI Index and ΔPSE. Spearman's ρ (PD among all groups, RFE_{20S} and RFE_{40S} not normally distributed) was calculated between PD and ΔPSE, between RFE_{20S} and ΔPSE_{20S} and between RFE_{40S} and ΔPSE_{40S}.

3.3 Results

3.3.1 General analysis

The synchronicity effect was found significant on the RHI Index (Fig. 3.5, top-left graph). Indeed, the score of the synchronous VHI (20S) resulted significantly greater than the asynchronous control condition (20A) (t = 8.849, p<0.001). However, the elongation effect was not found significant (Fig. 3.5, top-right graph): no significant difference in RHI Index score was found between the synchronous conditions 20S vs 40S (t=0.145, p=1.000). Neither the synchronicity nor the elongation effect was found significant on PD (Fig. 3.5, middle graphs; 20S vs 20A: t=1.941, p=0.116 and 40S vs 20S: t=1.132, p=0.526). Nevertheless, PD resulted significantly greater than 0 following the synchronous conditions (20S: t=3.035, p=0.004; 40S: t=3.499, p<0.001) but not following the asynchronous one (20A: t=0.118, p=0.906) and no significant difference of PD pre-measures (pre-PM) was found neither between 20A and 20S nor between 20S and 40S (p=1.000 for both comparisons). No significant effect of synchronicity was found on ΔPSE (Fig. 3.5, bottom-left graph; 20S vs 20A: t=1.139, p=0.518), nor any significant elongation effect (Fig. 3.5, bottom-right graph; 40S vs 20S: t=-1.611, p=0.224). However, ΔPSE was found significantly lower than 0 only following the 40S condition (Fig. 3.5, bottom graphs; 20A: t=-1.717, p=0.091; 20S: t=0.316, p=0.753; 40S: t=-2.295, p=0.025) and no significant difference of ΔPSE pre-measures was found neither between 20A and 20S nor between 20S and 40S (p=1.000 for both comparisons).
No significant correlation was found between any measure (Fig. 3.6; ρ(RHI Index, ΔPSE)=-0.085, p=0.325; r(PD, ΔPSE)=-0.127, p=0.142; $\rho(RFE_{20S}$, ΔPSE_{20S})=-0.094, p=0.538; $\rho(RFE_{40S}$, ΔPSE_{40S})=-0.050, p=0.743).

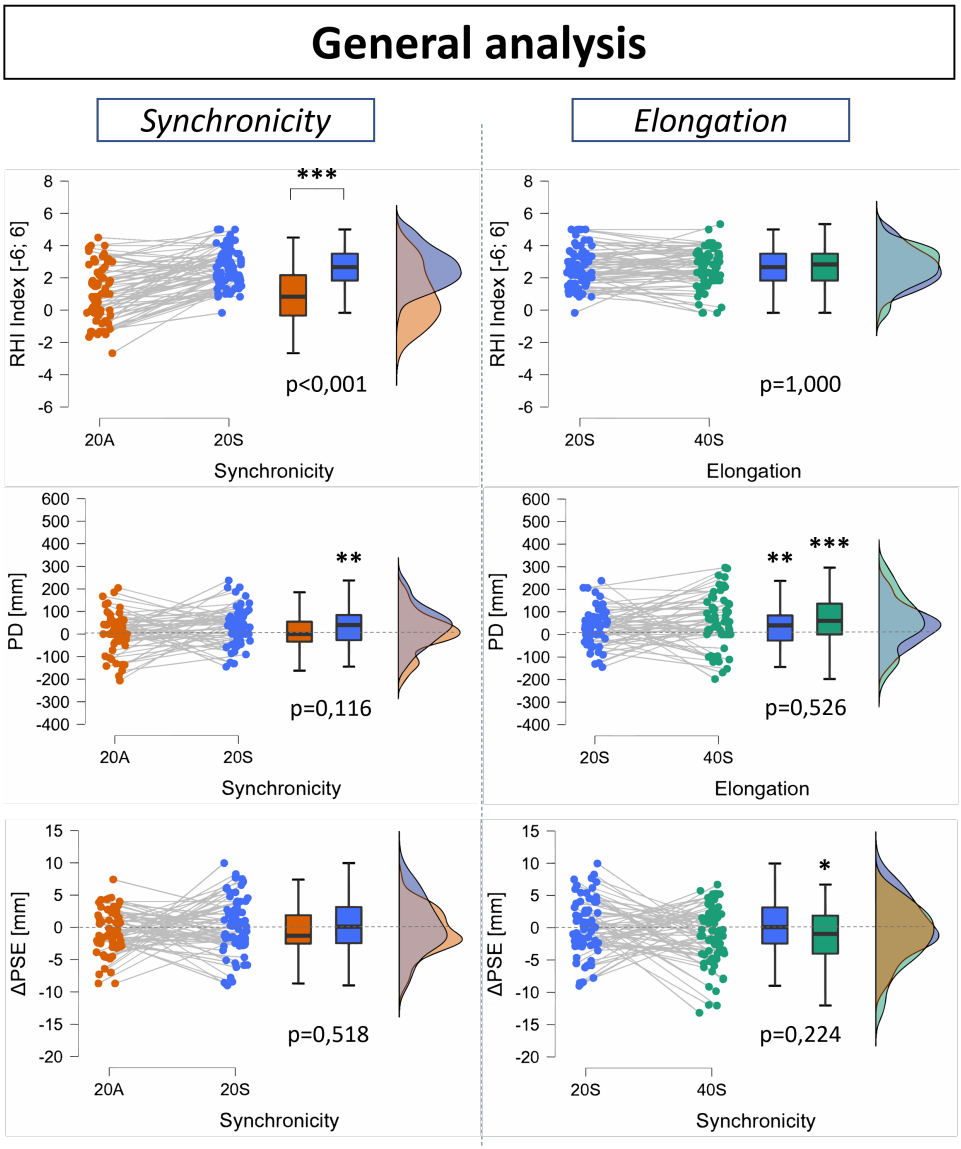

Figure 3.5: Raincloud plots showing results of the **within-subjects** analysis on the *synchronicity* effect (left) and *elongation* effect (right) on the RHI Index (top), PD (middle) and ΔPSE (bottom). Asterisks on top of brackets indicate the significance of a comparison and asterisks without brackets indicate the significance of a difference from 0. For each graph the displayed p-value is the p-value of the statistical test between the compared conditions.

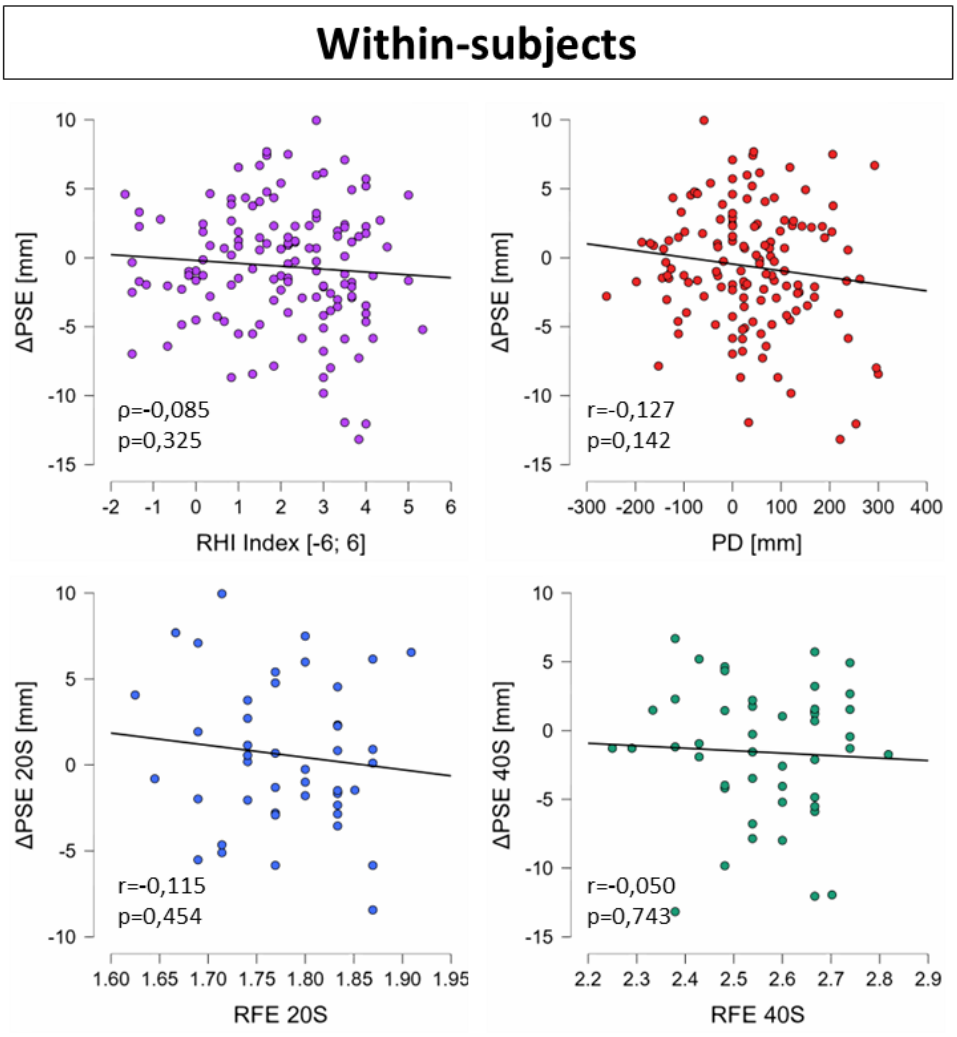

Figure 3.6: Correlations plots of the **within-subjects** analysis: RHI Index and ΔPSE (top left), PD and ΔPSE (top right), RFE_{20S} and ΔPSE_{20S} (bottom left), and RFE_{40S} and ΔPSE_{40S} (bottom right).

3.3.2 First condition analysis

The synchronicity effect was found significant on the RHI Index (Fig. 3.7, top-left graph). Indeed, the score of the synchronous VHI resulted significantly greater than the asynchronous control condition (20S vs 20A: t=3.473, p=0.002). However, no significant effect of elongation was found on the RHI Index (Fig. 3.7, top-right graph; 20S vs 40S: t=0.606, p=1.000).
No significant difference between conditions was found in the Pre PM (20S vs 20A: t=0.004, p=1.000 and 40S vs 20S: t=1.063, p=0.588) and all conditions were found to elicit a significant PD (Fig. 3.7, middle line graphs; 20A: t=2.737, p=0.012; 20S: t=3.547, p=0.002; 40S: t=3.116, p=0.005). However, no significant effect of synchronicity nor elongation was found on PD (20S vs 20A: t=0.770, p=0.892; 40S vs 20S: t=-0.999, p=0.646).
No significant difference in Pre PSE was found between conditions (20S vs 20A: t=1.463, p=0.302) nor between 40S and 20S (t=1.029, p=0.620). All conditions were found to elicit a ΔPSE significantly lower than 0 (Fig. 3.7, bottom line graphs; 20A: t=-2.608, p=0.016; 20S: t=-2.288, p=0.033; 40S: t=-6.232, p<0.001). No significant effect on synchronicity was found on ΔPSE (20S vs 20A: t=0.096, p=1.000), but the elongation effect proved significant (40S vs 20S: t=-2.551, p=0.030).
The correlation between RHI Index and ΔPSE was found close to significance (Fig. 3.8, left graph; r=-0.225, p=0.069) but no significant correlation between any measure was found (ρ(PD,ΔPSE)=0.116, p=0.353; $\rho(RFE_{20S},\Delta PSE_{20S})$=-0.229, p=0.331; $\rho(RFE_{40S},\Delta PSE_{40S})$=-0.374, p=0.104).

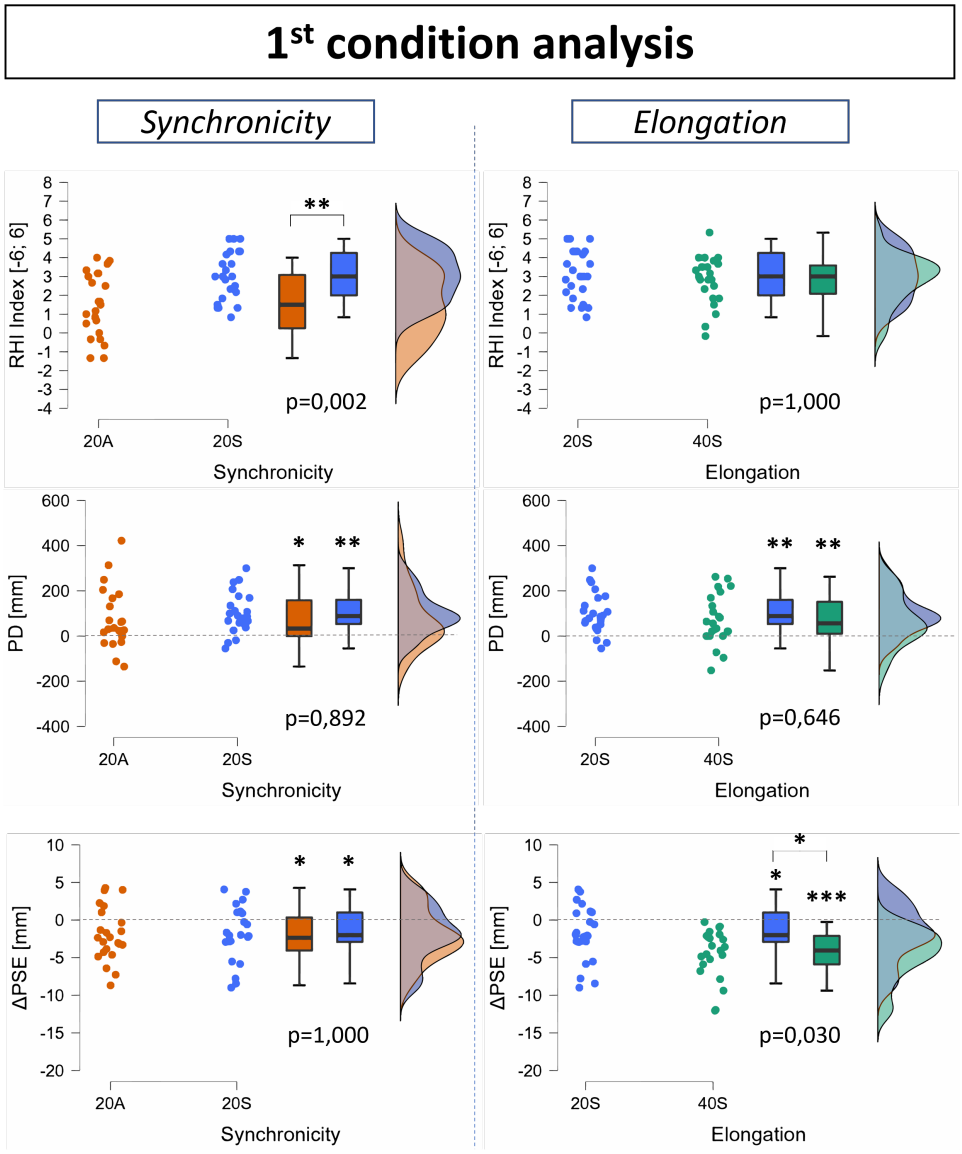

Figure 3.7: Raincloud plots showing results of the **between-subjects** analysis on the *synchronicity* effect (left) and *elongation* effect (right) on the RHI Index (top), PD (middle) and ΔPSE (bottom). Asterisks on top of a bracket indicate the significance of a comparison and asterisks without bracket indicate the significance of a difference from 0. For each graph the displayed p-value is the p-value of the statistical test between the compared conditions.

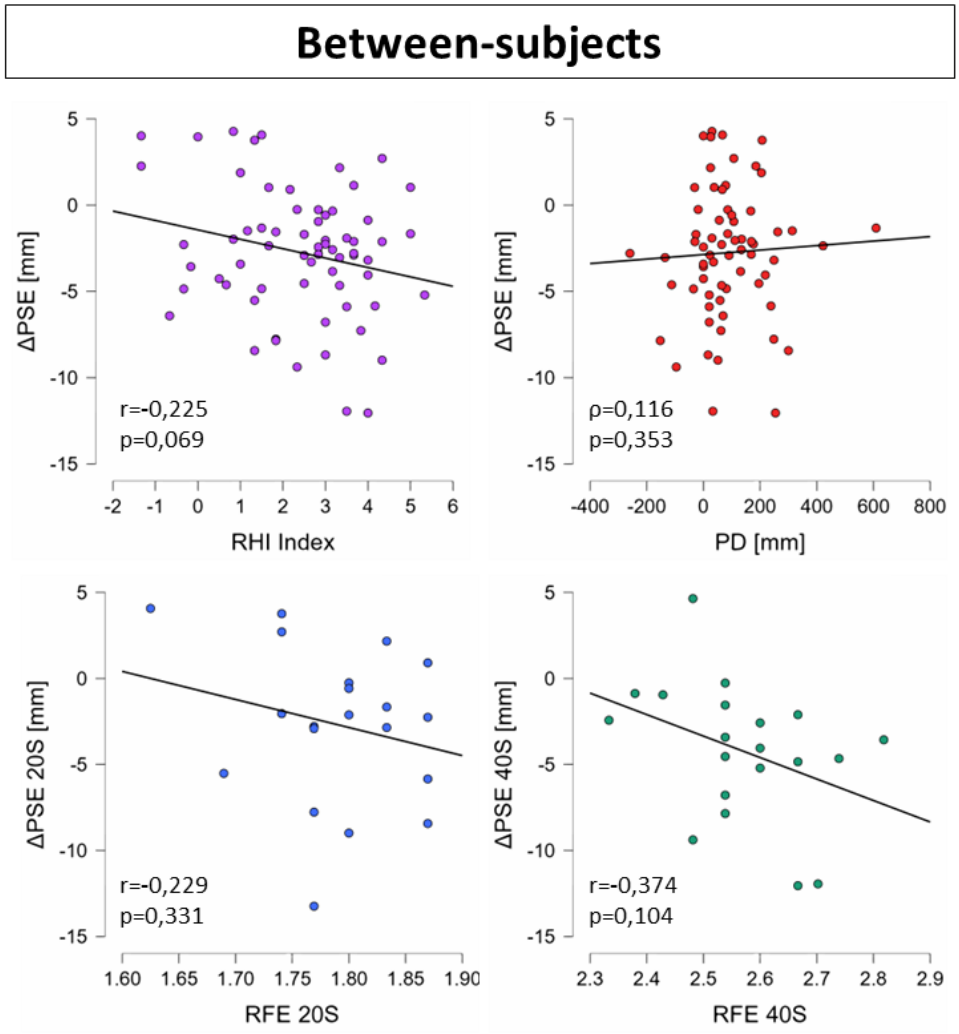

Figure 3.8: Correlations plots of the **between-subjects** analysis: RHI Index and ΔPSE (top left), PD and ΔPSE (top right), RFE_{20S} and ΔPSE_{20S} (bottom left), and RFE_{40S} and ΔPSE_{40S} (bottom right).

3.4 Discussion

The aim of the study was to understand whether the change in TDP following a bodily illusion demonstrated by previous studies [114, 116] could be achieved through embodiment over a fake limb. We used a VHI paradigm with an elongated forearm in a 1PP virtual environment to induce the bodily illusion of owning an elongated forearm and assessed the resulting change in TDP using a TDPT. The experimental protocol exposed participants to synchronous VHI with two different forearm elongations and to an asynchronous VHI as a control condition. In this novel study, we attempted to establish a link between embodiment and TDP. The embodiment illusion proved effective, as participants perceived a significantly higher level of ownership (from the RHI Index in both analyses) after a synchronous VHI compared to an asynchronous condition. Our experiment confirms previous findings on the effectiveness of virtual reality together with synchronous visuo-tactile stimulation in eliciting ownership over a virtual limb [89, 120]. It also confirms previous results showing that it is possible to embody a fake hand placed farther than the real one along the distal plane in a RHI or VHI paradigm [41, 88, 97]. The first condition analysis on PD revealed that participants perceived a significant proprioceptive drift of the position of their real hand towards the position of the virtual hand at the end of the virtual forearm after all VHI conditions, even the asynchronous one (PD significantly greater than 0 for all conditions), without a significant effect of synchronicity. Those results come in line with previous studies ([121] in a real environment, [90] in VR) which suggests a dissociation between ownership due to congruent visuo-tactile integration and proprioceptive drift (also introduced by [36]), the latter likely to be led by visuo-proprioception [92]. Nevertheless, Rhode and colleagues further detailed that long asynchronous stimulation (i.e 120s) prevents the proprioceptive drift. On the contrary, we found PD to be robust to asynchronous stimulation (PD value significantly higher than 0 and no significant difference between asynchronous and synchronous conditions in the first condition analysis). Our stimulation was slightly shorter (i.e. 90s); however, we did not consider that such limited difference in stimulation duration (i.e., 30s) could affect the outcome. We suggest here that the robustness of the PD is due to the strength of the visuo-proprioceptive integration in the case of a VHI in an 1PP immersive virtual reality, which corroborates the findings of Perez-Marcos and colleagues [122]. However, it is also worth to say that such PD significantly greater than 0 in asynchronous condition could be due also by the differences among groups of participants in providing the proprioceptive measure. Indeed, considering the results of the within-subjects

general analysis where is expected a limitation of this effect, we observe a PD significantly greater than 0 only for the synchronous conditions. Although no significant difference was found among conditions, this finding in general analysis seems to suggest an effect of synchronicity on PD. We could, hence, hypothesize that even if visuo-tactile synchronicity is not the leading effect in the manifestation of PD in VHI, it might nevertheless enhance it. The first condition analysis on ΔPSE proved that participants perceived an increase in TDP on the forearm after all elongated VHI conditions and the effect of the virtual forearm elongation on the TDP was confirmed (ΔPSE due to 40S significantly lower than ΔPSE due to 20S). Although no significant effect of elongation was found between the two synchronous conditions in the general analysis, the fact that only the 40S condition elicited a significant increase in TDP (ΔPSE due to 40S significantly lower than 0) was highlighted, confirming the findings of first condition analysis. However, in general, none of the analyses showed an effect of synchronicity of the VHI on the modification of the TDP. Therefore, the presence of the elongation effect in the absence of a significant synchronicity effect, combined with the absence of correlation between RHI Index and ΔPSE in both analyses suggests that the modification of the TDP is dissociated from the elicited embodiment of the virtual hand by the VHI paradigm. Still, elongation of a virtual forearm perceived in a virtual environment here proves to effectively increase the TDP on the corresponding real forearm. In line with the change in TDP caused by the visual modification of body proportions performed with lenses by Taylor-Clarke and colleagues [114], we suggest here that the increase of TDP results at least from the visual experience of the virtual body, thus that visual feedback plays the main role in the modification of the body schema whereas congruent visuo-tactile feedback leading to ownership here appears irrelevant. This is also partly in line with another study where a change in the visually perceived sizes of objects was found after participants experienced in 1PP VR vision and agency over a virtual hand of modified dimensions without any form of congruent visuo-tactile stimulation [123]. Nevertheless, it is possible that the observed modification of TDP might still be linked to the embodiment of the virtual body since ownership over a virtual body can be elicited solely by vision in the case of an immersive 1PP experience [124–128]. However, no measure taken in our study can attest the veracity of this hypothesis. It must be mentioned that one limit of this study is the lack of a break between the conditions underwent by participants. Indeed, participants underwent all conditions successively without removing the headset nor moving their left arm. Therefore, no proper "reset" of the experimental conditions took place between the different conditions, and

thus the effects of one condition on ownership and body schema modification might have been transferred to the successive condition. This issue can affect the results of the general analysis but not of the first condition analysis, giving a greater relevance to the analysis of the first condition results despite an a priori greater standard deviation in the data with respect to the general analysis (due to inter-subjects variability). Furthermore, it has been demonstrated in a classical RHI that ownership over the fake hand has decreased five minutes after the end of the visuo-tactile stimulation [129]. In our experimental protocol, the TDPT lasts around ten minutes and is performed before participants answer the questionnaire. It is therefore likely that the ownership data we registered are underestimated for the synchronous conditions with respect to the direct post-illusion feeling of ownership. This underestimation of the RHI Index would not question the highlighted effect of synchronicity on ownership, which is present nevertheless, but it might have affected the correlation results between the RHI Index and the ΔPSE. Finally, PD has been previously presented as a measure of the body schema [2, 130–132]. The presence of a significant effect of elongation on the variation of the TDP in the absence of one on the PD, coupled to the absence of significant correlation between ΔPSE and PD suggests that the assessment of the TDP (i.e., exteroception) is more sensitive measurement than the PD metric (i.e., proprioception) to measure a modification of the body schema involving a change of the perceived dimensions of a limb.

3.5 Conclusion

In our everyday life, we interact with the environment using our body to sense. Like any sensor, our perception requires specific reference frames to measure parameters accurately. For instance, to perceive tactile distances we rescale our perception based on the currently perceived dimensions of the touched body part. It is believed that rescaling process involves the implicit model of the metric properties of our body constructed by the brain: the body schema. Several studies have proven the latter by modifying the body schema of participants through own body size modifications illusions and observing a correlated modification of the TDP. However, to our knowledge none had investigated it following a modification of the body schema through the embodiment of an artificial (i.e virtual) body part. In this study we investigated the effects on TDP of an embodied virtual elongated forearm. Even though we found an increase of the TDP positively associated to the virtual forearm elongation, no link has been found between the perceived

embodiment over the virtually elongated arm resulting from the VHI and the perceived augmentation of the TDP, suggesting that the alteration of the body schema has taken place mainly through 1PP visual feedback over the elongated body part.

Chapter 4

A Novel Platform for Robot-Aided Transcranial Magnetic Stimulation

4.1 Introduction

TMS functioning as well as its applications have been introduced in Chapter 1. TMS is usually carried out by an expert operator who manually holds the coil on the subjects scalp [133]. However, the weight of coils coupled with the duration of TMS sessions both in clinical and research environments can make it difficult for operators to maintain the required position and orientation for an accurate stimulation. Errors in position and orientation can greatly decrease the resulting intensity and location of the stimulation [134–137], thus compromising the efficacy of the treatment or the reproducibility of the research study. Therefore, neuronavigation systems guiding in real-time TMS operators in the correct placement of the coil on the subject's scalp have emerged and are now widely used [138]. They mainly consist in a computer vision software coupling a stereotaxic system with a 3D model of the brain and scalp correlating geometrical data of the subject's scalp with their personal or average magnetic resonance imaging (MRI) [139]. Nevertheless, despite the significant help of neuronavigation in stimulation accuracy, the latter still remains dependent on operator variability [140]. To tackle this issue, a wide range of robot-aided TMS systems have been proposed [141–146]. Besides improving accuracy, repeatability and reproducibility of the stimulation, they can also improve patients and operators' comfort and compensate for patients' head movements. Although, a few commercial systems are already

available [147–149], their cost and their "black box" characteristic are their main drawbacks. It is indeed impossible to implement additional custom protocols for calibration, placement of the coil and stimulation, and the lack of a common standardized use procedure make it difficult to compare and reproduce results from different studies using robot-aided TMS. A first semi-custom neuronavigated robot-aided TMS platform was formerly developed. The system consisted in a seven degrees-of-freedom (dof) robot (Panda, Franka Emika GmbH) holding a TMS coil, an infrared camera (Polaris Vicra, Northern Digital Inc.) tracking the movement of the head of the subject wearing optical markers, and an commercial neuronavigation software (E.M.S srl). This preliminary platform enabled to develop a novel hand-eye and robot-world calibration methodology and control approach, and to successfully validate them by showing a better performance of the robotic system in coil positioning than a human expert operator [150, 151]. The platform however presented two main drawbacks. The first one being the neuronavigator, a commercial software that despite its efficacy, was not open-source which thus prevented the access to some data and denied the possibility to add any other functionality. The second drawback was the sampling frequency of the infrared cameras ($20Hz$) which was too low to generate a smooth trajectory for the robot to follow while minimizing its latency and end-effector jerk. We thus developed a novel platform using more efficient yet cheaper infrared cameras and an open-source neuronavigation software based on which we developed new functionalities. Besides, by improving the real-time compensation of head movements of the robotic TMS platform, we would also open the way to new experimental possibilities required for the embodiment platform such as transcranial magnetic stimulation during a task requiring movement of the subject.

4.2 Development

4.2.1 Platform description

The platform maintains the TMS coil in the desired pose on the subject's head by tracking and compensating for the subject's head movement in real-time. The robotic manipulator used in the platform is a 7-dof manipulator (Panda, Franka Emika GmbH) that holds a TMS coil (D70 Alpha Coil, figure of eight, Magstim Co Ltd) on its end-effector thanks to a 3D-printed adaptor. The robot is equipped with torque sensors in each joint and its controller runs at a frequency of $1kHz$. The motion tracking is performed thanks to two Optitrack 13W infrared cameras (NaturalPoint Inc.) that track the

position of reflective optical markers. The cameras' sampling frequency is set at their maximum i.e $240Hz$. Our neuronavigator is based on the open-source neuronavigator NeuRRonav [152] developed by the NeuRRo Lab of the University of Michigan Medical School with the game engine Unity in C# language. The NeuRRonav software had been developed with an older version of Unity (Unity 5.4.1f.1). However, with the scope of unifying several Unity projects into one in the future, it has been decided to work with a more recent version of Unity, with which we were already working for other projects (see section 2.2). Thus, the first step of the customization of the software has been to fix its compatibility issues with our more recent versions of Unity (Version 2018.3.3f1).

4.2.2 Communication

The Optitrack cameras track the position of the optical markers attached on rigid bodies (one strapped on the subject's head, the other one attached to the TMS coil). Thanks to ethernet cables, the cameras are connected to and powered by a Power-over-Ethernet (PoE) switch (Netgear Inc.) in turn connected to a Windows computer. The data captured by the cameras are live-streamed to the Optitrack Motive software (version 2.1.1 Final, running on the Windows PC) which computes in real-time the position and orientation (pose) of the rigid bodies based on the position of their optical markers. Rigid bodies' pose information is then live-streamed to the neuronavigation software in Unity, also running on the Windows PC, thanks to the Optitrack plug-in for Unity (Unity Plugin, version 1.1.0). It embeds a NatNet client/server networking protocol for real-time communication using UDP. The robot control application we have developed has been programmed in C++ language using Qt libraries and runs on a Linux computer (running OS Ubuntu 16.04 LTS). To live-stream the relevant information (poses of the head and selected hotspot for stimulation) from the neuronavigator to the robot control application, we developed a UDP communication between both computers. We developed the sender part of the UDP in C# on the neuronavigator and the receiver part in C++ on the robot control application. Finally, output torque commands coming from the robot control application are sent to the robot controller through TCP/IP.

4.2.3 Neuronavigation & Calibration protocol

The neuronavigation software NeuRRonav is a graphical user interface integrating motion capture that enables to visualize on a computer screen the

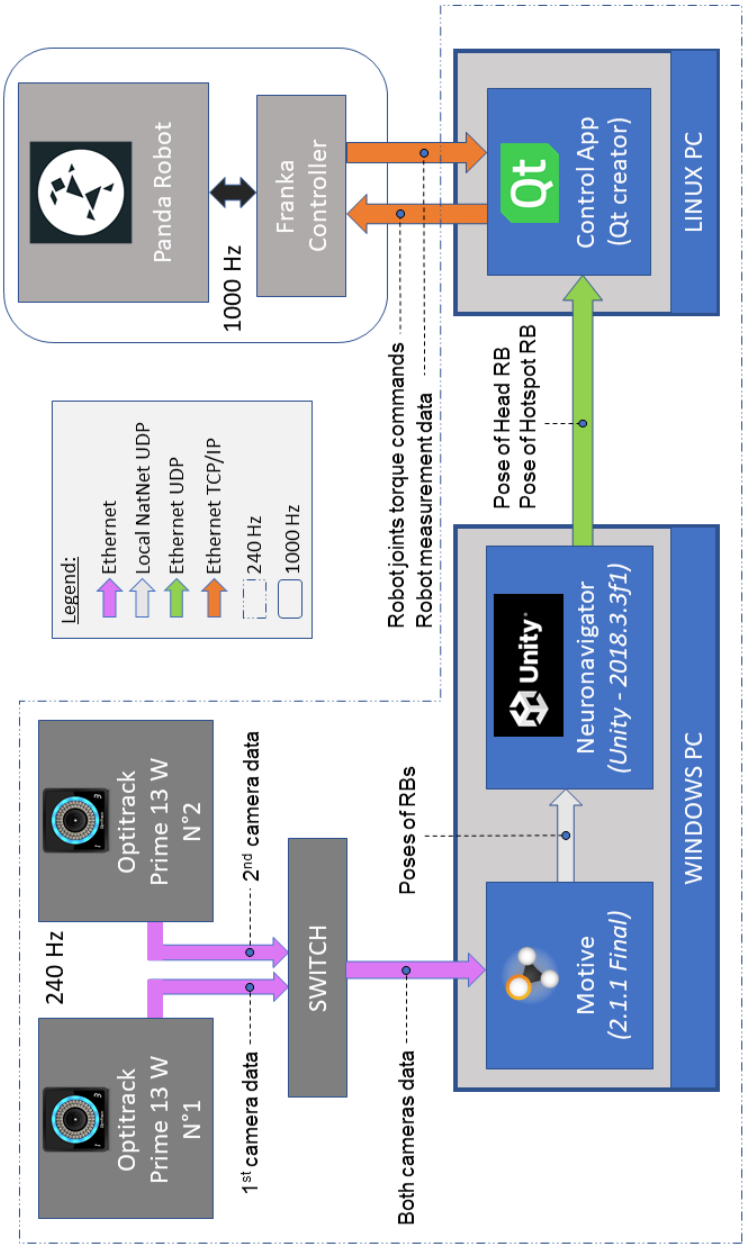

Figure 4.1: Communications and data flow within the robot-aided TMS platform.

virtual model of the subject's head and of the TMS coil as well as their respective poses in the workspace.

Four real tools equipped with motion tracking optical makers are used with the neuronavigation software: a calibration tool, a stylus, a head marker and a coil marker. The first step consists in calibrating the stylus length into the neuronavigator by placing its tip at the center of the calibration tool. By doing so the motion tracking system communicates to the neuronavigation software the orientation and length of the stylus' rod with respect to the optical markers placed on its handle. With this information the neuronavigator can recreate the exact virtual model of the stylus and replicate in real time its position and orientation (pose) in the virtual environment. The next step consists in calibrating the virtual model of the TMS coil. To do so, we place the tip of the stylus at the center, top and right extremities of the coil's stimulation surface. The neuronavigator uses these points to create the coil's virtual model and to define its pose with respect to the pose of the real coil's marker so that the neuronavigator can replicate in real time the movement of the real coil on the virtual one. One this is done, we can perform the the robot-cameras reference frames calibration following the methodology presented in [151]. The final step of the calibration consists in creating the virtual model of the subject's head. To do so, we attach firmly the head marker on the subject's forehead, then we successively place the tip of the stylus on five fiducial points of the subject's head (inion, right tragus, left tragus, nasion, vertex). By doing so, we communicate the relative position of the fiducial points with respect to the head marker to the software which then fits a generic virtual head model to the subject's head proportions. The pose of the subject's virtual head then follows the pose of the subject's real head in real time.

Once the calibration is finished, we can start creating the stimulation hotspots. The TMS operator manually moves the robot (controlled in a transparent mode at that moment) in order to place the stimulation surface of the coil on the subject's head and starts looking for the hotspot. Once it has been found, the corresponding pose of the coil (center point, also called focus) with respect to the subject's head is saved and an arrow-shaped virtual object pointing towards the hotspot is created at the corresponding pose in the neuronavigator. It is possible to create as many hotspots as it is desired and the hotspot whose pose has to be streamed to the robot control can be selected by clicking on it in the neuronavigator.

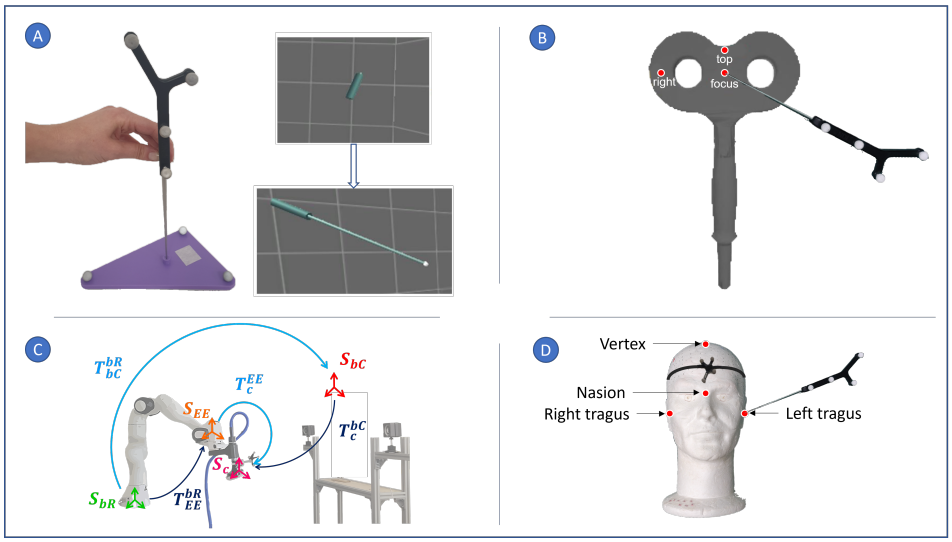

Figure 4.2: Robot-aided TMS platform calibration steps. **Panel A**: Stylus Calibration. **Panel B**: Coil calibration with coil (seen from below), calibration points and stylus on focus point. **Panel C**: Robot-cameras calibration. See [151] for details about the calibration process. **Panel D**: Head model calibration with stylus on left tragus and head marker on subject's forehead.

4.3 Validation and comparison of control approaches

4.3.1 Rationale

On the developed platform presented in section 4.2 we implemented and compared three different control approaches for the head motion compensation (homogeneous and selective impedance controls and hybrid force-position control), testing their performance during head movements both in term of contact force and tracking accuracy. The possibility to administer TMS while subjects perform tasks or even walk may indeed open-up new horizons in neuroscience. However, while following head's movement, robotic systems must limit interaction forces guaranteeing patients' safety. Hence the relevance of the control evaluation not only in term of accuracy but also in term of physical interaction. To simulate simple (translations and rotations) and complex head movements (head oscillations during walking on a treadmill), we employed another robot to move a dummy head, assessing

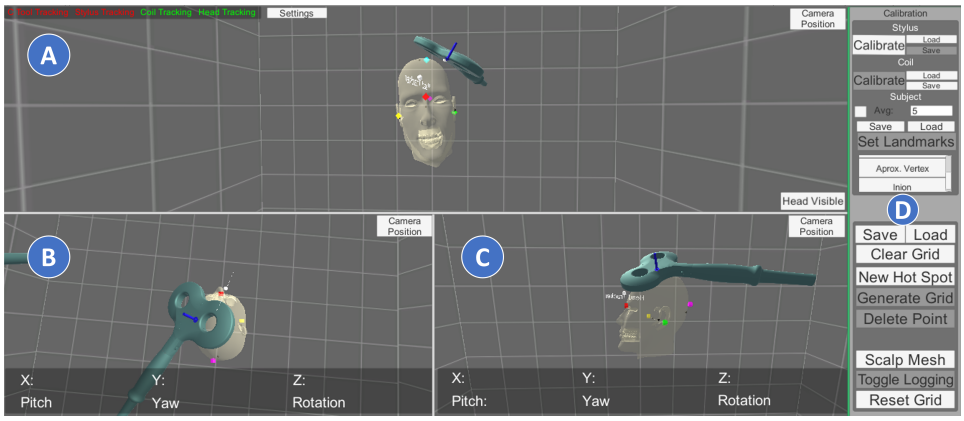

Figure 4.3: NeuRRonav software grahical user interface after calibration. **Panel A**: front view of the head model with fiducials points (colored cubes), and coil on hotspot (blue arrow). **Panel B**: top-view. **Panel C**: left-side-view. **Panel D**: Buttons canvas.

the performance of the TMS platform both in static and dynamic conditions. For this study, we used a second Panda manipulator, hereafter called "support robot", placed at 1m distance from the TMS robot, and holding the mock-up head to simulate human movements. Simple movements of the head have been implemented on the Franka Emika Desk web application, whereas more complex head movement such as walking simulation, have been implemented in a secondary control application (using C++ language and Qt libraries). The complete platform of this study together with the reference frames of the coil and support robot are display on Fig. 4.4.

4.3.2 Control approaches

Control algorithm of the TMS robot aims to move the coil on the scalp and to keep it on the hotspot maintaining a correct position and orientation while compensating for head movements. Besides pose tracking to ensure high stimulation accuracy, the system must guarantee subjects' safety. For this reason contact forces at the coil need to be limited.
We implemented three different control approaches: i) impedance control with homogeneous impedance; ii) impedance control with selective impedance; iii) hybrid position-force control.

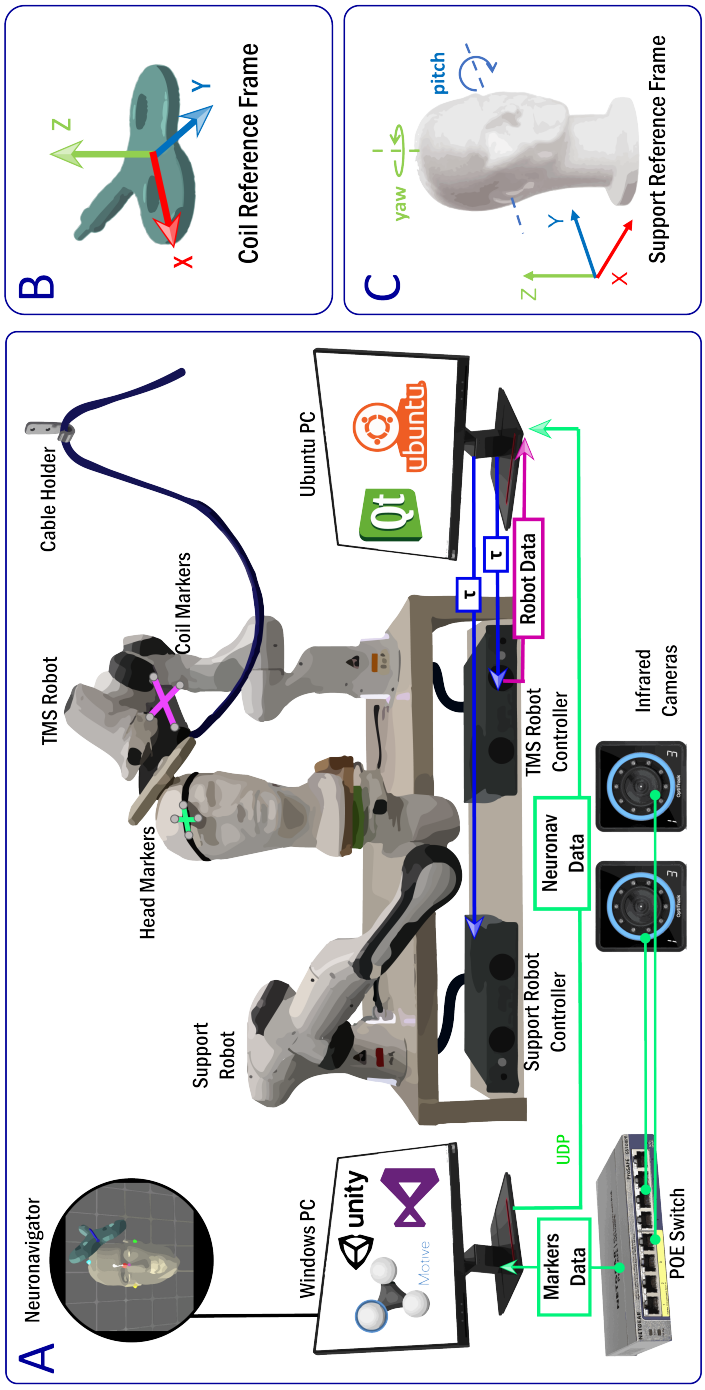

Figure 4.4: **Panel A**: Experimental setup. **Panel B**: Coil reference frame with z axis along the stimulation direction and x and y axis defining the stimulation plane on which the position error is computed. Coil frame is centered in the focal point of the magnetic stimulation field, at the centre of the two wings. **Panel C**: Support reference frame used to define directions of translation and rotation of the head.

Impedance control

Impedance control allows to maintain the coil on the hotspot, without direct regulation of the contact force but adjusting the impedance between the robot and the environment [153]. Commanded joint torques are computed according to the following equation:

$$\tau = J^T[K(x_d - x) - D(J\dot{q})] + C\dot{q} + G \tag{4.1}$$

with τ being the 7x1 joint torque vector and J the 6x7 Jacobian relative to the robot base frame; x_d and x the desired and current end-effector pose in the cartesian space with respect to the robot base frame and expressed as 6x1 vectors. $\dot{q}$ is the 7x1 joint velocities vector. K and D are respectively the stiffness and damping 6x6 matrices. C is the contribution of the centrifugal and Coriolis forces and finally G is the 7x1 gravity forces vector.
Furher details on the definition of x_d relative to the stimulation target can be found in [151].

Homogeneous impedance

In the first approach, the impedance is homogeneous i.e the same on every axes of the coil reference frame. K and D result in:

$$K_{homogeneous} = diag(K_t, K_t, K_t, K_r, K_r, K_r)$$
$$D_{homogeneous} = diag(D_t, D_t, D_t, D_r, D_r, D_r) \tag{4.2}$$

where x, y and z axes of the impedance matrices refer to the coil reference frame as shown in Fig. 4.4 B. In the present study $K_t = 2500$ N/m, $K_r = 50$ N/rad, $D_t = \sqrt{K_t}$ Ns/m and $D_r = \sqrt{K_r}$ Ns/rad. The implemented code for this approach is available at https://github.com/ANoccaro/Robot-aidedTMS.

Selective impedance

The second approach employs a heterogeneous impedance, selectively reducing its value only along the stimulation direction, i.e. the direction of contact with the scalp. Such selective impedance aims to increase the safety and comfort (compliance coil behavior towards the head) while maintaining high accuracy in the coil positioning (stiff behavior in orientation and position on the stimulation plane). Thus the diagonal stiffness and damping matrices

become:

$$K_{selective} = diag(K_t, K_t, K_z, K_r, K_r, K_r)$$
$$D_{selective} = diag(D_t, D_t, D_z, D_r, D_r, D_r) \quad (4.3)$$

with $K_z < K_t$, being z the stimulation direction relative to the coil reference frame (Fig. 4.4 B). In the experimental validation the following values were employed: $K_t = 2500$ N/m, $K_z = 1500$ N/m, $K_r = 50$ N/rad, $D_{t|z} = \sqrt{K_{t|z}}$ Ns/m and $D_r = \sqrt{K_r}$ Ns/rad.

Hybrid force-position control

The hybrid force-position approach decomposes the task space into unconstrained directions along which the system is controlled in position and constrained directions in which it is controlled in force [154], [155]. Position control is usually used to accurately place the coil on the target area, compensating for head movements, while force control is designed to regulate the force applied along the normal direction of the scalp [143]. To avoid stability problems of the force control during clear non-contact situations we first move the coil on the desired position with the homogeneous impedance control described earlier. Once the robot has reached the desired position on the scalp, it switches to the hybrid force-position control. We chose a 5 N commanded force to be applied by the robot as a compromise between the necessary force for accurate positioning and forces applied by conventional hand-held TMS procedures [156].
The hybrid control commands the torques of each joint according the following equation:

$$\tau = J^T[\Omega(K(x_d - x) - D(J\dot{q})) + \overline{\Omega}(F_d + K_f(F_d - F_s) - K_{vf}(J\dot{q})) + C\dot{q} + G \quad (4.4)$$

where Ω and $\overline{\Omega}$ select the directions along which the robot is controlled in position (XY plane in the coil reference frame as depicted in Fig. 4.4 B) and in force (the Z axis) and are defined as follows:

$$\Omega = \begin{bmatrix} R_c S_t {}^bR_c^T & 0 \\ 0 & {}^bR_c S_r {}^bR_c^T \end{bmatrix};$$
$$\overline{\Omega} = \begin{bmatrix} {}^bR_c(I - S_t){}^bR_c^T & 0 \\ 0 & {}^bR_c(I - S_r){}^bR_c^T \end{bmatrix} \quad (4.5)$$

with ${}^{b}R_c$ the rotation matrix from the robot base to the coil reference frame, I the identity matrix and S_t and S_r respectively the 3x3 translation and rotation selective matrix expressed in the coil reference frame (Fig. 4.4 B). In particular $S_t = diag(1, 1, 0)$ and $S_r = diag(1, 1, 1)$, with non-zero elements on the direction to be controlled in position and zero elements on the directions to be controlled in force.
Referring to Eq. 4.4, F_d and F_s are respectively the desired force and the current 6x1 force vector at the coil reference frame expressed with respect to the robot base frame; F_s is estimated using the FCI libraries and measures of the torque sensors embedded into each robot joint. $K_f = 0.9$ and $K_{vf} = 0.2$ Ns/m represent respectively the force control gain and the damping along the force controlled direction.

F_d is defined as follows:

$$F_d = Ad^T \cdot {}^{coil}F_d \tag{4.6}$$

with ${}^{coil}F_d = [0, 0, 5, 0, 0, 0]^T$ N the desired force with respect to the coil frame and Ad the adjoint matrix needed to express the desired interaction at the coil with respect to the base reference frame. Ad is defined as:

$$Ad = \begin{bmatrix} {}^{coil}R_b & \hat{p} \cdot {}^{coil}R_b \\ 0 & {}^{coil}R_b \end{bmatrix} \tag{4.7}$$

with ${}^{coil}R_b$ and p being respectively the rotation matrix from the coil reference frame to the robot base reference frame and the position vector of the robot base reference frame expressed in the coil frame. $\hat{p}$ and p are defined as follows:

$$\hat{p} = \begin{bmatrix} 0 & -p_3 & p_2 \\ p_3 & 0 & -p_1 \\ -p_2 & p_1 & 0 \end{bmatrix} ; \; p = \begin{bmatrix} p_1 \\ p_2 \\ p_3 \end{bmatrix} \tag{4.8}$$

4.3.3 Experimental protocol

The three control approaches were tested and evaluated simulating first simple head translations and rotations and then simulating head movements while walking on a treadmill.

Translations The support robot moved the dummy head along each axis -one at a time- of the support frame (Fig. 4.4 C), here also corresponding to the support robot base frame), performing a series of 5 translations always

starting from the same point. Control algorithms were tested for translation distances of 10 mm, 20 mm and 30 mm in both positive and negative directions, each one for velocities of 0.2 m/s and 0.5 m/s, for a total of 36 different series of movement [157].

Rotations A second test was performed for head rotation, from 0° to 30°, simulating head pitch (Fig. 4.4 C), i.e. the "yes" movement. Five series of rotations were performed at velocities of $9°/s$ and $18°/s$ for a total of 6 different series of movements. Each series of movements, both for translations and rotations, is composed of 10 movements (5 back and forth) separated in time by a 2 s pause during which the head remained still.

Walking on treadmill A third dynamical test was conducted simulating the head movement of of a person walking on a treadmill [158]. The support robot was commanded so that the dummy head would follow a sinusoidal-like trajectory defined by the following equations:

$$z_h(t) = z_h(0) + A_z sin(2\pi f_t t) \tag{4.9}$$

$$R_h(t) = R_h(0) R_y(t) \tag{4.10}$$

with z_h and R_h the vertical position and orientation of the dummy head with respect to the support base frame (Fig. 4.4 C). $z_h(0)$ and $R_h(0)$ represent values at time $t = 0$, whereas R_y is the elementary rotation matrix around the y axis, here corresponding to the pitch direction, and computed as follows:

$$R_y = \begin{bmatrix} cos\theta & 0 & sin\theta \\ 0 & 1 & 0 \\ -sin\theta & 0 & cos\theta \end{bmatrix} \tag{4.11}$$

$$\theta(t) = A_\theta sin(2\pi f_\theta t) \tag{4.12}$$

To simulate walking with slow velocity (0.6 m/s) the translation and pitch amplitude were respectively set to $A_t = 10\ mm$ and $A_\theta = 2°$; while the frequency of vertical movements and pitch rotations were respectively set to $f_t = 1\ Hz$ and $f_\theta = 1\ Hz$ [158].

4.3.4 Data Analysis

Performance were evaluated both in static and dynamic conditions, i.e. relatively to the achieved values of the investigated metrics at the end of the

head movement and during actual head motion, respectively. The following measures were used:

- Position (E_{xy}: cartesian norm on the stimulation plane, E_z: error along the stimulation axis) and orientation (E_ϕ: norm in the SO(3) space) error of the coil with respect to the selected target both in static and dynamic conditions;
- Initial latency (L_{start}): the time interval between the start of head movement and the start of coil movement, to understand how quickly the system tracks head movement;
- Settling time (L_{end}), considering the time interval between the end of the head movement and the end of the coil movement to analyze the settling time of the robotic control system;
- Interaction forces F_z between the stimulation coil and the mock-up head.

For the translation movements, performance were compared using a two-way Kruskal-Wallis test (after having evaluated the non-normal distributions with Shapiro-Wilk test) with control approach and direction of movement as factors. Post-Hoc analysis was conducted using Mann-Whitney test with Bonferroni correction. Performance comparison among the three controls during head rotations and simulated walking was conducted with a one-way ANOVA, except for the contact force values analyzed with a one-way Kruskal-Wallis test and a Bonferroni corrected Mann-Whitney post-hoc test.

4.3.5 Results

Tracking errors and interaction forces, for head translation movements, did not show significant differences along directions of movement or velocities of the head. Thus we reported only the comparison between control algorithms regardless to the direction or velocity of the head translation. In static conditions (i.e. at the end of head movements), errors in coil positioning on the stimulation plane and in orientation are comparable between the homogeneous ($E_{XY} = 0.003 \pm 0.001\ m$, $E_\phi = 1.56 \pm 0.5°$) and selective ($E_{XY} = 0.003 \pm 0.0008\ m$, $E_\phi = 1.64 \pm 0.46°$) impedance controls, and lower ($p < 0.001$) for the hybrid control ($E_{XY} = 0.0027 \pm 0.0008 m$, $E_\phi = 1.07 \pm 0.5°$) (Fig. 4.5 A-B). In term of distance from the target along the stimulation direction, homogeneous impedance control shows the highest error and widest distribution ($E_Z = 0.002 \pm 0.0008\ m$), while the hybrid control achieves the

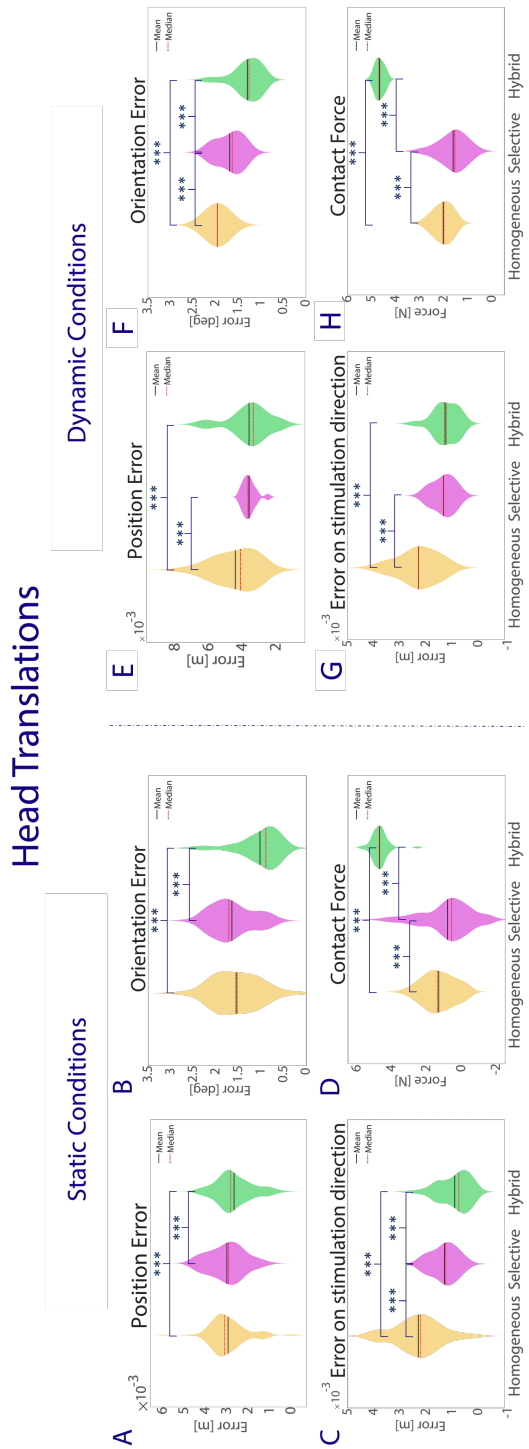

Figure 4.5: Performances evaluated in static and dynamic conditions for the homogeneous impedance (yellow), selective impedance (purple) and hybrid control (green) approaches during head **translation** movements. **Panels A & E**: position error (norm on the stimulation plane). **Panels B & F**: orientation error. **Panels C & G**: position error on the stimulation direction. **Panel D & H**: contact force.

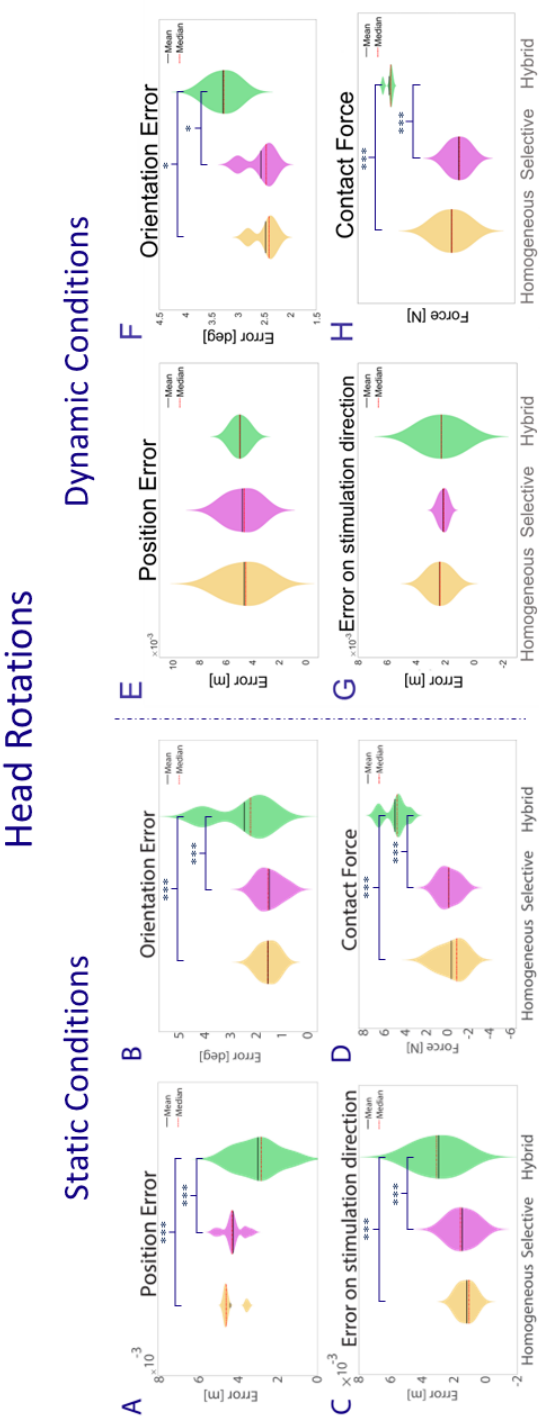

Figure 4.6: Performances evaluated in static and dynamic conditions for the homogeneous impedance (yellow), selective impedance (purple) and hybrid control (green) approaches during head **rotation** movements. **Panels A & E**: position error (norm on the stimulation plane). **Panels B & F**: orientation error. **Panels C & G**: position error on the stimulation direction. **Panel D & H**: contact force.

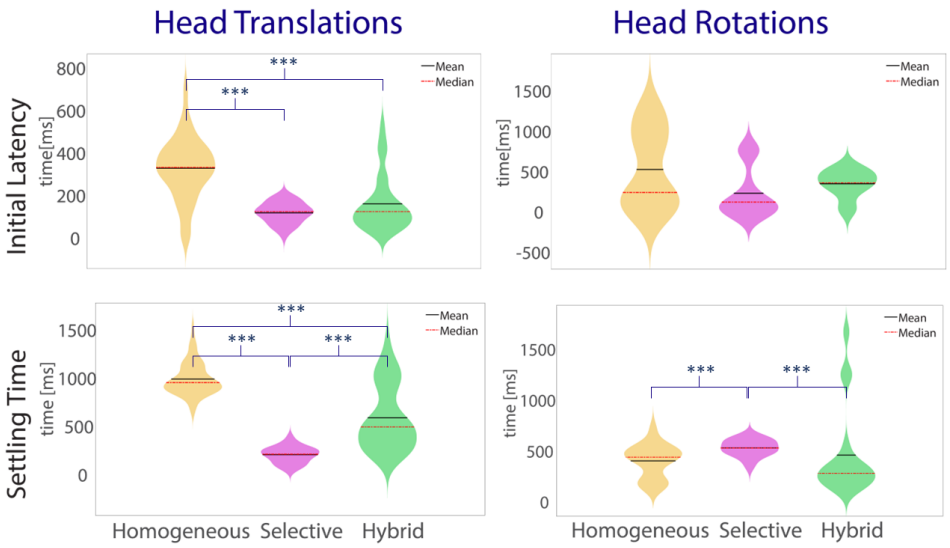

Figure 4.7: Starting latency (top) and settling time (bottom) for of head translations (left) and rotations (right) for the the homogeneous impedance (yellow), selective impedance (purple) and hybrid control (green) approaches.

lowest error values ($E_Z = 0.0009 \pm 0.0006\ m$) (Fig. 4.5 C; all p values < 0.001).

Contact forces are more spread in impedance controls, with higher values in the homogeneous approach ($F_Z = 1.32 \pm 0.92\ N$) than in the selective one ($F_Z = 0.83 \pm 1.44\ N$) ($p < 0.001$). On the other hand, hybrid control shows a compact distribution ($F_Z = 4.59 \pm 0.73\ N$) around the desired force value ($5\ N$), significantly higher than both the impedance controls (all p values < 0.001). Same results in term of contact force are obtained also in dynamic conditions (Fig. 4.5 D).

Performances of the selective impedance control in dynamic conditions in terms of coil positioning error on the plane ($E_{XY} = 0.0036 \pm 0.0004\ m$) and on the stimulation direction ($E_Z = 0.0014 \pm 0.0005\ m$) (Fig. 4.5 A-C) both show results significantly comparable to the hybrid control ($E_{XY} = 0.0038 \pm 0.0012 m$, $E_Z = 0.0012 \pm 0.0004 m$) and better than the homogeneous impedance one ($E_{XY} = 0.0044 \pm 0.0011\ m$, $E_Z = 0.0023 \pm 0.0008\ m$) ($p = 0.014$ in position error and $p < 0.001$ in stimulation direction position error). Comparisons of control approaches in terms of orientation error and contact force result similar to the ones in the static evaluation during translation movements (Fig. 4.5 B-D) except for the orientation error in the

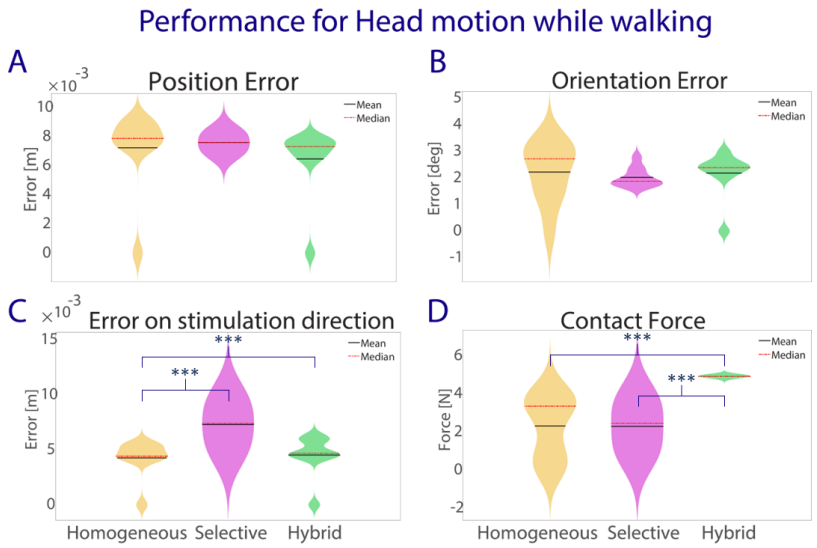

Figure 4.8: Performances evaluated in dynamic conditions for the homogeneous impedance (yellow), selective impedance (purple) and hybrid control (green) approaches during walking head movements. **Panel A**: position error (norm on the stimulation plane). **Panel B**: orientation error. **Panel C**: position error on the stimulation direction. **Panel D**: contact force.

selective impedance approach ($E_\phi = 1.70 \pm 0.28°$) that is lower ($p < 0.001$) than the one achieved with the homogeneous control ($E_\phi = 1.97 \pm 0.24°$). Similar results on contact forces can be found for static condition of head rotations (Fig. 4.6 D). Positioning errors on the plane are however significantly lower for the hybrid approach than for both impedance approaches ($p < 0.001$ in both cases) (Fig. 4.6 A), whereas orientation and position on the stimulation direction errors are significantly higher for the hybrid approach than for the impedance ones ($p = 0.001$ for both orientation error comparisons, and $p < 0.001$ for both position on stimulation direction error comparisons) (Fig. 4.6 B-C). Homogeneous impedance control proves to require the highest time to follow the head translations ($338.4 \pm 144.8\,ms$) and to settle after the motion ($1022 \pm 192.4\,ms$) (Fig. 4.7 A-C), whereas the selective impedance approach presents more compact distributions (initial latemcy=$128.5 \pm 49.3 ms$, settling time= $227.8 \pm 86.5 ms$), respectively comparable to and better (all $p < 0.001$) than the hybrid approach in term of initial latency and settling time ($L_{start} = 185 \pm 169.9\,ms$, $L_{end} = 617.7 \pm 364.3\,ms$). In case of head rotations, initial latencies are all equivalent among control ap-

proaches. However, settling latencies are significantly higher for the selective impedance approach ($L_{end} = 547.3 \pm 82\,ms$) than for both the homogeneous impedance approach ($L_{end} = 394.4 \pm 186.9\,ms$, $p = 0.015$) and the hybrid approach ($L_{end} = 476.7 \pm 448\,ms$, $p = 0.006$), and homogeneous and hybrid approaches show equivalent settling latencies.
No significant differences occur in the position and orientation error among the three controls if evaluated for simulated head movements while walking (Fig. 4.8 A-B), even though the selective impedance control still shows the most compact distribution. Error on the stimulation direction (Fig. 4.8 C) is instead higher for the selective impedance control ($E_Z = 0.007 \pm 0.002\,m$) than the homogeneous ($E_Z = 0.0048 \pm 0.0006\,m$, $p = 0.003$) and hybrid ($E_Z = 0.005 \pm 0.0008\,m$, $p = 0.009$) approaches. Contact force (Fig. 4.8 D), similarly to simple head movements results, is lower for the two impedance controls than for the hybrid control. Considering control algorithms performances during dynamical rotation movements, all three approaches are equivalent in terms of position tracking. Hybrid control performs worse ($E_\phi = 3.29 \pm 0.26°$) than the impedance controls (homogeneous: $E_\phi = 2.47 \pm 0.24°$, selective: $E_\phi = 2.56 \pm 0.30°$) in orientation ($p = 0.018$ versus homogeneous, $p = 0.032$ versus selective), whereas all three controls shows similar performances in positioning on stimulation direction. Finally, identically to the other results on contact force, the hybrid approach shows significantly higher forces with a data distribution centered on the $5\,N$ value.

4.3.6 Discussion

Considering head translation movements, the hybrid control approach appears as the most efficient algorithm with better performances than the impedance ones. The absence of position control on the stimulation direction ensures a permanent contact of the coil on the head of the subjects, essential for an effective stimulation.
Actively controlling the force applied on subjects head proves to maintain it constant and to avoid undesired variations -which instead occur in the impedance controls- improving the safety. Negative values in interaction forces using the impedance approaches could be due to either the coil weight model not handling big variations of the flexible coil cable configuration or additional torque acting on the coil if it touches the head not exactly with the center of the stimulation plane. An online estimation and compensation of the coil cable payload could mitigate this issue.
Stable performance of the hybrid control where achieved for an absolute

force value of 5 N; further investigation is necessary to understand if results are robust at lower force values and tests in real TMS sessions are needed to assess related subjects' comfort.
Now considering the head rotations and the walking-on-a-treadmill related movements, no control approach can be considered advantageous compared to the others, despite the consistency of pose error of the selective algorithm and the already mentioned advantage of the hybrid control on force distribution. Overall position and orientation error values remain acceptable for all three control approaches for the translation movements. However, more complex movements such as head rotations or walking movements prove more challenging for all three control algorithms as they show higher errors, especially on coil planar and directional positions, or even on orientation for the hybrid control on rotation movement.
Selective impedance and hybrid approaches prove to be effective in the compensation of small head movements both in static and dynamic conditions and thus employable in movement-based TMS experimentation. Whereas hybrid control is better equipped at continuous stimulation on the same target by keeping the contact on the head, selective impedance could be used to sequentially stimulate several targets -thanks to the position control on all the axis and the low latency and settling time- with high safety thanks to the compliance behavior towards the scalp.
Results highlight also the necessity for further improvements of the presented control approaches in order to go deeper in movement-based TMS involving complex and repetitive motions like walking.

4.4 Conclusion

We developed a robot-aided TMS platform able to track and compensate for subjects' head movements, integrating infrared motion capture, a graphical user interface and the control of a 7 dof robot. We tested three control approaches on a moving mannequin and validated the platform through the investigation of which control would present the best performances in an experimental protocol involving movement of the subject. The robot-aided TMS system component is thus ready to be integrated into the final embodiment platform and also for experimental application. Indeed, the platform is currently being used for a study on the neuromodulation of performances during a pointing task. The task requires minimal movements of the head but the successive stimulation of two different hotspots. Thus, for this experiment we are using a mixed control approach, i.e the hybrid

control for head movement compensation during the pointing task and the selective impedance control during hotspots position shifting.
Furthermore, additional features of the robot-aided TMS platform are planned or currently under development, including double coil stimulation (involving two robots), automatic scalp numerical reconstruction from detected contacts of the robot on the head, and automatic hotspot research with a closed loop control integrating a relationship between coil pose, stimulation intensity and elicited motor evoked potential (MEP).

Chapter 5

Electrophysiological study of a preferred hand posture in the body schema

5.1 Background

Body schema was previously introduced as a *dynamic* representation of the metric properties of our body in our brain, integrating information about limb dimensions and position in space (see chapters 1 and 3). Specific attention was given to the "online" characteristic of the body schema, in the sense that it is constructed and permanently updated from individual afferent multimodal somatosensory inputs received when perceiving the environment [159]. However, recent studies have brought to light a possible *static* component of the body schema, suggesting the existence of a universally predefined and preferred limbs configuration in space i.e a standard body posture which would promote a more efficient interaction with the environment [160]. The first evidences for the existence of such a default spatial representation of our body dates back to the seventies, in studies in which eyes-closed participants who underwent anesthetic block of the sensory and motor nerves of the arm reported feeling their phantom arm (their perceived arm, in contrast with their real arm) in a standardized position dissociated with the the position of their arm at the moment of the anesthesia [161, 162]. Further investigations have brought behavioral proofs to the presence of a standard body posture: arm crossing with respect to a normal uncrossed posture flawed the localization of touch of participants until corrected by the brain process of taking into account the current position of the arms. It suggested a conflict between

a preset postural model of the arms and the actual limb configuration [163], corroborated by similar studies on localization of touch with crossed fingers [164, 165] as well as on visuo-tacile interaction or saccades with crossed hands [166, 167]. The body schema is integrated in brain processes for perception and motor planning for action, and our hands are primordial for interaction with our environment. Thus, information about a favored hand posture appears precious to study the motor control of the the hand and the related pathologies, as well as for the development of dexterous hand prostheses and their optimal integration in the body schema of amputees. The pronated index-up thumb-down position of the hand has proved to be preferred to the supinated thumb-up index-down posture, from a tactile sensory discrimination task [168] and from behavioral and physiological evidence in motor control [113]. However, to our knowledge there is no electrophysological evidence present in the literature of such a standard hand posture. Thus, we used electroencephalography (EEG) to investigate the brain responses to electrotactile stimulation of the hand in index-up thumb-down and index-down thumb-up postures, hereafter respectively referred as the "standard" and "inverse" postures, stimulating the median nerve, the index finger, or the thumb. We expected an overall stronger amplitude of the sensory evoked potentials (SEP) following the median nerve stimulation with the hand in the standard posture with respect to the inverse posture, and a main effect of the posture on the SEP amplitude as well as an interaction between the posture effect and the stimulated finger effect on the SEP following finger stimulation.

5.2 Materials and Methods

5.2.1 Participants

Sixteen participants were enrolled in the experiment: 8 females, all right-handed, aged 25.7±4.3. All participants reported to have normal tactile sensation of the hand and wrist. All participants provided written informed consent before the experiment in accordance with the Declaration of Helsinki and following amendments. The experiment was conducted after approval of the Ethics Committee of Università Campus Bio-Medico di Roma (EMBODY protocol).

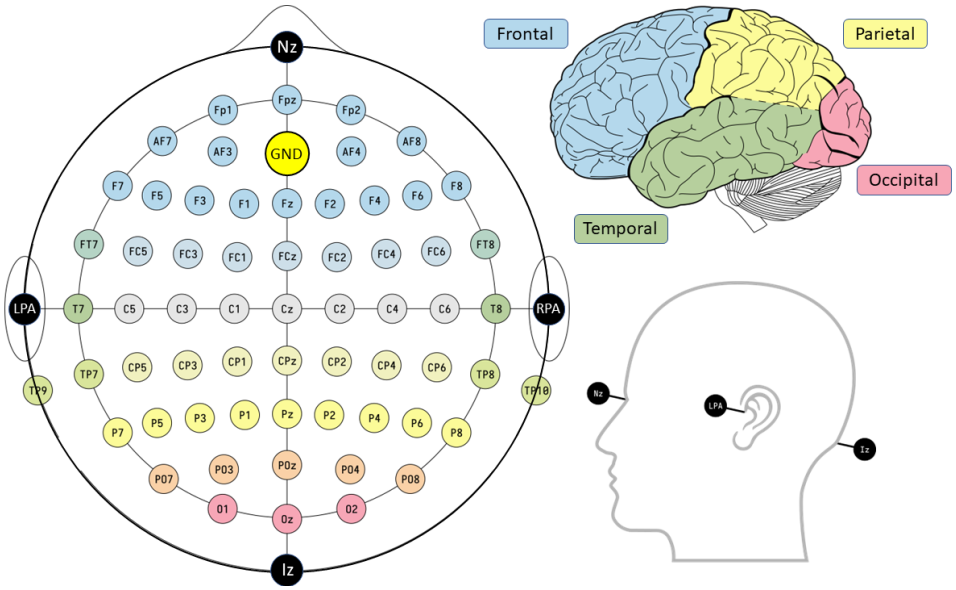

Figure 5.1: EEG electrode positions in the 10-10 convention system using modified combinatorial nomenclature, along with the fiducials and associated lobes of the brain. Adapted from [169].

5.2.2 Experimental Setup

To record the electric field caused by neurons activation in the cerebral cortex, we equipped subjects with an EEG cap (g.GAMMAcap - G.Tec Medical Engineering GmbH) of the 10-10 modified combinatorial nomenclature convention [170] set with 62 active electrodes (g.SCARABEO - G.Tec Medical Engineering GmbH). The 10-10 convention stands for 10%-10% which means that one electrode is placed every 10% of the distance between the nasion and the inion on the nasion-vertex-inion (NVI) line (9 electrodes on the NVI line: Fpz, AFz, Fz, FCz, Cz, CPz, Pz, PO, Oz) and one electrode every 10% of the distance between the left preauricular (LPA) and the right preauricular (RPA) on the LPA-vertex-RPA (LVR) line (9 electrodes the LVR line: T7, C5, C3, C1, Cz, C2, C4, C6, T8). The remaining 44 electrodes are evenly distributed on the rest of the scalp (see Fig. 5.1). The elasticity of the cap enables to evenly stretch the cap to fit it on the subjects head maintaining the 10-10 convention. To place the cap on the subjects head, the experimenter identifies the vertex location of the subjects scalp by measuring the middle point of the nasion-inion distance on the NVI line, and places the central Cz electrode of the cap on the vertex. Once the cap is correctly

placed on the subject's scalp, conductive gel is carefully inserted between electrodes and the scalp to ensure an optimum conductivity. Thanks to the design of the electrodes, the gel can be injected below every electrodes through holes provided for this purpose using syringes.
Once the gel has been inserted, the conductivity of every electrodes can be inspected through the g.HISYS software (g.HIsys for Simulink - G.Tec Medical Engineering GmbH) and gel quantity can be adjusted in case of low-conductivity electrodes. We used the arbitrary threshold of 50 $K\Omega$ as a maximum acceptable resistivity. The reference electrode is attached to the earlobe ipsilateral to the electrical stimulation side, thus to the right earlobe. The ground electrode is the AFz electrode. Electrodes signal was amplified by the g.HIamp biosignal amplifier and the corresponding g.HISYS software and recorded through the g.RECORDER software (G.Tec Medical Engineering GmbH).
The right hand was investigated. For the electrical stimulation, subjects are equipped with three sets of electrodes. They wear only one set at a time. The median nerve stimulation set of electrodes is placed on the anterior side of the wrist, longitudinally along the median nerve. Since a correct positioning of the electrodes on the median nerve should trigger a twitch of the thumb finger upon stimulation, the positioning is adjusted by performing light electrical stimulations until the twitch occurs. For the median nerve stimulation, we set the stimulation intensity at the minimum required intensity to elicit a twitch of the thumb. A set of ring electrodes is used for the index and thumb finger stimulation. The anode is placed on the intermediate phalanx and the cathode on the proximal phalanx for the index finger, and the anode on the distal phalax and catode on the proximal phalanx for the thumb finger. For each finger, the stimulation intensity is set as twice the sensory threshold of the subject, each finger having its own stimulation intensity. The stimulation pattern was implemented on a custom micro-controller and the pattern was simultaneously sent to the stimulation system (Digitimer DS7A - Digitimer Ltd.) and to the amplifier through the electrode connector box.
During the whole duration of the experiment subjects are seated comfortably in a chair, at rest. They are asked to relax and to stare at a point in front of them. Their right arm elbow is resting on the armrest, with their right hand in the air in the posture corresponding to the tested condition. They are asked to maintain the opened pinching posture with their index and thumb finger, and to keep the other fingers of the hand in a resting semi-closed position, without contracting the muscles to fully close them (see Fig. 5.3).

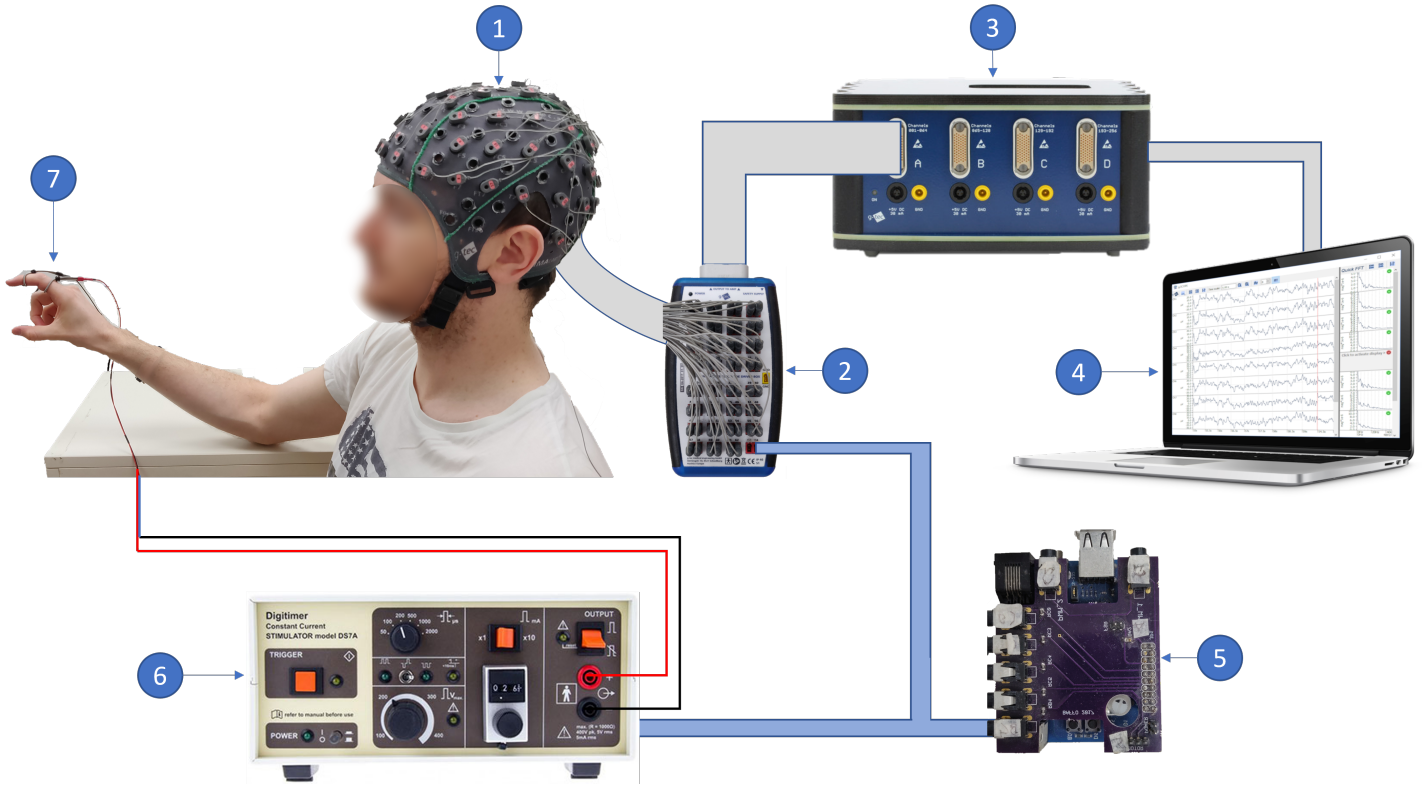

Figure 5.2: Experiemtal setup with with standard hand posture and index stimulation. **1.**EEG cap. **2.**Electrodes connector box. **3.**g.HIamp biosignal amplifier. **4.**PC equipped with g.HISYS and g.RECORDER softwares for amplification parameters and data acquisition. **5.**Custom micro-controller generating the stimulation pattern. **6.**Digitimer DS7A stimulation system. **7.**Anode (black) and cathode (red) stimulation electrodes.

Figure 5.3: Standard (left) and inverse (right) hand postures tested in the experiment. Adapted from [113].

5.2.3 Experimental Protocol

The experiment is a 2-by-2 design with FINGER and POSTURE as factors. Index and Thumb are the levels of the factor FINGER and Standard and Inverse are the levels of the factor POSTURE. Since sensory evoked potential caused by the stimulation of a nerve differs greatly from the sensory evoked potential caused by the stimulation of a finger, the median nerve stimulation has not been integrated into this design and analysed separately to avoid introducing a false main effect of the stimulation spot factor in the statistical analysis.
The conditions are tested in a semi-random order. First the stimulation spot is chosen randomly but then both postures for this stimulation spot are successively tested in a random order. This is done so the position of the electrodes remains the same between conditions for the same stimulation spot, to avoid introducing variability in the data due to slightly different electrodes positions on the same stimulation spot for different postures.
The stimulation frequency is $2.6Hz$ and we perform 550 stimulations per condition, thus a recording lasts approximatively 210s. The EEG recording sampling frequency is $4800Hz$. Including setup and experimental phase, the comprehensive experiment duration approximates one hour.

5.2.4 Data processing

Stimulation Artefact Interpolation

Data processing is performed with Brainstorm [171]. Surface electrical stimulation for sensory evoked potentials investigation is known to have the major drawback of being recorded by the EEG electrodes. It manifests on

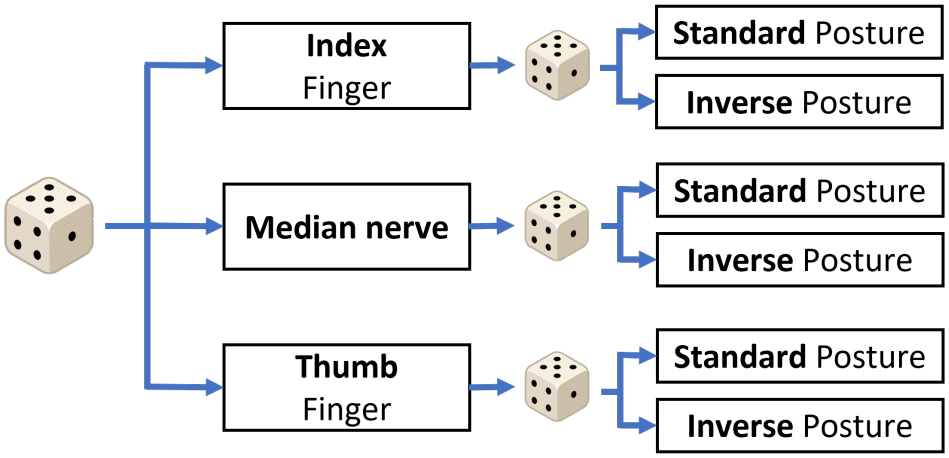

		FINGER		Median nerve
		Index	Thumb	
POSTURE	Standard	*ind_std*	*tmb_std*	*med_std*
	Inverse	*ind_inv*	*tmb_inv*	*med_inv*

Figure 5.4: Experimental protocol (top) and design (bottom) of the EEG study.

the EEG trace as a peak in the signal synchronized with the stimulation and can be of several orders of magnitude greater then the physiologic EEG activity. Since the origin of theses peaks are not physiological, they do not represent neural activity and are thus called stimulation artifacts. The origins of this stimulation artifact have been identified as the volume conducted currents, the displacement currents and the electromagnetically coupled currents [172, 173]. Several techniques have been developed over time to counter the stimulation artefact, from hardware equipment modification to software algorithms [174, 175]. In the present case, the stimulation artefact is removed by performing an offline interpolation of the signal around each trigger on a $[-2ms, 5ms]$ time interval with a spline curve (Fig. 5.5, A-B).

Filtering

Mainly due to the different impedances between the electrodes, recorded raw traces do not have the same mean value over time. Thus the next step was to remove the continuous components by applying a high-pass filter on the traces a $1Hz$. Furthermore, frequencies higher than $250Hz$ are not of interest in our study, thus we then applied a low-pass filter on all signals at $250Hz$. Looking at the power spectrum density (PSD) of the filtered data, we noticed a great power amplitude at $50Hz$, $100Hz$, $150Hz$, and $200Hz$, representing the power line frequency and its harmonics. Those specific frequencies not being of interest in our investigation and introducing an important noise in the EEG signal, we applied four notch filters at the previously mentioned frequencies (Fig. 5.5, B-C-D).

Downsampling

For computational speed, we then downsampled the signals from its $4800Hz$ sampling frequency to a frequency of $1024Hz$.

Bad channels identification

Due to imperfect fit of the EEG headset on the scalp of the subject or to deficient electrodes, some channels might show aberrant values. Identifying those channels directly on the whole trace of the recording might prove difficult, therefore we aslo inspect the PSD to look for channels with incoherent power amplitude over large frequency bands. Additionally, to identify remaining bad channels it can be interesting to look at the event related potential (ERP) of the signal. To compute the ERP of a recording, the signal must first be decomposed into epochs. An epoch is a segment on the signal taken at a fixed interval of time around each trigger event. The chosen time interval in our study was $[-50ms, 300ms]$. We thus have a total number of 550 epochs per recording. The ERP is computed by averaging all the epochs. By averaging the epochs, we also remove some noisy brain activity not related to the response to the electrical stimulation. If an electrode is not properly recording the brain activity, its signal will be incoherent with the rest of the channels' signal, and will be easily identifiable on the ERP. Once the bad channels are identified, the signal of each one of them is interpolated by performing the arithmetic mean of the signal of the manually selected surrounding channels. Bad channels were manually identified for every recording. In the whole data processing, 2.9 ± 2.6 [mean $\pm$ standard deviation] channels were interpolated (Fig. 5.5, D and Fig. 5.6, E).

Independent Components Analysis

Up to this point, we have performed several cleaning steps but the signal can still contain high amplitude events recorded by the EEG system that do not represent brain activity related to the electrical stimulation (Fig. 5.6, E). Those high amplitude events are called "artifacts", and can represent for instance eye movements, blinking or remaining bad channels. To remove those artifact from our signal, we used the Independent Components Analysis (ICA) technique, first described by Jutten and Herault in 1986 [176] and first applied to EEG data by Makeig et al. [177]. The ICA is a signal processing method used to separate independent sources linearly mixed in several sensors. In the case of EEG, electric fields coming from different brain sources can project and overlap over identical electrodes. Each electrode thus records a mixture of brain signals coming from separated sources, hence the use of ICA to identify them. ICA tries to recover a version of the original sources by applying an unmixing matrix to the recorded data, following the equation:

$$U = WX \tag{5.1}$$

where X is the matrix of the recorded signal (lines represent the EEG channels and columns the time steps), U is the matrix of the independent sources activities (lines represent the components, columns the time steps) and W is the unmixing matrix (lines represent the components, columns the channels). Compared to the Principal Component Analysis (PCA) method [178] that tries and finds the uncorrelated components of the data representing the largest variation using an orthogonal uncorrelation matrix W, ICA tries and finds the components of the data that are statistically independent from each other without placing constraint on the matrix W. A great number of ICA algorithms have been implemented over the years, among the most popular ones beeing Infomax [179], JADE [180] or FastICA [181]. We used the Infomax algorithm available in Brainstorm (which calls the EEGLAB function runica.m [182]). For temporal and computational efficacy, for each participants we concatenated along the time axis all three recordings (one per condition) in order to perform one single ICA per participant. Once independent components are computed, artifacts components have to be rejected. Independent components selection is performed through a visual investigation of the topoplot (a spatial representation of the channels data on a schematic scalp), of the components ERP and their PSD. There exist two different approaches for independent components rejection. One is an exclusive approach consisting in keeping only the components containing

the brain response of interest to the scientific question investigated. This approach is valid when the investigated brain activity is precisely defined beforehand (frequencies, latencies), but is too restrictive when the study is exploratory. In the latter case, a conservative approach is used: to avoid excluding any neural response out of the analysis, only the obvious artifacts components are discarded, too keep the number of removed components to a minimum. In this study, we thus used the second approach, and 5.1 ± 1.9 [mean ± standard deviation] components were removed (Fig. 5.6, F-G).

Re-referencing

To improve visualization and interpretation of the data, we need to re-reference the signal. An evolution of the signal recorded at the reference electrode affects all the others electrodes and thus the trace of our recording (Fig. 5.6, G). It is necessary to remove the influence of the reference electrode on the rest of the signal to retain only the amplitude evolution of the trace due to the brain activity we are investigating. We thus perform an average re-referencing of the signal, which consists, for each time step, in computing the arithmetic mean value of all electrodes at that time step and to subtract this mean value to all electrodes (Fig. 5.6, H).

$$\forall t \in [t_i, t_f], \forall i \in [0, N_c], V_{i,rref}(t) = V_i(t) - \frac{1}{N_c} \sum_{k=1}^{N_c} V_k(t) \qquad (5.2)$$

where t is the time step, t_i is the first time step of the recording, t_f is the last time step of the recording, i is the number of the electrode, N_c the total number of electrodes, $V_{i,rref(t)}$ the amplitude of the average re-referenced signal of electrode i at time step t, and $V_i(t)$ the amplitude of the signal of the electrode i at time step t before the average re-referencing. The average re-referenced signal is thus centered on the $0\,\mu V$ value of the amplitude.

Finally, we observed a remaining stimulation artifact after the previous processing steps (Fig. 5.6, H) and thus performed an second stimulation artifact interpolation around each trigger of each recording but this time over a specific time window for each recording within the range of $[-6ms, 6ms]$ (Fig. 5.7, I). Then, ERPs of the pre-processed trace were computed (Fig. 5.7, J) as well as the grand average (GA) of each condition (Fig. 5.8 and Fig. 5.9). The GA is the mean of ERPs over all subjects by conditions.

For visualization clarity, the data in Fig. 5.5, 5.6, and 5.7 is displayed on a time segment ([22s, 42s]) of the trace of one of the subjects' recording

(median nerve stimulation, inverse posture). Green dots in the superior part of the graphs are stimulation events. In superimposed view, all channels' signal are displayed on the same Y axis (signal amplitude) origin, whereas in the split view, each channel's signal is displayed on a different Y axis (line), in the channels numerical order. In the split view, all channels' signal are displayed with the same scale, displayed on the top right corner. In the superimposed view, the green line at the bottom of the graph separated from the channels' trace is the global field power (GFP) of the signal. The segment below the time axis is the timeline of the signal. The red segment indicates the time segment of the currently displayed signal with respect to the whole recording (whole segment). Red and green lines of the timeline represent respectively discarded (beginning and end of the recording) and studied parts of the signal.

5.2.5 Data analysis

The cleaned data were exported out of Brainstorm and processed through Fieldtrip [183] which benefits from adaptable toolboxes for specific statistical analysis. We analyzed the main effect of *POSTURE* on the ERP amplitude following median nerve stimulation and the main effects of *FINGER* and *POSTURE* as well as their interaction the ERP amplitude following the fingers electrotactile stimulation. To do so, we employed cluster-based (over time and space) permutation tests [184, 185] on the whole ERP time-window ([-50;+300]ms) with the Montecarlo method and 1000 permutations. Each effect was evaluated at the sample level with dependant samples T-tests (since each main effect has only two levels) using $\alpha = 0.05$ as thresholding value. We used the "maxsum" statistical test under the permutation distribution. Since we wanted to separate positive from negative clusters of channels, we set the sample level T-tests as two-sided, thus taking an alpha value of $\alpha = 0.025$ for the permutation test. To avoid combining clusters representing different sources, we set as 2 the minimum number of channels that must be in common between two clusters so that their are considered as one.
Considering the median nerve stimulation, we investigated the *POSTURE* effect on the ERP amplitude comparing conditions *med_std* and *med_inv*. Considering the 2x2 experimental design, to analyse *POSTURE* effect on the ERP amplitude, we computed for each subject the average of the ERP between conditions *ind_std* and *tmb_std* into a new condition *std* and did the same for conditions *ind_inv* and *tmb_inv* into condition *inv*. We then ran the cluster-based permutation analysis to compare conditions *std* and *inv*. We proceeded in an identical way to investigate the *FINGER* effect,

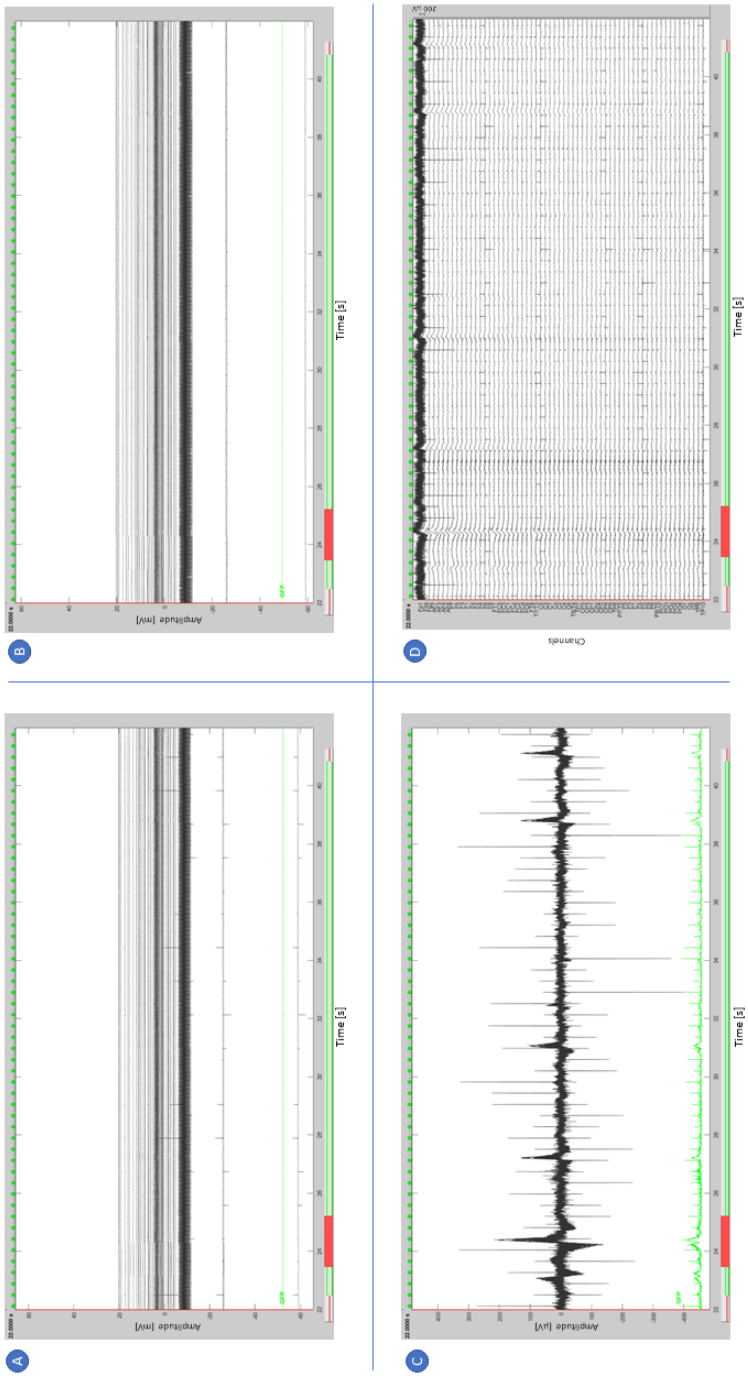

Figure 5.5: EEG signal pre-processing steps (1/3). **Panel A**: raw EEG signal in a superimposed view. **Panel B**: EEG signal after stimulation artifact interpolation (superimposed view). **Panel C**: EEG signal after band and notch filtering (superimposed view). **Panel D**: EEG signal after band and notch filtering (split view).

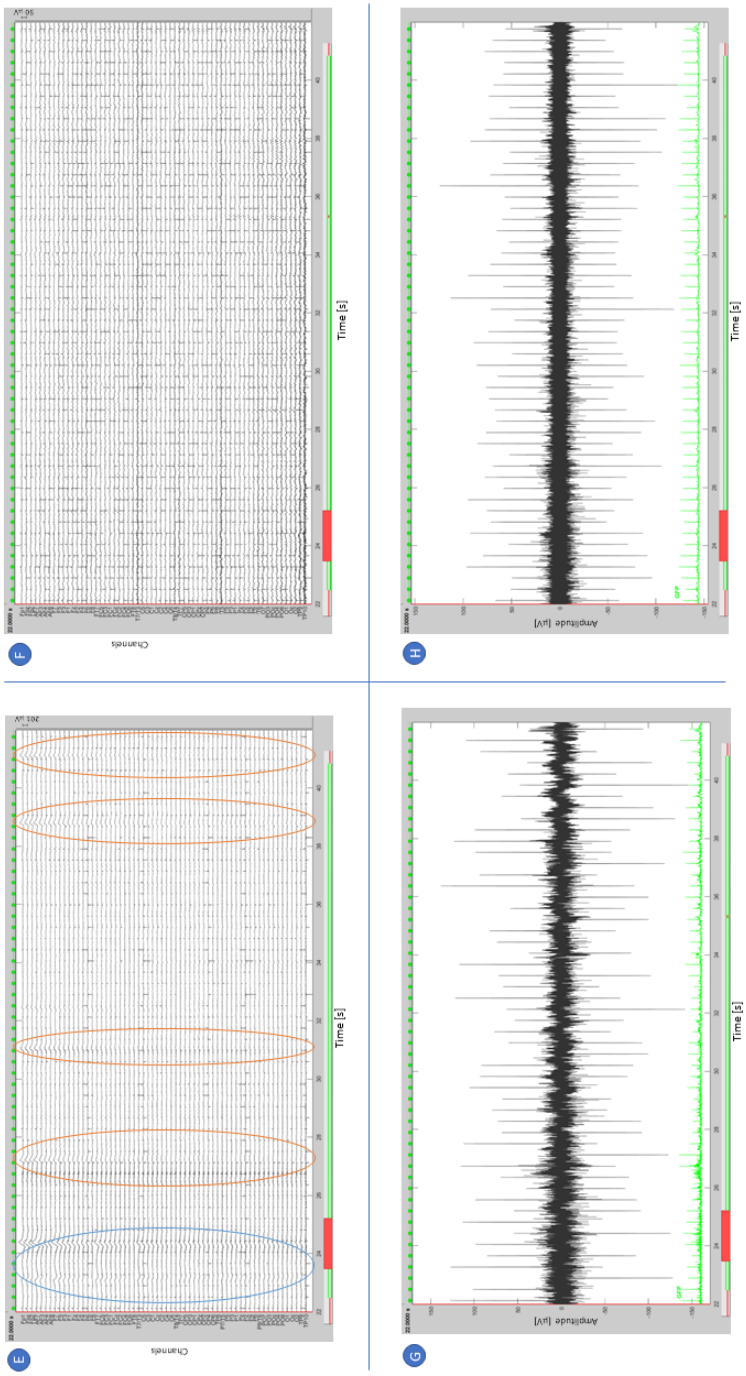

Figure 5.6: EEG signal pre-processing steps (2/3). **Panel E**: EEG signal after bad channels (Fp1) interpolation (split view). Circled segments are typical artifacts present in the signal (blue: horizontal eye movement; orange: blinking). **Panel F**: EEG signal after artifact components removal (split view). **Panel G**: EEG signal after artifact components removal (superimposed view). **Panel H**: EEG signal after average re-referencing (superimposed view).

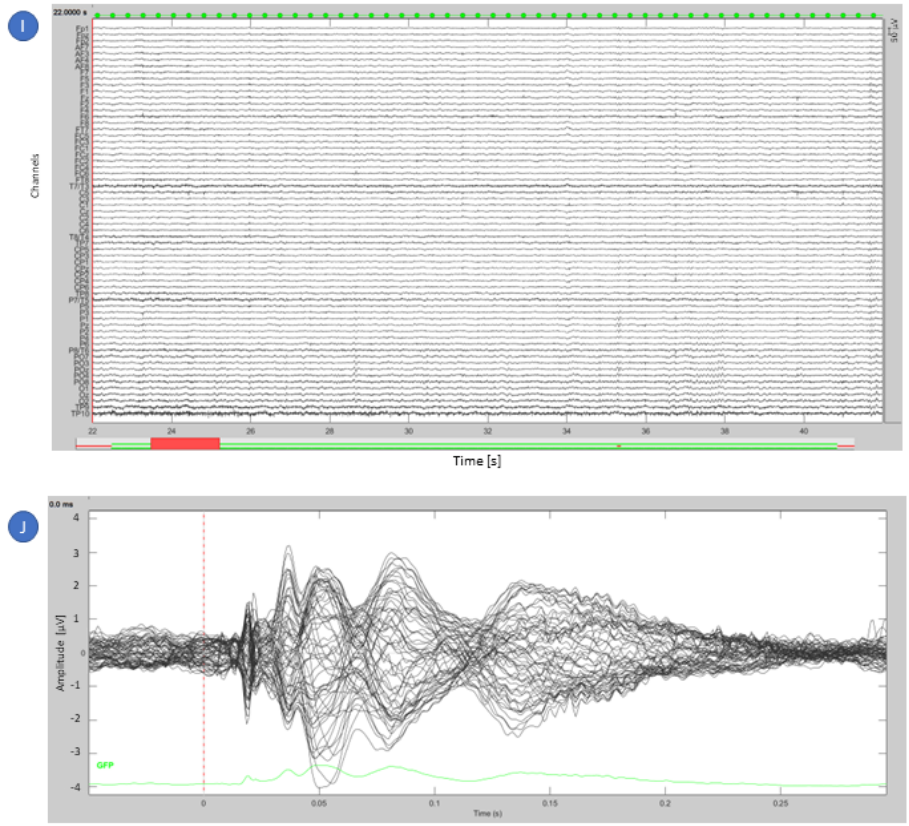

Figure 5.7: EEG signal pre-processing steps (3/3). **Panel I**: EEG signal after second stimulation artifact interpolation (split view). **Panel J**: Clean ERP after pre-processing of the EEG signal.

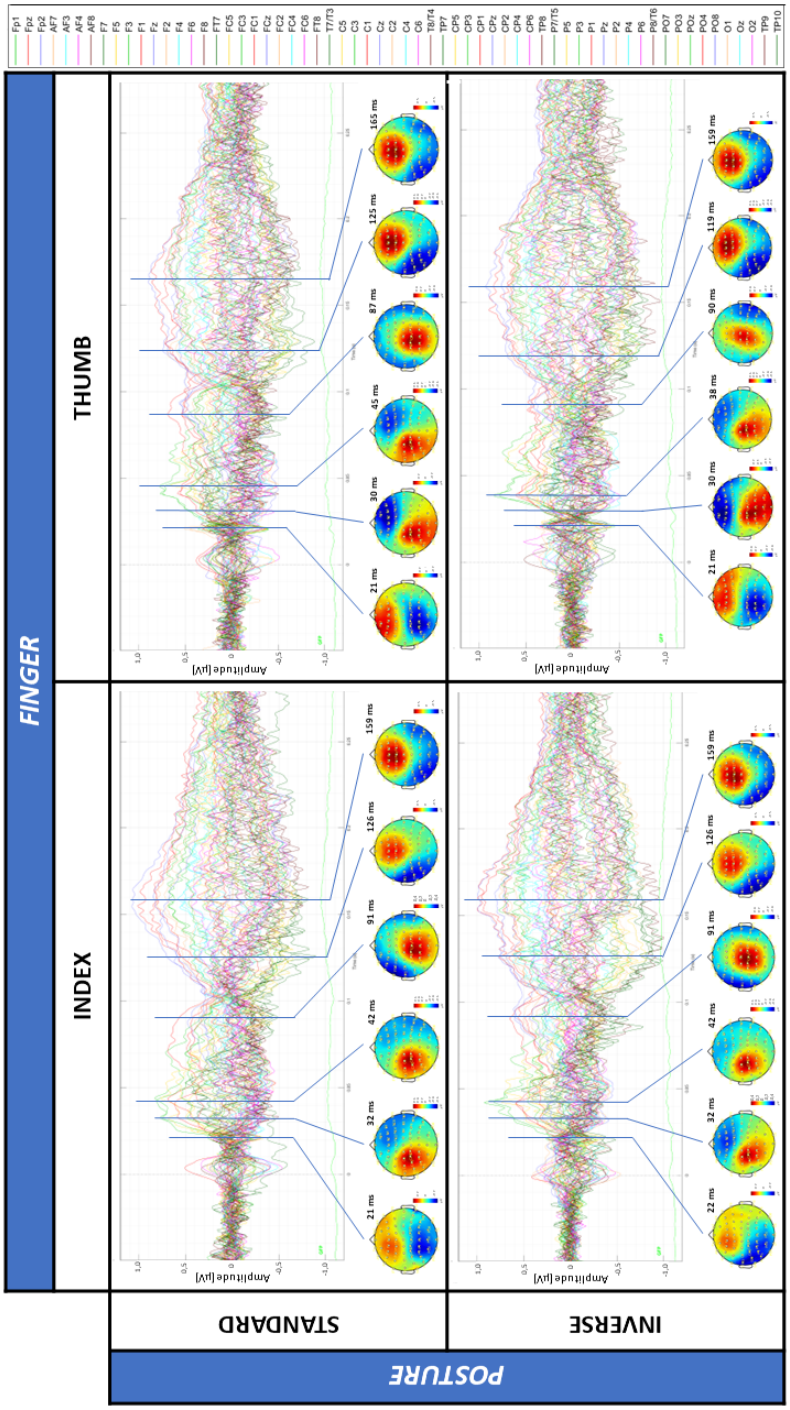

Figure 5.8: Grand averages and relative topoplots of the four conditions of the 2x2 experimental design.

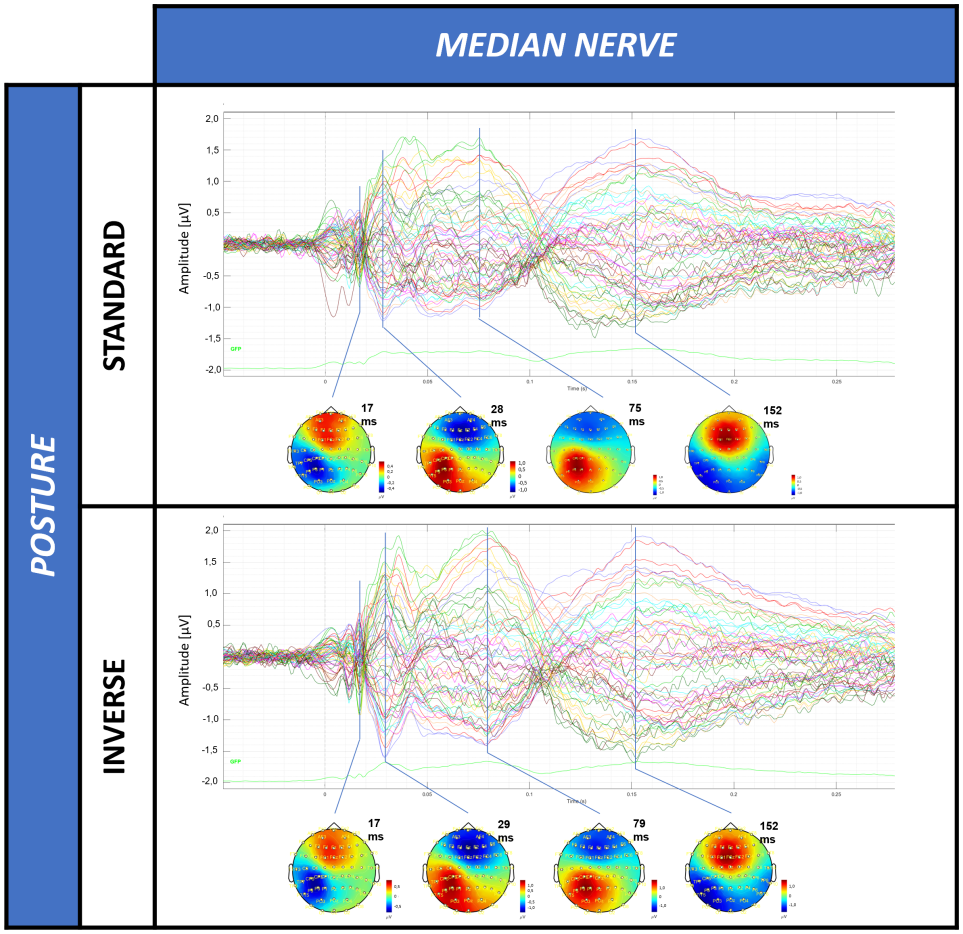

Figure 5.9: Grand averages and relative topoplots for both postures after median nerve stimulation.

averaging the ERP of conditions *ind_std* and *ind_inv* into condition *ind* and conditions *tmb_std* and *tmb_inv* into condition *tmb* and running the cluster-based permutation between condition *ind* and *tmb*. Finally, to investigate the interaction between effects, we computed for each subject the difference between the ERP of condition *ind_std* and *ind_inv* on one side and the difference between the ERP of condition *tmb_std* and *tmb_inv* on the other side and ran the cluster-based permutation analysis between the differences, thus testing the interaction between *std* vs *inv* and *ind* vs *tmb*.

5.3 Results

No significant cluster was found for the *POSTURE* effect on the ERP amplitude following median nerve stimulation (Table 5.1). Considering the 2x2 design, no significant cluster was found for any of the studied effects on the ERP amplitude following finger stimulation, nor for their interaction (Table 5.2). Thus no significant effect of *POSTURE* nor *FINGER* nor of their interaction was found on the ERP amplitude following finger or median nerve stimulation.

5.4 Discussion

We did not find any evidence of a preferred hand posture from an electrophysiology point of view in the amplitude of the brain response following electrotactile stimulation that would corroborate the behavioral and physiological evidences found in the existing literature. Nevertheless, some additional analyses on the latency of the brain responses of interest are required to understand if there is any effect of the hand posture or finger stimulation (or interaction between both) on the time necessary for the brain to process the electrotactile stimulation.

5.5 Conclusion

Despite the lack of significant result from the study so far, the investigation of a preferred hand posture in the body schema from an electrophysiology point of view enabled the author to obtain hands-on knowledge on the acquisition, processing and analysis of EEG data, which is necessary for the development and data analysis of future experimental protocols on the electrophysiological study of the embodiment.

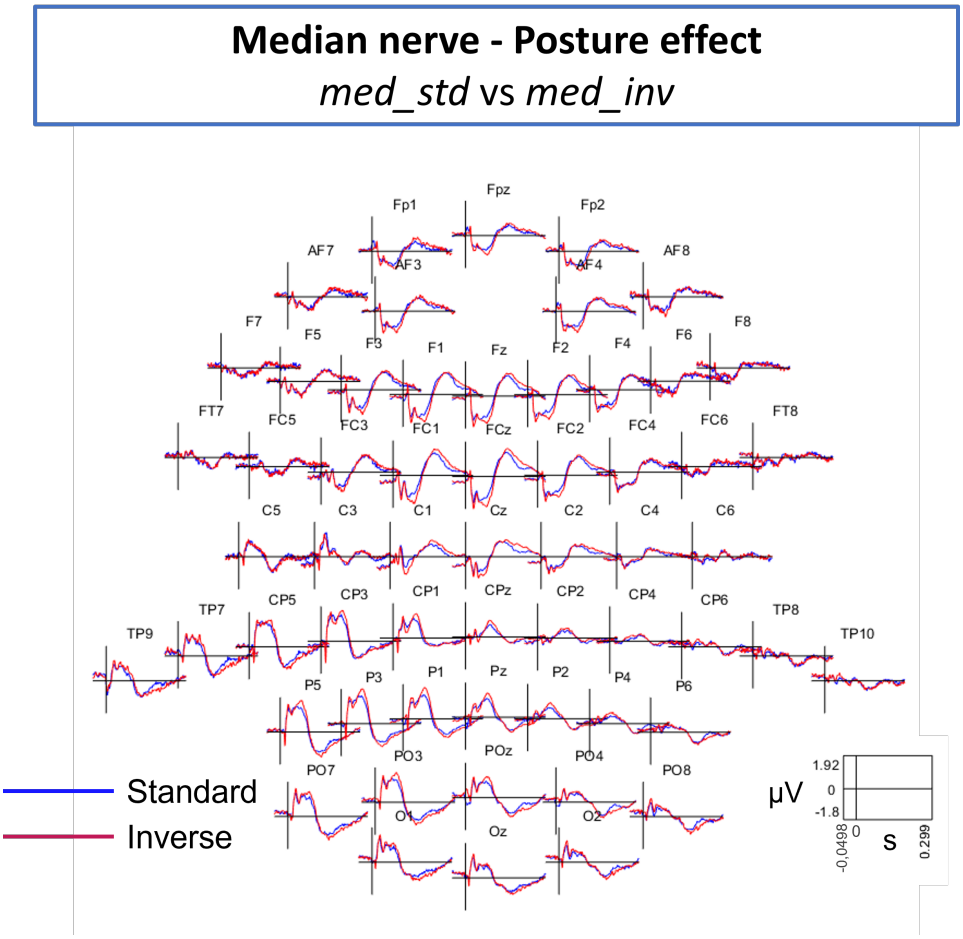

Figure 5.10: Multiplot of the **posture effect** (GA of each condition displayed by channel on the channels topography) on the brain response following **median nerve stimulation** in a standard (blue) and inverse (red) posture.

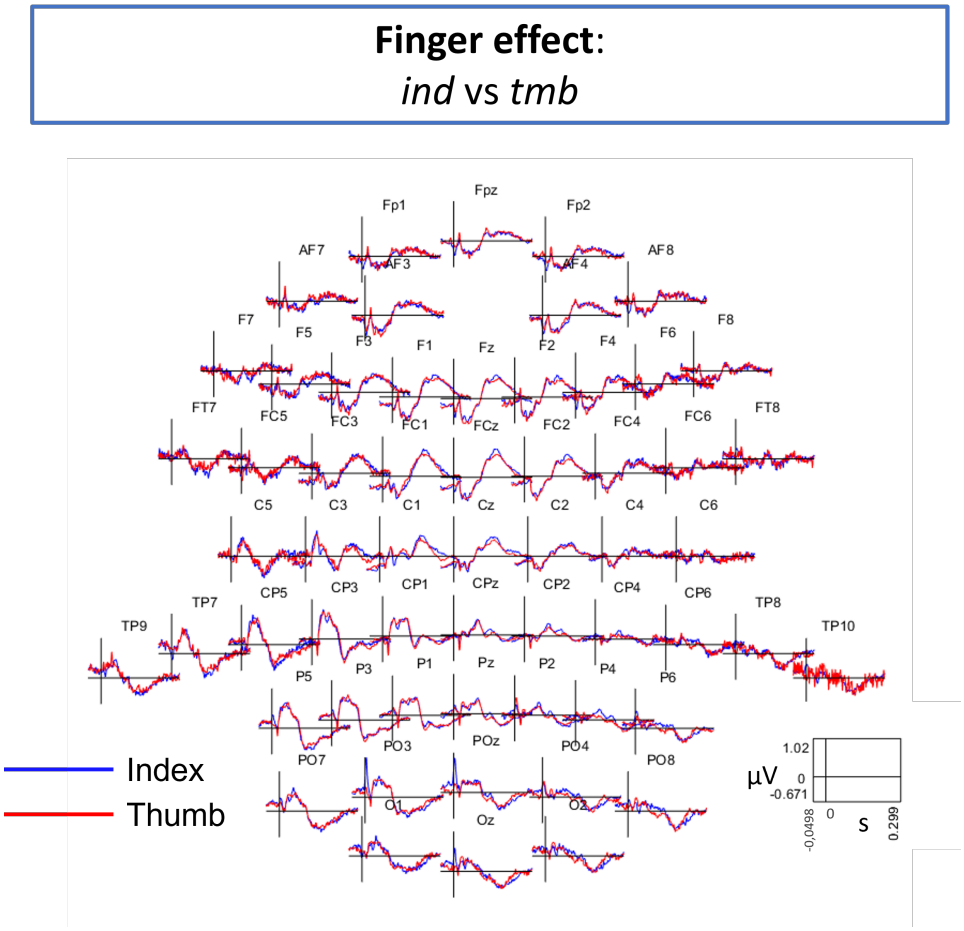

Figure 5.11: Multiplot of the **finger effect** (GA of each condition displayed by channel on the channels topography) on the brain response following **finger stimulation** on the index (blue) and on the thumb (red) finger.

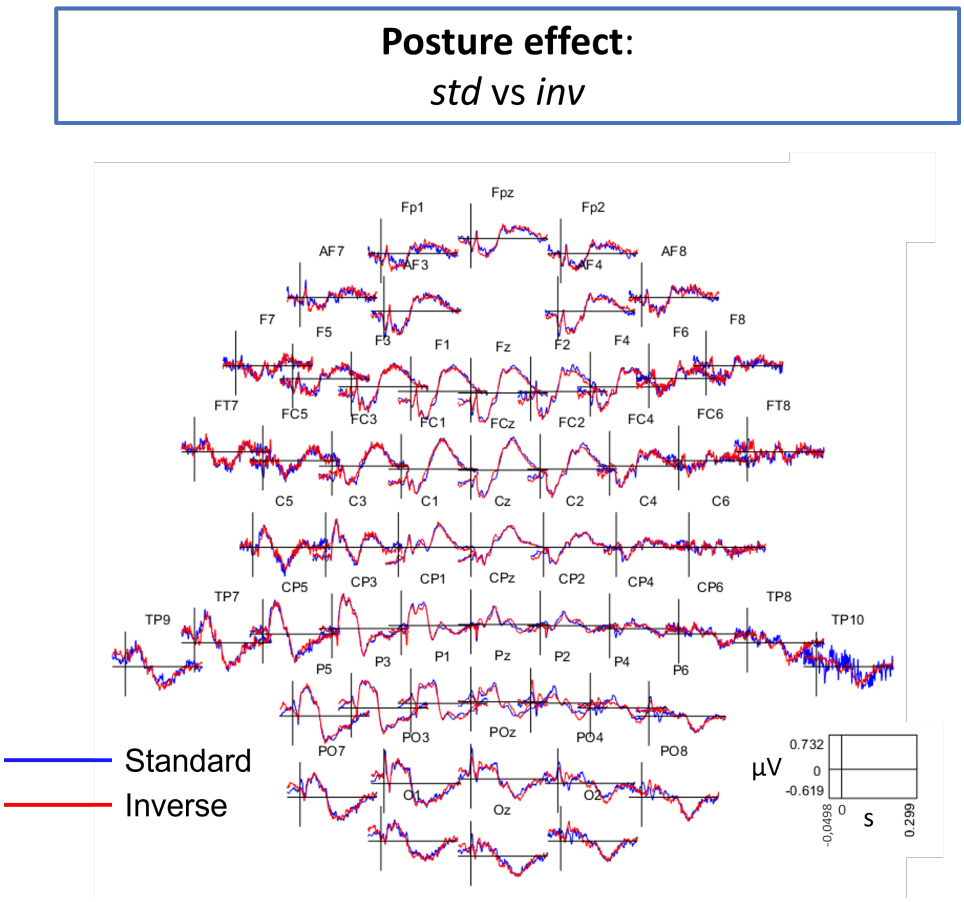

Figure 5.12: Multiplot of the **posture effect** (GA of each condition displayed by channel on the channels topography) on the brain response following **finger stimulation** in the standard (blue) and inverse (red) position.

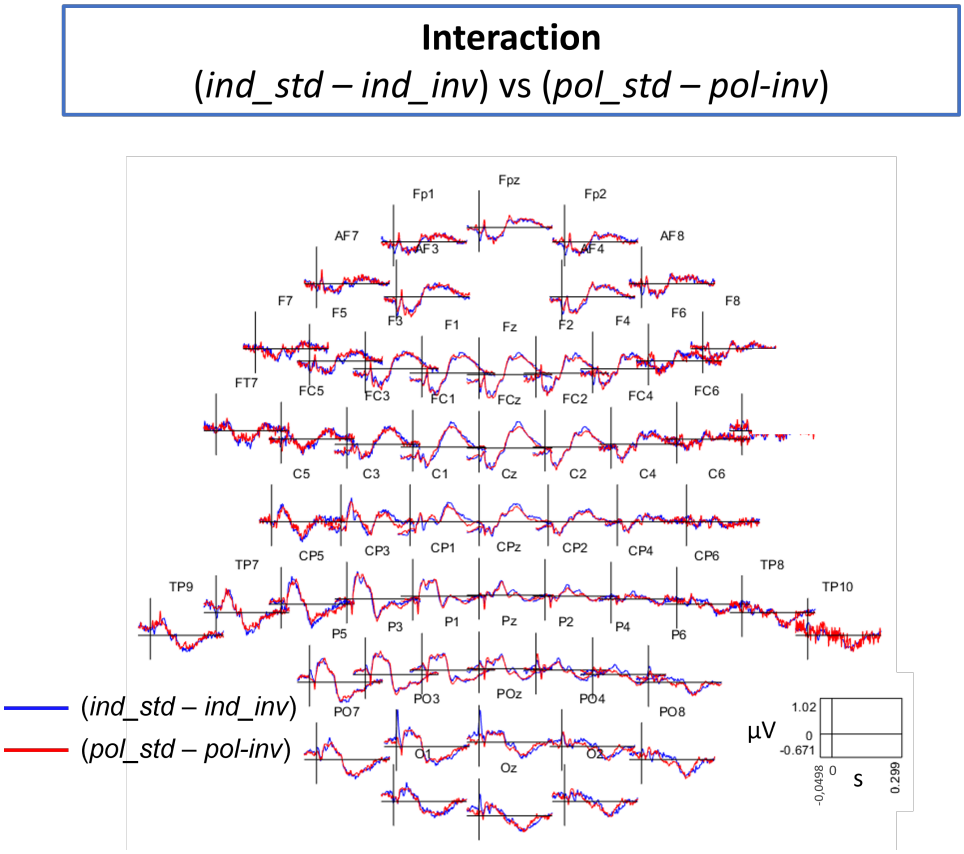

Figure 5.13: Multiplot of the **interaction effect** (GA of each condition displayed by channel on the channels topography). on the brain response following **finger stimulation** in the standard (blue) and inverse (red) position.

Median : Standard VS Inverse			
Positive Clusters		Negative Clusters	
p	t	p	t
0.230	288.216	0.163	-372.361
0.386	191.055	0.185	-333.386
0.394	187.008	0.676	-79.262
0.646	93.214	0.718	-70.662
0.947	29.831	0.957	-24.455
0.951	28.755	0.992	-14.895
0.969	22.301	0.993	-14.508
0.984	18.856	0.997	-10.175
0.986	18.403	0.998	-8.063
0.987	17.877	0.998	-7.974
0.998	13.593	1.000	-6.504
0.998	13.483		
0.999	8.380		
0.999	8.129		
0.999	7.606		
0.999	7.538		
0.999	7.217		

Table 5.1: Results of the cluster-based permutation analysis for the *POSTURE* effect on the amplitude of the ERP following median nerve stimulation. p and t are respectively the p-value and t-value of each cluster.

Finger : Index VS Thumb				Posture : Standard VS Inverse				Interaction : Finger*Posture			
Positive Clusters		Negative Clusters		Positive Clusters		Negative Clusters		Positive Clusters		Negative Clusters	
p	t	p	t	p	t	p	t	p	t	p	t
0.532	114.276	0.262	-225.248	0.717	67.907	0.441	-126.348	0.545	114.276	-225.248	0.243
0.650	86.246	0.992	-20.550	0.875	43.869	0.451	-124.364	0.681	86.246	-20.550	0.995
0.726	71.128	0.997	-16.338	0.915	37.392	0.633	-83.723	0.758	71.128	-16.338	0.995
0.860	48.749	0.997	-15.612	0.926	34.912	0.653	-79.557	0.875	48.749	-15.612	0.997
0.877	45.471	0.997	-14.881	0.966	25.701	0.726	-67.570	0.888	45.471	-14.881	0.998
0.936	33.244	0.997	-13.429	0.968	25.620	0.792	-57.057	0.960	33.244	-13.429	0.999
0.962	26.853	0.999	-10.427	0.993	16.144	0.792	-56.310	0.983	26.853	-10.427	1.000
0.983	20.974	1.000	-9.484	0.999	8.548	0.820	-51.882	0.993	20.974	-9.484	1.000
0.996	16.106	1.000	-9.046	0.999	8.165	0.930	-35.555	1.000	16.106	-9.046	1.000
0.996	15.912	1.000	-7.379	0.999	7.846	0.996	-16.203	1.000	15.912	-7.379	1.000
0.999	12.294	1.000	-7.320	0.999	7.680	1.000	-7.481	1.000	12.294	-7.320	1.000
0.999	10.359	1.000	-7.027	0.999	7.506			1.000	10.359	-7.027	1.000
0.999	9.815	1.000	-6.854	1.000	6.820			1.000	9.815	-6.854	1.000
1.000	7.729			1.000	6.728			1.000	7.729		
1.000	7.185							1.000	7.185		
1.000	7.026							1.000	7.026		
1.000	6.905							1.000	6.905		
1.000	6.834							1.000	6.834		

Table 5.2: Results of the cluster-based permutation analysis for the *FINGER* and *POSTURE* effects and their *INTERACTION* on the amplitude of the ERP following finger stimulation. p and t are respectively the p-value and t-value of each cluster.

Chapter 6

Conclusion

The present work proposes the development and validation of components of a novel platform which purpose is to be a comprehensive test bench for a wide range of in depth studies with healthy and amputated participants aimed at expanding knowledge on embodiment. The first component which has been designed is a sub-platform integrating virtual reality and infrared-based motion capture into a virtual reality environment. In the first chapter, we presented its hardware and software development and the preliminary feasibility study of a virtual hand illusion paradigm with an elongated virtual forearm through the developed platform. The results of the feasibility study were in line with the existing literature and it was therefore decided to proceed and use the platform for further studies on embodiment and the body schema.
Indeed, we presented in the second chapter a study ran with a high number of participants on the embodiment of an elongated arm through a virtual hand illusion paradigm and its effect on the tactile distance perception, which modification is a sign of body schema alteration. Results of the study showed that the elongation of a virtual forearm experienced in a first-person perspective in a virtual environment increases the tactile distance perception on the corresponding real forearm. However, even though the embodiment illusion over the virtual hand was perceived, we did not find any effect of the synchronicity of the virtual hand illusion paradigm on the effective modification of the tactile distance perception. This might suggest that in our study, the visual feedback in a first-person perspective of the elongated forearm was strong enough to elicit its embodiment and thus a modification of the body schema. Thus, embodiment of a virtual limb with the developed platform is effective and modifies the body schema, but further investigation

is needed to understand the respective weight of the different sensorimotor modalities in the multisensory integration responsible for the embodiment in virtual environments.
With the objective to understand in details the brain areas to stimulate and the neuromodulation paradigms necessary to enhance the embodiment, we presented in the third chapter the development of a robot-aided TMS platform integrating infrared-based motion tracking, a graphical user interface and a seven-degrees-of-freedom robot holding the TMS coil. We successively presented the validation of the functioning of the platform through a study of the performances of three control approaches aimed at compensating for subjects' movement during experimentation in order to keep the coil on the stimulation hotspot during dynamic tasks while ensuring subjects complete safety. The robot-aided TMS platform was successfully tested and we settled that the hybrid control approach would best fit dynamical tasks targeting a single hotspot whereas the selective impedance control would best fit dynamical tasks in which several hotspots have to be successively stimulated.
Finally, monitoring the brain activity during embodiment experimentation would give important clues on how and when this process takes place in the human brain. Hence, the author developed hands-on knowledge on electroencephalographic monitoring of the brain activity through a electrophysiologic study of a preferred hand posture in the body schema, addressed in the forth and last chapter.

Taking a step back, two sub-components of the desired platform have been independently developed and validated, and the third subcomponent has been studied. The future work is plural. On one side, additional features of the robot-aided TMS platform can be developed towards a more autonomous functioning of the TMS administration. Secondly, a realistic and adaptive virtual model of a hand prosthesis should be implemented to more directly act of its features and study the following modulation of its embodiment. Finally, the main future project is to integrate together the so far independent components and to validate the resulting platform through a comprehensive experimental study. This study could investigate in a virtual environment the weight of vision, agency, tactile feedback and of their interactions in the multisensory integration process responsible for the embodiment, stimulating the related brain areas in Sham and real stimulation conditions while monitoring the resulting brain activity.

Bibliography

[1] Matthew R Longo. "Types of body representation". In: *Perceptual and emotional embodiment*. Routledge, 2015, pp. 125–142.

[2] Frédérique De Vignemont. "Body schema and body image—Pros and cons". In: *Neuropsychologia* 48.3 (2010), pp. 669–680.

[3] Matthew R Longo, Elena Azañón, and Patrick Haggard. "More than skin deep: body representation beyond primary somatosensory cortex". In: *Neuropsychologia* 48.3 (2010), pp. 655–668.

[4] Eric Stice and Heather E Shaw. "Role of body dissatisfaction in the onset and maintenance of eating pathology: A synthesis of research findings". In: *Journal of psychosomatic research* 53.5 (2002), pp. 985–993.

[5] Matthew R Longo and Patrick Haggard. "An implicit body representation underlying human position sense". In: *Proceedings of the National Academy of Sciences* 107.26 (2010), pp. 11727–11732.

[6] Matthew R Longo and Patrick Haggard. "Implicit body representations and the conscious body image". In: *Acta Psychologica* 141.2 (2012), pp. 164–168.

[7] Dennis R Proffitt and Sally A Linkenauger. "Perception viewed as a phenotypic expression". In: *Action science: Foundations of an emerging discipline* 171 (2013).

[8] Laurence R Harris, Michael J Carnevale, et al. "How our body influences our perception of the world". In: *Frontiers in psychology* 6 (2015), p. 819.

[9] Marianne L Simmel. "On phantom limbs". In: *AMA Archives of Neurology & Psychiatry* 75.6 (1956), pp. 637–647.

[10] Troels S Jensen, Børge Krebs, et al. "Immediate and long-term phantom limb pain in amputees: incidence, clinical characteristics and relationship to pre-amputation limb pain". In: *Pain* 21.3 (1985), pp. 267–278.

[11] Søren Bach, Morten F Noreng, and Niels U Tjéllden. "Phantom limb pain in amputees during the first 12 months following limb amputation, after preoperative lumbar epidural blockade". In: *Pain* 33.3 (1988), pp. 297–301.

[12] Herta Flor, Thomas Elbert, et al. "Phantom-limb pain as a perceptual correlate of cortical reorganization following arm amputation". In: *Nature* 375.6531 (1995), pp. 482–484.

[13] Herta Flor. "Phantom-limb pain: characteristics, causes, and treatment". In: *The Lancet Neurology* 1.3 (2002), pp. 182–189.

[14] Herta Flor. "Maladaptive plasticity, memory for pain and phantom limb pain: review and suggestions for new therapies". In: *Expert review of neurotherapeutics* 8.5 (2008), pp. 809–818.

[15] Lone Nikolajsen and Kristian Friesgaard Christensen. "Phantom limb pain". In: *Nerves and Nerve Injuries* (2015), pp. 23–34.

[16] Olga Horgan and Malcolm MacLachlan. "Psychosocial adjustment to lower-limb amputation: a review". In: *Disability and rehabilitation* 26.14-15 (2004), pp. 837–850.

[17] Nicolas Burden, Jane Simpson, et al. "Prosthesis use is associated with reduced physical self-disgust in limb amputees". In: *Body image* 27 (2018), pp. 109–117.

[18] Vilayanur S Ramachandran and Diane Rogers-Ramachandran. "Synaesthesia in phantom limbs induced with mirrors". In: *Proceedings of the Royal Society of London. Series B: Biological Sciences* 263.1369 (1996), pp. 377–386.

[19] Vilayanur S Ramachandran and William Hirstein. "The perception of phantom limbs. The DO Hebb lecture." In: *Brain: a journal of neurology* 121.9 (1998), pp. 1603–1630.

[20] *REstoring the Self with embodiable HAnd ProsthesEs*. 2016. URL: `https://cordis.europa.eu/project/id/678908`.

[21] Cody L McDonald, Sarah Westcott-McCoy, et al. "Global prevalence of traumatic non-fatal limb amputation". In: *Prosthetics and orthotics international* (2021), p. 0309364620972258.

[22] Alan J Thurston. "Paré and prosthetics: the early history of artificial limbs". In: *ANZ journal of surgery* 77.12 (2007), pp. 1114–1119.

[23] TL Wellerson. "Historical development of upper extremity prosthetics". In: *Orthop Prosthet Appl J* 11.3 (1957), pp. 73–77.

[24] Dudley S Childress. "Historical aspects of powered limb prostheses". In: *Clin Prosthet Orthot* 9.1 (1985), pp. 2–13.

[25] B Popov. "The bio-electrically controlled prosthesis". In: *The Journal of Bone and Joint Surgery. British volume* 47.3 (1965), pp. 421–424.

[26] Robert N Scott. "Myoelectric control of prostheses and orthoses". In: *Bull. Prosthet. Res* 7 (1967), p. 93.

[27] Samreen Hussain, Sarmad Shams, and Saad Jawaid Khan. "Impact of medical advancement: Prostheses". In: *Computer Architecture in Industrial, Biomechanical and Biomedical Engineering* (2019), p. 9.

[28] Oluwarotimi Williams Samuel, Mojisola Grace Asogbon, et al. "Intelligent EMG pattern recognition control method for upper-limb multifunctional prostheses: advances, current challenges, and future prospects". In: *Ieee Access* 7 (2019), pp. 10150–10165.

[29] Max Ortiz-Catalan, Bo Håkansson, and Rickard Brånemark. "An osseointegrated human-machine gateway for long-term sensory feedback and motor control of artificial limbs". In: *Science translational medicine* 6.257 (2014), 257re6–257re6.

[30] Laura A Miller, Robert D Lipschutz, et al. "Control of a six degree of freedom prosthetic arm after targeted muscle reinnervation surgery". In: *Archives of physical medicine and rehabilitation* 89.11 (2008), pp. 2057–2065.

[31] E. A. Biddiss and T. T. Chau. "Upper limb prosthesis use and abandonment: A survey of the last 25 years". In: *Prosthetics and Orthotics International* 31.3 (2007), pp. 236–257. DOI: 10.1080/03093640600994581.

[32] Francesca Cordella, Anna Lisa Ciancio, et al. "Literature review on needs of upper limb prosthesis users". In: *Frontiers in neuroscience* 10 (2016), p. 209.

[33] Lauren C Smail, Chantelle Neal, et al. "Comfort and function remain key factors in upper limb prosthetic abandonment: findings of a scoping review". In: *Disability and rehabilitation: Assistive technology* 16.8 (2021), pp. 821–830.

[34] Craig D Murray. “An interpretative phenomenological analysis of the embodiment of artificial limbs”. In: *Disability and rehabilitation* 26.16 (2004), pp. 963–973.

[35] Craig D Murray. “Embodiment and prosthetics”. In: *Psychoprosthetics*. Springer, 2008, pp. 119–129.

[36] Matthew R Longo, Friederike Schüür, et al. “What is embodiment? A psychometric approach”. In: *Cognition* 107.3 (2008), pp. 978–998.

[37] Niclas Braun, Stefan Debener, et al. “The senses of agency and ownership: a review”. In: *Frontiers in psychology* 9 (2018), p. 535.

[38] Jared Medina, Priya Khurana, and H Branch Coslett. “The influence of embodiment on multisensory integration using the mirror box illusion”. In: *Consciousness and cognition* 37 (2015), pp. 71–82.

[39] Manos Tsakiris. “The multisensory basis of the self: from body to identity to others”. In: *The Quarterly Journal of Experimental Psychology* 70.4 (2017), pp. 597–609.

[40] Chandramouli Chandrasekaran. “Computational principles and models of multisensory integration”. In: *Current opinion in neurobiology* 43 (2017), pp. 25–34.

[41] K Carrie Armel and Vilayanur S Ramachandran. “Projecting sensations to external objects: evidence from skin conductance response”. In: *Proceedings of the Royal Society of London. Series B: Biological Sciences* 270.1523 (2003), pp. 1499–1506.

[42] Melita J Giummarra, Stephen J Gibson, et al. “Mechanisms underlying embodiment, disembodiment and loss of embodiment”. In: *Neuroscience & Biobehavioral Reviews* 32.1 (2008), pp. 143–160.

[43] Lee D Walsh, G Lorimer Moseley, et al. “Proprioceptive signals contribute to the sense of body ownership”. In: *The Journal of physiology* 589.12 (2011), pp. 3009–3021.

[44] Andreas Kalckert and H Henrik Ehrsson. “Moving a rubber hand that feels like your own: a dissociation of ownership and agency”. In: *Frontiers in human neuroscience* 6 (2012), p. 40.

[45] Simona Crea, Marco D’Alonzo, et al. “The rubber foot illusion”. In: *Journal of NeuroEngineering and Rehabilitation* 12.1 (2015), pp. 1–6.

[46] Giovanni Di Pino, Daniele Romano, et al. “Sensory-and action-oriented embodiment of neurally-interfaced robotic hand prostheses”. In: *Frontiers in Neuroscience* 14 (2020), p. 389.

[47] M Pinardi, F Ferrari, et al. "Doublecheck: a sensory confirmation is required to own a robotic hand, sending a command to feel in charge of it". In: *Cognitive Neuroscience* 11.4 (2020), pp. 216–228.

[48] Matthew Botvinick and Jonathan Cohen. "Rubber hands 'feel'touch that eyes see". In: *Nature* 391.6669 (1998), pp. 756–756.

[49] Paul D Marasco, Keehoon Kim, et al. "Robotic touch shifts perception of embodiment to a prosthesis in targeted reinnervation amputees". In: *Brain* 134.3 (2011), pp. 747–758.

[50] Stanisa Raspopovic, Marco Capogrosso, et al. "Restoring natural sensory feedback in real-time bidirectional hand prostheses". In: *Science translational medicine* 6.222 (2014), 222ra19–222ra19.

[51] Tamar R Makin, Frederique de Vignemont, and A Aldo Faisal. "Neurocognitive barriers to the embodiment of technology". In: *Nature Biomedical Engineering* 1.1 (2017), pp. 1–3.

[52] Fiona MZ Van den Heiligenberg, Tanya Orlov, et al. "Artificial limb representation in amputees". In: *Brain* 141.5 (2018), pp. 1422–1433.

[53] Marco D'Alonzo, Francesco Clemente, and Christian Cipriani. "Vibrotactile stimulation promotes embodiment of an alien hand in amputees with phantom sensations". In: *IEEE Transactions on Neural Systems and Rehabilitation Engineering* 23.3 (2014), pp. 450–457.

[54] Giovanni Di Pino, Angelo Maravita, et al. "Augmentation-related brain plasticity". In: *Frontiers in systems neuroscience* 8 (2014), p. 109.

[55] Konstantina Kilteni, Raphaela Groten, and Mel Slater. "The sense of embodiment in virtual reality". In: *Presence: Teleoperators and Virtual Environments* 21.4 (2012), pp. 373–387.

[56] M D'Alonzo, A Mioli, et al. "Different level of virtualization of sight and touch produces the uncanny valley of avatar's hand embodiment". In: *Scientific reports* 9.1 (2019), pp. 1–11.

[57] Craig D Murray, Emma L Patchick, et al. "Can immersive virtual reality reduce phantom limb pain". In: *Stud Health Technol Inform* 119 (2006), pp. 407–12.

[58] Michihiro Osumi, Kazunori Inomata, et al. "Characteristics of phantom limb pain alleviated with virtual reality rehabilitation". In: *Pain Medicine* 20.5 (2019), pp. 1038–1046.

[59] Craig D Murray, Emma Patchick, et al. “Immersive virtual reality as a rehabilitative technology for phantom limb experience: a protocol”. In: *CyberPsychology & Behavior* 9.2 (2006), pp. 167–170.

[60] Craig D Murray, Stephen Pettifer, et al. “The treatment of phantom limb pain using immersive virtual reality: three case studies”. In: *Disability and rehabilitation* 29.18 (2007), pp. 1465–1469.

[61] Jonathan Cole, Simon Crowle, et al. “Exploratory findings with virtual reality for phantom limb pain; from stump motion to agency and analgesia”. In: *Disability and rehabilitation* 31.10 (2009), pp. 846–854.

[62] Naoki Wake, Yuko Sano, et al. “Multimodal virtual reality platform for the rehabilitation of phantom limb pain”. In: *2015 7th International IEEE/EMBS Conference on Neural Engineering (NER)*. IEEE. 2015, pp. 787–790.

[63] M Osumi, A Ichinose, et al. “Restoring movement representation and alleviating phantom limb pain through short-term neurorehabilitation with a virtual reality system”. In: *European journal of pain* 21.1 (2017), pp. 140–147.

[64] Justin Dunn, Elizabeth Yeo, et al. “Virtual and augmented reality in the treatment of phantom limb pain: A literature review”. In: *NeuroRehabilitation* 40.4 (2017), pp. 595–601.

[65] Elisabetta Ambron, Alexander Miller, et al. “Immersive low-cost virtual reality treatment for phantom limb pain: Evidence from two cases”. In: *Frontiers in neurology* 9 (2018), p. 67.

[66] Thomas Rutledge, Deborah Velez, et al. “A virtual reality intervention for the treatment of phantom limb pain: development and feasibility results”. In: *Pain Medicine* 20.10 (2019), pp. 2051–2059.

[67] Patrice L Weiss, Rachel Kizony, et al. “Virtual reality in neurorehabilitation”. In: *Textbook of neural repair and rehabilitation* 51.8 (2006), pp. 182–97.

[68] Thais Massetti, Talita Dias Da Silva, et al. “The clinical utility of virtual reality in neurorehabilitation: a systematic review”. In: *Journal of central nervous system disease* 10 (2018), p. 1179573518813541.

[69] Giovanni Di Pino, Alessandro Mioli, et al. “Embodying an artificial hand increases blood flow to the investigated limb”. In: *Open Research Europe* 1 (2022), p. 55.

[70] H Henrik Ehrsson, Charles Spence, and Richard E Passingham. "That's my hand! Activity in premotor cortex reflects feeling of ownership of a limb". In: *Science* 305.5685 (2004), pp. 875–877.

[71] H Henrik Ehrsson, Nicholas P Holmes, and Richard E Passingham. "Touching a rubber hand: feeling of body ownership is associated with activity in multisensory brain areas". In: *Journal of neuroscience* 25.45 (2005), pp. 10564–10573.

[72] Patrick Haggard. "Sense of agency in the human brain". In: *Nature Reviews Neuroscience* 18.4 (2017), pp. 196–207.

[73] Bilal Alchalabi, Jocelyn Faubert, and David R Labbe. "EEG can Be used to measure embodiment when controlling a walking self-avatar". In: *2019 IEEE Conference on Virtual Reality and 3D User Interfaces (VR)*. IEEE. 2019, pp. 776–783.

[74] Li Ding, Jiayuan He, et al. "Mirror visual feedback combining vibrotactile stimulation promotes embodiment perception: an Electroencephalogram (EEG) pilot study". In: *Frontiers in Bioengineering and Biotechnology* 8 (2020), p. 553270.

[75] Filip Škola and Fotis Liarokapis. "Study of full-body virtual embodiment using noninvasive brain stimulation and imaging". In: *International Journal of Human–Computer Interaction* 37.12 (2021), pp. 1116–1129.

[76] Anthony T Barker, Reza Jalinous, and Ian L Freeston. "Non-invasive magnetic stimulation of human motor cortex". In: *The Lancet* 325.8437 (1985), pp. 1106–1107.

[77] Colleen K Loo and Philip B Mitchell. "A review of the efficacy of transcranial magnetic stimulation (TMS) treatment for depression, and current and future strategies to optimize efficacy". In: *Journal of affective disorders* 88.3 (2005), pp. 255–267.

[78] Giovanni Di Pino, Giovanni Pellegrino, et al. "Modulation of brain plasticity in stroke: a novel model for neurorehabilitation". In: *Nature Reviews Neurology* 10.10 (2014), pp. 597–608.

[79] Marjolein PM Kammers, Lennart Verhagen, et al. "Is this hand for real? Attenuation of the rubber hand illusion by transcranial magnetic stimulation over the inferior parietal lobule". In: *Journal of cognitive neuroscience* 21.7 (2009), pp. 1311–1320.

[80] Davide Crivelli and Michela Balconi. "The agent brain: a review of non-invasive brain stimulation studies on sensing agency". In: *Frontiers in Behavioral Neuroscience* 11 (2017), p. 229.

[81] Michela Bassolino, Matteo Franza, et al. "Non-invasive brain stimulation of motor cortex induces embodiment when integrated with virtual reality feedback". In: *European Journal of Neuroscience* 47.7 (2018), pp. 790–799.

[82] URL: `https://psychscenehub.com/psychinsights/transcranial-magnetic-stimulation-for-depression/`.

[83] Sotaro Shimada, Kensuke Fukuda, and Kazuo Hiraki. "Rubber hand illusion under delayed visual feedback". In: *PloS one* 4.7 (2009), e6185.

[84] Marjolein PM Kammers, Frederique de Vignemont, et al. "The rubber hand illusion in action". In: *Neuropsychologia* 47.1 (2009), pp. 204–211.

[85] Henning Holle, Neil McLatchie, et al. "Proprioceptive drift without illusions of ownership for rotated hands in the "rubber hand illusion" paradigm". In: *Cognitive neuroscience* 2.3-4 (2011), pp. 171–178.

[86] Anne M Aimola Davies, Rebekah C White, and Martin Davies. "Spatial limits on the nonvisual self-touch illusion and the visual rubber hand illusion: subjective experience of the illusion and proprioceptive drift". In: *Consciousness and Cognition* 22.2 (2013), pp. 613–636.

[87] Harriet Dempsey-Jones and Ada Kritikos. "Handedness modulates proprioceptive drift in the rubber hand illusion". In: *Experimental brain research* 237.2 (2019), pp. 351–361.

[88] Andreas Kalckert, A Perera, et al. "Rubber hands in space: the role of distance and relative position in the rubber hand illusion". In: *Experimental Brain Research* 237.7 (2019), pp. 1821–1832.

[89] Mel Slater, Daniel Pérez Marcos, et al. "Towards a digital body: the virtual arm illusion". In: *Frontiers in human neuroscience* (2008), p. 6.

[90] Ke Ma and Bernhard Hommel. "The role of agency for perceived ownership in the virtual hand illusion". In: *Consciousness and cognition* 36 (2015), pp. 277–288.

[91] Bigna Lenggenhager, Tej Tadi, et al. "Video ergo sum: manipulating bodily self-consciousness". In: *Science* 317.5841 (2007), pp. 1096–1099.

[92] Maria V Sanchez-Vives, Bernhard Spanlang, et al. "Virtual hand illusion induced by visuomotor correlations". In: *PloS one* 5.4 (2010), e10381.

[93] Ye Yuan and Anthony Steed. "Is the rubber hand illusion induced by immersive virtual reality?" In: *2010 IEEE Virtual Reality Conference (VR)*. IEEE. 2010, pp. 95–102.

[94] Ke Ma and Bernhard Hommel. "The virtual-hand illusion: effects of impact and threat on perceived ownership and affective resonance". In: *Frontiers in psychology* 4 (2013), p. 604.

[95] Mel Slater, Bernhard Spanlang, et al. "First person experience of body transfer in virtual reality". In: *PloS one* 5.5 (2010), e10564.

[96] Martin Riemer, Jörg Trojan, et al. "The rubber hand universe: On the impact of methodological differences in the rubber hand illusion". In: *Neuroscience & Biobehavioral Reviews* 104 (2019), pp. 268–280.

[97] Konstantina Kilteni, Jean-Marie Normand, et al. "Extending body space in immersive virtual reality: a very long arm illusion". In: *PloS one* 7.7 (2012), e40867.

[98] Ian P Howard, Brian J Rogers, et al. *Binocular vision and stereopsis*. Oxford University Press, USA, 1995.

[99] *Vive Specs*. 2022. URL: `https://developer.vive.com/resources/hardware-guides/vive-specs-user-guide/`.

[100] Diederick C Niehorster, Li Li, and Markus Lappe. "The accuracy and precision of position and orientation tracking in the HTC vive virtual reality system for scientific research". In: *i-Perception* 8.3 (2017), p. 2041669517708205.

[101] Miguel Borges, Andrew Symington, et al. "HTC vive: Analysis and accuracy improvement". In: *2018 IEEE/RSJ International Conference on Intelligent Robots and Systems (IROS)*. IEEE. 2018, pp. 2610–2615.

[102] Gergely Nagymáté and Rita M Kiss. "Application of OptiTrack motion capture systems in human movement analysis: A systematic literature review". In: *Recent Innovations in Mechatronics* 5.1. (2018), pp. 1–9.

[103] *Optitrack 13W Specs*. 2022. URL: `https://optitrack.com/cameras/primex-13w/specs.html`.

[104] *LeapMotion Specs*. 2022. URL: `https://www.ultraleap.com/datasheets/Leap_Motion_Controller_Datasheet.pdf`.

[105] *Optitrack Unity Plugin*. 2022. URL: https://optitrack.com/support/downloads/plugins.html#unity-plugin.

[106] *Leap Motion Unity Plugin*. 2022. URL: https://developer.leapmotion.com/releases/core-assets-434-wpszx-mmgl5.

[107] *SteamVR Unity Plugin*. 2022. URL: https://valvesoftware.github.io/steamvr_unity_plugin/.

[108] Marco D'Alonzo and Christian Cipriani. "Vibrotactile sensory substitution elicits feeling of ownership of an alien hand". In: *PloS one* 7.11 (2012), e50756.

[109] H. E. Ross and D. J. Murray. *E.H. Weber on the Tactile Senses*. 2nd ed. Psychology Press, 1996. DOI: 10.4324/9781315782089.

[110] S. Weinstein. "Intensive and extensive aspects of tactile sensitivity as a function of body part, sex and laterality". In: *The skin senses* (1968), pp. 195–222.

[111] Barry G Green. "The perception of distance and location for dual tactile pressures". In: *Perception & Psychophysics* 31.4 (1982), pp. 315–323.

[112] Andrea Serino and Patrick Haggard. "Touch and the body". In: *Neuroscience & Biobehavioral Reviews* 34.2 (2010), pp. 224–236.

[113] Daniele Romano, Alessandro Mioli, et al. "Behavioral and Physiological Evidence of a favored Hand Posture in the Body Representation for Action". In: *Cerebral Cortex* 31.7 (2021), pp. 3299–3310.

[114] Marisa Taylor-Clarke, Pamela Jacobsen, and Patrick Haggard. "Keeping the world a constant size: Object constancy in human touch". In: *Nature neuroscience* 7.3 (2004), pp. 219–220.

[115] James R Lackner. "Some proprioceptive influences on the perceptual representation of body shape and orientation". In: *Brain* 111.2 (1988), pp. 281–297.

[116] Frédérique De Vignemont, Henrik H Ehrsson, and Patrick Haggard. "Bodily illusions modulate tactile perception". In: *Current Biology* 15.14 (2005), pp. 1286–1290.

[117] Nicola Bruno and Marco Bertamini. "Haptic perception after a change in hand size". In: *Neuropsychologia* 48.6 (2010), pp. 1853–1856.

[118] Björn Van Der Hoort, Arvid Guterstam, and H Henrik Ehrsson. "Being Barbie: the size of one's own body determines the perceived size of the world". In: *PloS one* 6.5 (2011), e20195.

[119] Zakaryah Abdulkarim and H Henrik Ehrsson. "No causal link between changes in hand position sense and feeling of limb ownership in the rubber hand illusion". In: *Attention, Perception, & Psychophysics* 78.2 (2016), pp. 707–720.

[120] Maria Pyasik, Gaetano Tieri, and Lorenzo Pia. "Visual appearance of the virtual hand affects embodiment in the virtual hand illusion". In: *Scientific reports* 10.1 (2020), pp. 1–11.

[121] Marieke Rohde, Massimiliano Di Luca, and Marc O Ernst. "The rubber hand illusion: feeling of ownership and proprioceptive drift do not go hand in hand". In: *PloS one* 6.6 (2011), e21659.

[122] D. Pérez-Marcos, M.V Sanchez-Vives, and M. Slater. "Is my hand connected to my body? The impact of body continuity and arm alignment on the virtual hand illusion". In: *Cognitive Neurodynamics* 6 (2012), pp. 295–305. DOI: 10.1007/s11571-011-9178-5.

[123] Sally A Linkenauger, Markus Leyrer, et al. "Welcome to wonderland: The influence of the size and shape of a virtual hand on the perceived size and shape of virtual objects". In: *PloS one* 8.7 (2013), e68594.

[124] Antonella Maselli and Mel Slater. "The building blocks of the full body ownership illusion". In: *Frontiers in human neuroscience* 7 (2013), p. 83.

[125] Enea Francesco Pavone, Gaetano Tieri, et al. "Embodying others in immersive virtual reality: electro-cortical signatures of monitoring the errors in the actions of an avatar seen from a first-person perspective". In: *Journal of Neuroscience* 36.2 (2016), pp. 268–279.

[126] Gaetano Tieri, Emmanuele Tidoni, et al. "Mere observation of body discontinuity affects perceived ownership and vicarious agency over a virtual hand". In: *Experimental brain research* 233.4 (2015), pp. 1247–1259.

[127] Giuseppe Spinelli, Gaetano Tieri, et al. "Wronger than wrong: Graded mapping of the errors of an avatar in the performance monitoring system of the onlooker". In: *NeuroImage* 167 (2018), pp. 1–10.

[128] Pierre Bourdin, Matteo Martini, and Maria V Sanchez-Vives. "Altered visual feedback from an embodied avatar unconsciously influences movement amplitude and muscle activity". In: *Scientific Reports* 9.1 (2019), pp. 1–9.

[129] Zakaryah Abdulkarim, Zineb Hayatou, and H Henrik Ehrsson. "Sustained rubber hand illusion after the end of visuotactile stimulation with a similar time course for the reduction of subjective ownership and proprioceptive drift". In: *Experimental brain research* 239.12 (2021), pp. 3471–3486.

[130] Frédérique De Vignemont. "Embodiment, ownership and disownership". In: *Consciousness and cognition* 20.1 (2011), pp. 82–93.

[131] Daniele Romano, Elisa Caffa, et al. "The robot hand illusion: Inducing proprioceptive drift through visuo-motor congruency". In: *Neuropsychologia* 70 (2015), pp. 414–420.

[132] Noel Segura Meraz, Masafumi Sobajima, et al. "Modification of body schema by use of extra robotic thumb". In: *Robomech Journal* 5.1 (2018), pp. 1–8.

[133] R. Sparing, D. Buelte, et al. "Effects of coil orientation on the electric field induced by TMS over the hand motor area". In: *Human Brain Mapping* 29.1 (2008), pp. 82–96. DOI: 10.1002/hbm.20360.

[134] I. Laakso, A. Hirata, and Y. Ugawa. "Effects of coil orientation on the electric field induced by TMS over the hand motor area". In: *Physics in Medicine and Biology* 59.1 (2014), pp. 203–218.

[135] L. Richter, G. Neumann, et al. "Optimal Coil Orientation for Transcranial Magnetic Stimulation". In: *PLOS ONE* 8.4 (2013), e60358. DOI: 10.1371/journal.pone.0060358.

[136] J. Gomez-Tames, A. Hamasaka, et al. "Atlas of optimal coil orientation and position for TMS: A computational study". In: *Brain Stimulation* 11.4 (2018), pp. 839–848.

[137] A. A. de Goede, E. M. Ter Braack, and M. van Putten. "Accurate Coil Positioning is Important for Single and Paired Pulse TMS on the Subject Level". In: *Brain topography* 31.6 (2018), pp. 917–930. DOI: 10.1007/s10548-018-0655-6.

[138] J. Ruohonen and J. Karhu. "Navigated transcranial magnetic stimulation". In: *Neurophysiologie Clinique/Clinical Neurophysiology* 40.1 (2010), pp. 7–17.

[139] B. Langguth, T. Kleinjung, et al. "rTMS for the treatment of tinnitus: The role of neuronavigation for coil positioning". In: *Neurophysiologie Clinique/Clinical Neurophysiology* 40.1 (2010), pp. 45–58.

[140] A. T. Sack, R. C. Kadosh, et al. "Optimizing Functional Accuracy of TMS in Cognitive Studies: A Comparison of Methods". In: *Journal of Cognitive Neuroscience* 21.2 (2009), pp. 207–221.

[141] J. L. Lancaster, S. Narayana, et al. "Evaluation of an image-guided, robotically positioned transcranial magnetic stimulation system". In: *Human brain mapping* 22.4 (2004), pp. 329–340.

[142] C. Lebossé, P. Renaud, et al. "A robotic system for automated image-guided transcranial magnetic stimulation". In: *2007 IEEE/NIH Life Science Systems and Applications Workshop*. IEEE. 2007, pp. 55–58.

[143] L. Zorn, P. Renaud, et al. "Design and evaluation of a robotic system for transcranial magnetic stimulation". In: *IEEE Transactions on Biomedical Engineering* 59.3 (2011), pp. 805–815.

[144] Romuald Ginhoux, Pierre Renaud, et al. "A custom robot for transcranial magnetic stimulation: first assessment on healthy subjects". In: *2013 35th Annual International Conference of the IEEE Engineering in Medicine and Biology Society (EMBC)*. IEEE. 2013, pp. 5352–5355.

[145] J. Meincke, M. Hewitt, et al. "Automated TMS hotspot-hunting using a closed loop threshold-based algorithm". In: *NeuroImage* 124.Pt.4 (2016), pp. 509–517. DOI: /10.1016/j.neuroimage.2015.09.013.

[146] S. Harquel, J. Diard, et al. "Automatized set-up procedure for transcranial magnetic stimulation protocols". In: *NeuroImage* 153 (2017), pp. 307–318. DOI: 10.1016/j.neuroimage.2017.04.001.

[147] URL: https://www.ant-neuro.com/products/smartmove.

[148] URL: http://www.axilumrobotics.com/en/tms-robot.

[149] URL: http://www.ying-chi.net/en/Product/index/cid/25.html.

[150] A. Noccaro, L. Raiano, et al. "Evaluation of Hand-Eye and Robot-World Calibration Algorithms for TMS Application". In: *2018 7th IEEE International Conference on Biomedical Robotics and Biomechatronics (Biorob)* (2018), pp. 1115–1119. DOI: 10.1109/BIOROB.2018.8487930.

[151] A. Noccaro, A. Mioli, et al. "Development and Validation of a Novel Calibration Methodology and Control Approach for Robot-Aided Transcranial Magnetic Stimulation (TMS)". In: *IEEE Transactions on Biomedical Engineering* 68.5 (2021), pp. 1589–1600.

[152] J. Rodseth, E. P. Washabaugh, and C. Krishnan. “A novel low-cost approach for navigated transcranial magnetic stimulation”. In: *Restorative neurology and neuroscience* 35.6 (2017), pp. 601–609.

[153] N. Hogan. “Impedance control: An approach to manipulation: Part I—Theory”. In: (1985).

[154] O. Khatib. “A unified approach for motion and force control of robot manipulators: The operational space formulation”. In: *IEEE Journal on Robotics and Automation* 3.1 (1987), pp. 43–53.

[155] V. Ortenzi, R. Stolkin, et al. “Hybrid motion/force control: a review”. In: *Advanced Robotics* 31.19-20 (2017), pp. 1102–1113.

[156] W.N.W. Zakaria, R. Tomari, and R. Ngadengon. “Active Head Motion Compensation of TMS Robotic System Using Neuro-Fuzzy Estimation”. In: *MATEC Web of Conferences* 56 (2016), p. 07001.

[157] L. Richter, L. Matthäus, and A. Schlaefer A.and Schweikard. “Fast robotic compensation of spontaneous head motion during Transcranial Magnetic Stimulation (TMS)”. In: *IET Conference Proceedings* (2010), pp. 872–877.

[158] E. Hirasaki, S. T. Moore, et al. “Effects of walking velocity on vertical head and body movements during locomotion”. In: *Experimental brain research* 127.2 (1999), pp. 117–130.

[159] Henry Head and Gordon Holmes. “Sensory disturbances from cerebral lesions”. In: *Brain* 34.2-3 (1911), pp. 102–254.

[160] Daniele Romano, Luigi Tamè, et al. “The standard posture of the hand.” In: *Journal of Experimental Psychology: Human Perception and Performance* 45.9 (2019), p. 1164.

[161] Ronald Melzack and PR Bromage. “Experimental phantom limbs”. In: *Experimental neurology* 39.2 (1973), pp. 261–269.

[162] Philip R Bromage and Ronald Melzack. “Phantom limbs and the body schema”. In: *Canadian Anaesthetists’ Society Journal* 21.3 (1974), pp. 267–274.

[163] Shinya Yamamoto and Shigeru Kitazawa. “Reversal of subjective temporal order due to arm crossing”. In: *Nature neuroscience* 4.7 (2001), pp. 759–765.

[164] Alyanne M De Haan, Helen A Anema, and H Chris Dijkerman. “Fingers crossed! An investigation of somatotopic representations using spatial directional judgements”. In: (2012).

[165] Tobias Heed, Jenny Backhaus, and Brigitte Röder. "Integration of hand and finger location in external spatial coordinates for tactile localization." In: *Journal of Experimental Psychology: Human Perception and Performance* 38.2 (2012), p. 386.

[166] Elena Azañón and Salvador Soto-Faraco. "Changing reference frames during the encoding of tactile events". In: *Current biology* 18.14 (2008), pp. 1044–1049.

[167] Krista E Overvliet, E Azañón, and Salvador Soto-Faraco. "Somatosensory saccades reveal the timing of tactile spatial remapping". In: *Neuropsychologia* 49.11 (2011), pp. 3046–3052.

[168] Daniele Romano, Francesco Marini, and Angelo Maravita. "Standard body-space relationships: Fingers hold spatial information". In: *Cognition* 165 (2017), pp. 105–112.

[169] L. R. Krol. *EEG electrode positions in the 10-10 system using modified combinatorial nomenclature, along with the fiducials and associated lobes of the brain.* 2020. URL: https://en.wikipedia.org/wiki/10%5C%E2%5C%80%5C%9320_system_(EEG)#/media/File:EEG_10-10_system_with_additional_information.svg.

[170] G. H. Klem. "The ten-twenty electrode system of the international federation. the internanional federation of clinical nenrophysiology". In: *Electroencephalogr. Clin. Neurophysiol. Suppl.* 52 (1999), pp. 3–6. URL: https://ci.nii.ac.jp/naid/10030008057/en/.

[171] F. Tadel, S. Baillet, et al. "Brainstorm: A User-Friendly Application for MEG/EEG Analysis". In: *Computational Intelligence and Neuroscience* 2011 (2011), p. 13. DOI: https://doi.org/10.1155/2011/879716.

[172] K. C. McGill, K. L. Cummins, et al. "On the Nature and Elimination of Stimulus Artifact in Nerve Signals Evoked and Recorded Using Surface Electrodes". In: *IEEE Transactions on Biomedical Engineering* BME-29.2 (1982), pp. 129–137. DOI: 10.1109/TBME.1982.325019.

[173] L. McLean, R. N. Scott, and P. A. Parker. "Stimulus artifact reduction in evoked potential measurements". In: *Archives of Physical Medicine and Rehabilitation* 77.12 (1996), pp. 1286–1292. ISSN: 0003-9993. DOI: https://doi.org/10.1016/S0003-9993(96)90194-X.

[174] Soojin Lee, Martin J McKeown, et al. "Removal of high-voltage brain stimulation artifacts from simultaneous EEG recordings". In: *IEEE Transactions on Biomedical Engineering* 66.1 (2018), pp. 50–60.

[175] Andy Zhou, Benjamin C Johnson, and Rikky Muller. "Toward true closed-loop neuromodulation: artifact-free recording during stimulation". In: *Current opinion in neurobiology* 50 (2018), pp. 119–127.

[176] C. Jutten and J. Herault. "Blind separation of sources, part I: An adaptive algorithm based on neuromimetic architecture". In: *Signal Processing* 24.1 (1991), pp. 1–10. ISSN: 0165-1684. DOI: https://doi.org/10.1016/0165-1684(91)90079-X.

[177] S. Makeig, A.J. Bell, et al. "Independent component analysis of electroencephalographic data". In: *Advances in Neural Information Processing Systems 8: Proceedings of the 1995 Conference* 8 (1996), p. 145.

[178] I.T. Jolliffe. *Principal Component Analysis*. 2nd ed. Springer, 2002. DOI: https://doi.org/10.1007/b98835.

[179] A. J. Bell and T. J. Sejnowski. "An Information-Maximization Approach to Blind Separation and Blind Deconvolution". In: *Neural Computation* 7.6 (1995), pp. 1129–1159. DOI: 10.1162/neco.1995.7.6.1129.

[180] J-F Cardoso. "High-Order Contrasts for Independent Component Analysis". In: *Neural Computation* 11.1 (1999), pp. 157–192. ISSN: 0899-7667. DOI: 10.1162/089976699300016863.

[181] A. Hyvärinen and E. Oja. "Independent component analysis: algorithms and applications". In: *Neural Networks* 13.4–5 (2000), pp. 411–430. ISSN: 0893-6080. DOI: 10.1016/S0893-6080(00)00026-5.

[182] A. Delorme and S. Makeig. "EEGLAB: an open source toolbox for analysis of single-trial EEG dynamics including independent component analysis". In: *Journal of Neuroscience Methods* 134.1 (2004), pp. 9–21. ISSN: 0165-0270. DOI: https://doi.org/10.1016/j.jneumeth.2003.10.009.

[183] Robert Oostenveld, Pascal Fries, et al. "FieldTrip: open source software for advanced analysis of MEG, EEG, and invasive electrophysiological data". In: *Computational intelligence and neuroscience* 2011 (2011).

[184] Eric Maris and Robert Oostenveld. "Nonparametric statistical testing of EEG-and MEG-data". In: *Journal of neuroscience methods* 164.1 (2007), pp. 177–190.

[185] Jona Sassenhagen and Dejan Draschkow. “Cluster-based permutation tests of MEG/EEG data do not establish significance of effect latency or location”. In: *Psychophysiology* 56.6 (2019), e13335.

Appendix A

English version of the embodiment questionnaire of the VT-VHI (Chapter 2) and VHI (Chapter 3):

VT-VHI & VHI Embodiment Questionnaire – English Version		
Embodiment Statements	**Q1**	It seemed like I felt the touch of the paintbrush on the spot on which I was seeing the hand being touched.
	Q2	It seemed like the touch I was feeling were due to the touch of the paintbrush on the hand I was seeing.
	Q3	It felt like the hand I was seeing were my own hand.
Control Statements	**Q4**	It felt like my real hand were moving towards the hand I was seeing.
	Q5	It felt like I had three arms or three hands.
	Q6	It felt like the touch I was perceiving were coming from somewhere between my hand and the hand I was seeing.
	Q7	It felt like my real hand were turning virtual.
	Q8	It felt like the hand I was seeing was moving towards my real hand.
	Q9	The hand I was seeing was starting to look like my real hand, in terms of shape, skin tone, freckles, or other characteristics.

Italian version of the embodiment questionnaire of the VT-VHI (Chapter 2) and VHI (Chapter 3):

VT-VHI & VHI Embodiment Questionnaire – Italian Version		
Embodiment Statements	**Q1**	Sembrava di sentire il tocco del pennello nel punto in cui vedevo toccare la mano
	Q2	Sembrava che il tocco che sentivo fosse causato dal tocco del pennello sulla mano che vedevo
	Q3	Sembrava come se la mano che vedevo fosse la mia
Control Statements	**Q4**	Sembrava come se la mia vera mano si stesse spostando verso la mano che vedevo
	Q5	Sembrava come se avessi tre braccia o tre mani
	Q6	Sembrava come se il tocco che percepivo provenisse da qualche parte tra la mia mano e la mano che vedevo
	Q7	Sembrava come se la mia vera mano stesse diventando virtuale
	Q8	Sembrava come se la mano che vedevo si stesse spostando verso la mia vera mano
	Q9	La mano che vedevo cominciava ad assomigliare alla mia vera mano, in termini di forma, tonalità del carnato, lentiggini, o altre caratteristiche

Appendix B

English version of the embodiment questionnaire of the VMT-VHI (Chapter 2):

VMT-VHI Embodiment Questionnaire – English Version		
Embodiment Statements	**Q1**	It seemed like I felt the touch of the cardboard on the spot on which I was seeing the virtual hand.
	Q2	It seemed like the touch I was feeling were due to the touch of the hand I was seeing.
	Q3	It felt like the hand I was seeing were my own hand.
Control Statements	**Q4**	It felt like I had more then two arms or two hands.
	Q5	It felt like the touch I was perceiving were coming from somewhere between my hand and the hand I was seeing
	Q6	It felt like my real hand were moving towards the hand I was seeing.

Italien version of the embodiment questionnaire of the VMT-VHI (Chapter 2):

VMT-VHI Embodiment Questionnaire – Italian Version		
Embodiment Statements	**Q1**	Sembrava di sentire il tocco della carta nel punto in cui vedevo la mano virtuale.
	Q2	Sembrava che il tocco che sentivo fosse causato dal tocco della mano che vedevo
	Q3	Sembrava come se la mano che vedevo fosse la mia
Control Statements	**Q4**	Sembrava come se avessi più di due braccia o due mani.
	Q5	Sembrava come se il tocco che percepivo provenisse da qualche parte tra la mia mano e la mano che vedevo.
	Q6	Sembrava come se la mia vera mano si stesse spostando verso la mano che vedevo.